CHARACTERIZATION OF THE CHEMICAL EFFECTS OF CERIA SLURRIES FOR DIELECTRIC CHEMICAL MECHANICAL POLISHING

By

JEREMIAH TERRELL ABIADE

A DISSERTATION PRESENTED TO THE GRADUATE SCHOOL
OF THE UNIVERSITY OF FLORIDA IN PARTIAL FULFILLMENT
OF THE REQUIREMENTS FOR THE DEGREE OF
DOCTOR OF PHILOSOPHY

UNIVERSITY OF FLORIDA

2004

This dissertation is dedicated to my wife Kalia and daughter Asha; my parents Candy Grey and Renee McGee; my siblings, Marguerita, Paulette, Jonathan, Candon, Pilar, and Joshua. I also would like to dedicate this work to all of the elders of my family who were denied the educational experiences that I have been so fortunate to enjoy.

ACKNOWLEDGMENTS

First and foremost I would like to thank God for giving me the ability to complete this dissertation and surrounding me with such delightful people that have made this such an enlightening experience. I would also like to thank my advisor, Dr. Rajiv K. Singh, whose emphasis on sound reasoning, the fundamentals of materials science, and creative thinking has contributed immeasurably to my graduate experience. My committee, Dr. Brij Moudgil, Dr. Wolfgang Sigmund, Dr. Stephen Pearton, and Dr. Vaneica Young, have been extremely helpful. I would also like to thank Dr. Chang-won Park for his many insightful comments and for dutifully maintaining the CMP group, and Dr. Valentin Craciun and Dr. Hassan El-Shall for lending their expertise to particular areas of my research. I am also extremely grateful to Dr. Diola Bagayoko of Southern University for convincing me that the Ph.D. was a realistic goal to work toward.

I am extremely grateful to the National Science Foundation Alliance for Graduate Education and the Professoriate Program (NSF-AGEP), the UF College of Engineering Minority Fellowship Program, NSF-AGEP Dissertation Fellowship Program, and the Office of Graduate Minority Programs, the Particle Engineering Research Center (PERC), and the industrial partners of the PERC for financial support throughout my graduate program. Special thanks go to Dr. Anne Donnelly, Dr. Dovie Gamble, Dr. Terry Mills, Dr. Jonathan Earle, and Martha McDonald for encouragement, moral support and assistance with any problems I encountered. I would also like to thank the PERC and MAIC staff members Gary Schieffle, Gil Brubaker, John Henderson, Mike Beasley, Dr.

Emilia Hodge, Dr. Kevin Powers, Sophie Leone, Eric Lambers, Kerry Seiben, and Mike Tollon for their assistance throughout. I am extremely grateful for the assistance of Mr. James Albury of the ETD Office at the University of Florida. I would also like to extend my gratitude to Professor Brij Moudgil, Professor Paul Holloway, Professor Rolf Hummel, and Professor Robert Dehoff who have set great examples of lifetime excellence in both teaching and research.

I thank my colleagues, past and present, Uday Mahajan, Zhan Chen, Seung-Mahn Lee, Bahar Basim, Kyo-se Choi, Wonseop Choi, Wonseok Kim, Madhavan Esayanur, Suresh Yeruva, Kyoung-ho Bu, Su-Ho Jung, Sang Hyun Yoon, Han Ho Choi, Karthik Ramani, Anthony Stewart, Robert Crosby, Eboni Westbrooke, Lizandra Williams, Jeremiah Smith, Nakato Kibuyaga, and Samesha Barnes, for their contributions to this research with valuable discussions and friendship.

Of course I would like to thank my family and friends. My wife Kalia and daughter Asha have provided support, comfort, and love throughout this process. My parents, Candy Grey and Renee McGee; my siblings, Marguerita, Paulette, Jonathan, Candon, Pilar, and Joshua; and the rest of my family that have supported me throughout. Finally, thank you to the brothers of the Omega Psi Phi Fraternity, Beta Pi and Omicron Zeta Chapters.

TABLE OF CONTENTS

page

ACKNOWLEDGMENTS iv

LIST OF TABLES ix

LIST OF FIGURES x

ABSTRACT xiii

CHAPTER

1 INTRODUCTION 1

Background 1
Multilevel Metallization 2
Chemical Mechanical Polishing 2
Scope of the Dissertation 5

2 LITERATURE REVIEW 7

Introduction to Multilevel Metallization (MLM) 7
Motivation 7
Process Flow 9
Chemical Mechanical Polishing 10
CMP Components 12
Polishing pad 13
Wafer 15
Slurry 17
Silica-Silica CMP Mechanisms 18
Glass Polishing 19
Silica Hydrolysis 20
Silica CMP 22
Introduction to Shallow Trench Isolation (STI) 30
Ceria-Silica CMP Mechanisms 32
Chemical Tooth 33
Surface Defect 36
Particulate Generation 37
Ceria Surface Chemistry 38

3 MATERIALS AND METHODS 45

Introduction 45
Samples 45
Silica Wafers 45
Ceria Slurries 45
Ceria Thin Films 46
Functionalized Cantilevers 46
Cantilever oxidation 46
Particle attachment 46
CMP Equipment 47
CMP Tabletop Polishers 47
Friction Force Measurement Apparatus 48
Particle Characterization 49
Zeta Potential Measurement 49
Particle Size Analysis 51
Slurry Stability 52
Characterization of Silica Surface Morphology 53
Atomic Force Microscopy (AFM) 53
Scanning Electron Microscopy 55
X-ray Photoelectron Spectroscopy 56
Spectroscopic Ellipsometry (VASE) 58

4 THE EFFECT OF PRESSURE, PH, AND VELOCITY ON THE SILICA REMOVAL RATE AND SURFACE FINISH: A STATISTICAL DESIGN OF EXPERIMENTS 61

Introduction 61
Selecting a Statistical Design 63
Role of Pressure, Velocity, and pH in Silica CMP 64
Experimental 66
Results and Discussion 67
Removal Rate Response 67
Surface Finish Response 72
Summary 74

5 THE EFFECT OF CERIA SLURRY pH ON THE SILICA REMOVAL RATE, FRICTION FORCE, AND SURFACE MORHOLOGY DURING CHEMICAL MECHANICAL POLISHING 76

Introduction 76
Surfactant Based STI CMP 78
Fixed Abrasive Pads for STI CMP 80
Experimental 83
Results and Discussion 84
Ceria Slurry Characterization 84
Silica Removal Rate 88

Friction at the Ceria-Silica Interface 91
Surface Morphology 93
Comparison of pH Effects of Ceria-Silica to Silica-Silica CMP 94
Summary 97

6 NEAR SURFACE ANALYSIS OF POLISHED SILICA: CHARACTERIZATION OF THE CERIA-SILICA CHEMICAL REACTION 99

Introduction 99
Ceria CMP Models 99
Recent Progress 100
Experimental 104
Results and Discussion 105
Interaction Force Measurements 105
XPS Analysis 106
FE-SEM Analysis 109
Wear with Silica-Coated AFM Cantilevers 111
Summary 115

7 SUMMARY, CONCLUSIONS, AND SUGGESTIONS FOR FUTURE WORK ..117

Summary 117
Conclusions 120
Suggestions for Future Work 122

APPENDIX

A DEFINITION OF COMMON STATISTICAL TERMS 124

B BOX BEHNKEN DESIGN AND RESPONSES 125

LIST OF REFERENCES 127

BIOGRAPHICAL SKETCH 134

LIST OF TABLES

Table page

6-1 XPS binding energies for silica samples before and after polishing. 108

B-1 Box Behnken design for three factor experiment. 126

LIST OF FIGURES

Figure		page
1-1	Schematic illustration of a typical CMP tool.	1
1-2	Correlation of system-level variations with micro- and nanoscale effects and output parameters	4
2-1	Cross-section schematic of MLM structure with silica dielectric and aluminum metallization	7
2-2	Schematic depiction of cumulative increase in topography for non-planar MLM structures.	11
2-3	Degrees of planarization.	12
2-4	The effect of water on the mechanical properties of polyurethane chemistry	14
2-5	Current recorded for one stroke during tribological experiments on a tungsten substrate	17
2-6	Material removal rate of silica as a function of the concentration of silica slurries for different particle sizes	23
2-7	Indentation depth as a function of particle size.	24
2-8	Particle motion as a function of silica particle size and concentration.	29
2-9	Schematic depiction of device isolation:	31
2-10	Glass polish rate versus IEP of common abrasives.	33
2-11	Ceria crystal structure	39
2-12	Potential versus distance for a charged surface.	41
2-13	pH versus acid/base concentration.	43
3-1	SEM analysis of CMP pad	48
3-2	Schematic of in-situ friction force apparatus.	49

3-3 Schematic diagram of AFM apparatus. 54
4-1 Factor space for different statistical designs....67
4-2 Predictions of removal rate as a function of pressure and pH 69
4-3 Interaction profiles for removal rate as a function of pressure and pH 70
4-4 Predicted removal rate as a function of pressure, pH, and velocity....71
4-5 Predictions of RMS roughness as a function of pressure and pH....72
4-6 Interaction profiles for RMS roughness as a function of pressure and pH....73
4-7 Predicted removal rate as a function of pressure, pH, and velocity....74
5-1 SEM micrograph of fixed abrasive pad surface (200x) [Vel00]....80
5-2 Ceria slurry characteristics as a function of pH 84
5-3 Ceria slurry stability....85
5-4 FE-SEM image of ceria particles....86
5-5 Silica removal rate as a function of ceria slurry pH....89
5-6 Post-CMP slurry characteristics as a function of pH. 89
5-7 Zeta potential versus pH for ceria, silica, and co-dispersions....90
5-8 Friction force and removal rate....91
5-9 Qualitative comparison of electrostatic interactions....92
5-10 AFM topographical analysis of silica wafers....93
5-11 RMS roughness of silica wafers as a function of slurry pH. 94
5-12 pH dependent ceria-silica and silica-silica interactions. 95
6-1 Ratio of Ce M_5/M_4 white lines versus position....103
6-2 Interaction force....106
6-3 XPS analysis of silica....109
6-4 FE-SEM analysis of silica polished at pH 6.0. 110
6-5 FE-SEM analysis of silica polished at pH 2.5. 110

6-6 Ceria-silica wear at pH 2.5.....112
6-7 Ceria-silica wear at pH 4.5.....113
6-8 Ceria-silica wear at pH 6.0.....114
6-9 Ceria-silica wear at pH 11.0.....114
6-10 Silica-silica wear versus pH.....115
7-1 Schematic depiction of pH-dependent ceria-silica removal mechanism. 121

Abstract of Dissertation Presented to the Graduate School
of the University of Florida in Partial Fulfillment of the
Requirements for the Degree of Doctor of Philosophy

CHARACTERIZATION OF THE CHEMICAL EFFECTS OF CERIA SLURRIES FOR DIELECTRIC CHEMICAL MECHANICAL POLISHING

By

Jeremiah Terrell Abiade

December 2004

Chair: Rajiv K. Singh
Major Department: Materials Science and Engineering

In a little over a decade, chemical mechanical polishing (CMP) has grown from a niche application to an enabling technology for global planarization of virtually any material. Initially, CMP was limited to planarization of the silicon substrate during integrated circuit (IC) manufacturing. However, CMP has been successfully implemented in all phases of IC manufacturing. Since CMP is materials insensitive and the only process capable of producing globally planar surfaces, it is being investigated for new processing techniques like shallow trench isolation (STI), micro electromechanical systems (MEMS) fabrication, and a variety of other applications where the surface properties control device performance.

Despite the widespread acceptance of CMP, it remains the least understood step in the microelectronic device fabrication process. The emergence of novel technologies like STI that demand tighter control over the CMP process have stimulated increased interest in the fundamentals of the CMP process. In this work, the fundamental properties of ceria abrasives for STI CMP were studied.

Ceria slurries are promising for STI CMP because of their intrinsic preferential polishing of oxides over nitrides or polysilicon. This advantageous behavior has been attributed to a chemical reaction between the ceria abrasive and the oxide substrate. To date, ceria-silica polishing mechanisms have been supported by little to no experimental evidence. As a result of fundamental investigations, the silica polish rate and surface finish has been found to be a strong function of the ceria slurry pH, with the maximum polish rate occurring near the isoelectric point of ceria. An assortment of complementary surface analytical techniques was used to study the proposed abrasive-surface reaction that is widely attributed to ceria-silica CMP. The ceria-silica reaction has been confirmed by x-ray photoelectron spectroscopy (XPS), field emission scanning electron microscopy (FE-SEM), and atomic force microscopy (AFM) Finally, the surface chemistry of ceria has been reviewed and correlated with ceria-silica CMP observations.

CHAPTER 1
INTRODUCTION

Background

In little more than a decade, chemical mechanical polishing or chemical mechanical planarization (CMP) has grown from a niche application to an enabling technology for producing globally planar surfaces. Initially, CMP was developed to minimize topographical variations on Si substrates. The technology has since been applied to dielectrics (SiO_2, Si_3N_4, polymers, etc.), metals (W, Al, Cu, Pt, Ni), and semiconductors (SiC, GaN, silicon) for integrated circuit (IC) manufacturing and a variety of other emerging technologies such as microelectromechanical systems (MEMS) and organic light emitting diodes for flat panel displays. The use of CMP in such diverse technologies has created interest in fundamental aspects of the CMP process and development of novel designer slurries with tightly controlled polishing characteristics. Dielectric CMP processes essential for manufacturing metal-oxide-semiconductor field effect transistors (MOS-FETs) for microprocessor or dynamic random access memory (DRAM) applications are the focus of this research.

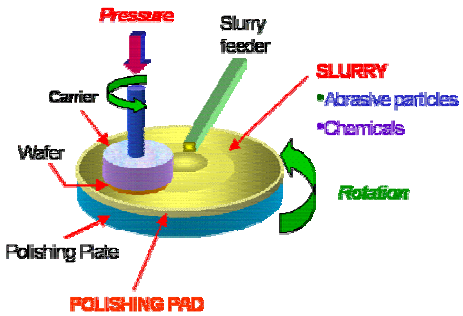

Figure 1-1 Schematic illustration of a typical CMP tool.

Multilevel Metallization

Generally, CMP systems consist of three main components: a polymeric polishing pad, the slurry with abrasive particles, and, of course, the surface to be polished (wafer) (figure 1.1). During CMP, the wafer is pressed against the compliant pad, which serves as a conduit for the abrasive particles that are suspended in an aqueous solution. Surface topography is reduced by simultaneous chemical and mechanical interactions that may be controlled by judicious selection of particle chemistry and slurry additives. The popularity of CMP in microelectronic device fabrication corresponds directly with device shrinkage, increasing wafer diameter, and an exponential increase in the number of IC components. For example, there were approximately 2300 transistors on a single chip in Intel's first generation of microprocessors. This number is expected to reach one billion by 2007 [ITRS03]. In fact, Intel recently manufactured chips with five hundred million transistors [Biz04]. Due to the finite wafer area available to chip manufactures, multilevel metallization (MLM) techniques were adopted. An IC fabricated via MLM techniques is analogous to construction in crowded urban areas like New York City or Tokyo. Once the available real estate has been consumed, the only option is to build vertical structures of increasing height. In MLM, alternating layers of dielectric and metal are deposited on the semiconducting substrate. Since topographical variations are additive, each layer must be globally planar before the next is deposited. To date, the CMP process is the only technique capable of producing globally planarized services [Ste97, Sin02, Eva02].

Chemical Mechanical Polishing

CMP is a deceptively complex process. Ideally, CMP should produce high removal rates (up to 800 nm/min), global planarity, good surface finish, and high selectivity to underlying barrier or isolation materials all with minimal defectivity, dishing, or erosion

[Sin02]. An additional complicating factor is the number of variables and their interactions that influence the CMP process. Despite its importance, the CMP process remains the least understood step during IC fabrication [Sin02]. In fact, early CMP processes were based on little more than an empirical understanding of CMP phenomena [Ste97, Sin02]. However, narrowing of the CMP process window because of the increasing needs of microelectronic device manufacturers has driven the need to reach a more mechanistic understanding of CMP. A major hurdle is the lack of understanding of interactions at the pad-particles-wafer interface. Conventional CMP processes rely heavily on end-point detection methods to terminate the CMP process before overpolishing ensues [Sin02]. Although the CMP process has matured significantly since its inception, efforts to understand wafer-slurry interactions still deserve considerable attention. This is especially true for emerging applications such as shallow trench isolation (STI), which requires alternative slurries with tunable properties for enhanced selectivity and planarity [Sin02, Eva04].

Initially, silica slurries were used to planarize interlevel dielectric (ILD) layers. However, the advent of new technologies coupled with increasingly stringent requirements for the CMP process has driven development of new abrasive particles for CMP slurries. Ceria slurries have stimulated widespread interest because of enhancements in material removal rate, surface finish, and selectivity over slurries formulated with silica abrasives. The replacement of local oxidation of silicon with STI has increased the demand for high selectivity slurries capable of removing the overburden of silica with minimal polishing of the underlying silicon nitride, which isolates active areas of the device. This shift to novel slurries is difficult without an understanding of the

slurry-wafer interactions. To develop CMP processes for STI, a thorough understanding of the variables that control the CMP process must be reached. In the early stages of CMP, empirical cause-and-effect observations of CMP performance as a function of applied pressure, carrier velocity, and pad type were utilized to explain CMP mechanisms. Years later, fundamental investigations were launched into the effect of process parameters such as slurry pH, abrasive size, and abrasive concentration to further explain CMP phenomena. Two major obstacles to understanding of CMP mechanisms are: the large number of process variables (figure 1.2) and their interactions and the lack of sufficiently sensitive techniques for measuring nano-scale phenomena during the CMP process. The CMP field has matured to the point of understanding that systematic investigations of micro- to nano-scale interactions at the pad-particles-wafer interface must be understood to extend the applicability of the CMP process to future generations of IC manufacturing.

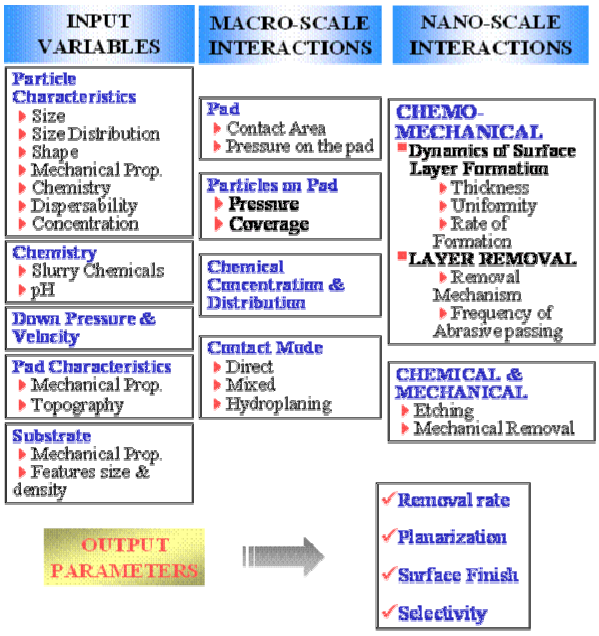

Figure 1-2 Correlation of system-level variations with micro- and nanoscale effects and output parameters in chemical. mechanical polishng [Sin02a].

Scope of the Dissertation

This study will focus specifically on dielectric CMP processes using ceria slurries. Despite the promise of ceria for STI CMP, few studies exist on the fundamentals of slurry-wafer interactions. Ceria–silica CMP mechanisms are assumed to be identical to ceria–glass polishing mechanisms. Furthermore, ceria CMP efforts are toward the use of surfactants to selectively adsorb onto the silicon nitride surface to enhance selectivity with respect to the overlying silica. Material removal during CMP takes place because of synergistic chemical and mechanical interactions. Ceria slurries are expected to have an enhanced chemical contribution to polishing. Therefore, investigations in this study are focused on chemical and surface chemical effects that control the CMP process. A synopsis of the efforts in this study follows.

Chapter 2 reviews the state-of-the-art of the CMP process. Motivations for the implementation of the CMP process are discussed. The roles of the pad, slurry, and wafer are covered in greater detail. Further, the current understanding of silica-silica CMP processes is summarized. A review of STI and STI CMP follows. Ceria behaves differently than silica both in solution and at the pad–wafer interface. Therefore, the surface chemistry of ceria will be reviewed.

Chapter 3 details the materials and methods used for this study. This work was approached with the viewpoint that CMP experiments alone are insufficient to explain polishing phenomena. Experiments and measurements were obtained using standard laboratory CMP equipment and surface sensitive characterization techniques.

Chapter 4 features a statistical examination of the effect of pressure, pH, and velocity on ceria–silica CMP. Studies that examine these crucial process parameters

neglect interactions between the variables. Using statistical methods the individual and synergistic effects may be ascertained.

Chapter 5 examines the effect of pH on the silica removal rate, surface finish, and in-situ lateral friction force. Particle characteristics (zeta potential and particle diameter): before and after CMP will be presented.

Chapter 6 is a study of the nano-scale phenomena that affect the CMP process. Atomic force microscopy (AFM), x-ray photoelectron spectroscopy (XPS), and field emission scanning electron microscopy (FE-SEM) have been used to characterize the extent of particle–wafer interactions during ceria-silica CMP.

Chapter 7 is a summary and offers conclusions of this work. A pH-dependent ceria-silica polishing model is proposed. Chapter 7 ends with some suggestions for future work for further enhancement of the STI CMP process.

CHAPTER 2
LITERATURE REVIEW

Introduction to Multilevel Metallization (MLM)

Motivation

It is impossible to provide a comprehensive review of CMP for IC fabrication without discussing multilevel metallization (MLM), figure 2-1. Modern ICs contain

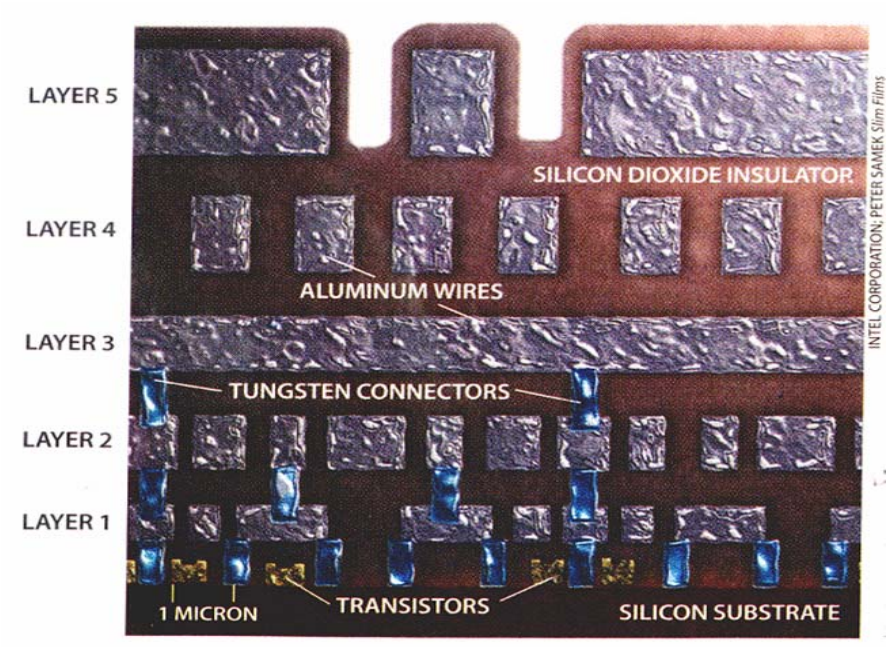

Figure 2-1 Cross-section schematic of MLM structure with silica dielectric and aluminum metallization [Sti97].

several million components (transistors, resistors, and capacitors) on a single chip. To form a circuit, these elements must be connected with some form of wiring. MLM provides a more efficient means of routing metal lines. Historically, each new generation of IC has involved a shrink of the device size [Wil93]. Device shrinkage results in improved speed, increased packing density, and greater functionality. MLM also provides

a means of separating long, winding metal lines resulting in increased yield and device reliability. CMP is an enabling technology for the production of MLM structures. Combined, these factors are responsible for the decline in prices and product dimensions for seemingly omnipresent items like the desktop or laptop computer, mobile phone, and calculator. As the device size decreases, and the number of components in the circuit increases, the interconnect becomes a limiting factor in chip performance.

The most widely used measure of IC performance is the product of the resistance in ohms (Equation 2.1) and capacitance in farads (Equation 2.2), commonly called the RC time constant (Equation 2.3), measured in seconds, which is the time required for a voltage at one end of a metal line to reach ~ 63% of its final value at the opposite end [Ste97].

$$R = \rho\, l/wd = \rho\, l/A \qquad (2.1)$$

$$C = \varepsilon wl/t \qquad (2.2)$$

$$RC = \rho\varepsilon\, l^2/td \qquad (2.3)$$

Where ρ is the resistivity of the metal line, l, w, d, and A are the length, width, thickness, and cross sectional area respectively and ε is the permittivity of the dielectric, which equals the insulator dielectric constant (ε_r) times the permittivity of free space (ε_o), and t is the thickness of the insulator. According to (Equation 2.3), the time constant may be lowered by using metal lines of lower resistivity (i.e. replacing Al with Cu), insulators with lower dielectric constants (i.e., porous silica, or polymeric materials instead of SiO_2), or by decreasing the length of the metal lines. Equation 2.3 does not show a direct dependence on line width, but as devices are continually miniaturized, the metal line thickness (d) and interlevel (ILD) thickness (t) are also scaled to smaller dimensions,

causing an increase in the time constant. Scaling the device dimensions is one alternative for improving device speed, since device delay decreases with decreasing feature size [Ste97]. However, for 0.5 μm features, interconnect delay accounts for ~ 25% of the total delay, while for 0.25 μm dimensions, ~ 50% of the delay is due to the interconnect [Ste97]. With continued scaling, interconnect performance dominates device speed resulting in diminishing returns as the dimensions are aggressively reduced. Any change that decreases ρ, l, ε, or increases t and d will enhance device speed by decreasing the interconnect delay. Since RC is proportional to l^2, the most dramatic decreases in interconnect delay can be achieved by avoiding long metal lines. This is possible using MLM [Wil93, Ste97].

Process Flow

The process flow for MLM is as follows [Wil93]: silicides (metal-Si compounds) are formed on the source, gate, and drain of MOS transistors as well as on doped polysilicon films that are used as resistors or contacts in bipolar circuits. Next, the pre-metal dielectric (ILD0) is deposited. The ILD0 and subsequent levels of dielectric (ILD1, 2, 3, ...) are different materials. Boron phosphate silicate glass (BPSG) [Ols93] is commonly chosen for the ILD0 layer whereas silica (SiO_2), silicon nitride (Si_3N_4), or silicon oxynitride (SiO_xN_y) are used for the ILD. Depending on the planarity requirements and thermal budget, planarization ensues via thermal flowing [Wil93], etchback [Che97], or CMP [Ste97]. The ILD0 layer is then patterned and etched to form contact holes through the oxide to the underlying structures or silicide. The holes or vias (V1, 2, …) are then filled by barrier film if none exists on silicide, then a conducting film (Al or W) is deposited. Currently, W is the metal of choice because of its ability to conformally fill high aspect ratio vias [Ire97]. The W is etched back to form a plug. The

interconnect metal (M1, 2, …) is then deposited. Cu has replaced Al as the metal of choice for the metal interconnect because of its low resistivity and improved electromigration resistance resulting in faster, more reliable devices [Lee03]. Vertical structures are built by replicating the procedure of dielectric deposition, etching to form vertical vias, patterning and interconnect deposition. The MLM process is completed by depositing a final dielectric layer that hermetically protects the underlying layers from corrosive ions, moisture, and solder chemicals. For feature sizes of ~100 μm, 12 metal layers are required when using Al interconnects and SiO_2 as the ILD. In contrast, only 6 levels are required using Cu interconnects and a low dielectric constant material [Sin98]. MLM is not a simple process. A variety of tools, materials, and techniques are involved. Stringent control must be maintained over each sequence in the process.

Chemical Mechanical Polishing

Initially, it may seem counter-intuitive to remove any of the dielectric or metal layers that have been so carefully deposited, especially by exposing the pristine environment of microelectronic fabs to such a dirty process as CMP. Topographical variations or thickness non-uniformities are deleterious to device performance [Ols93]. Also, in multilevel structures necessary for ICs, topographical variations are additive (stack-up effect) [Vie01]. There are several sources of topography generation during fabrication. Non-uniform deposition may occur if curved wafers are used. Wafer curvature may be because of intrinsic stress in the substrate [Ste97]. The fabrication process itself may contribute to non-planarity. Repetitive cycles of deposition, patterning, and etching are known to generate steps at the surface [Ste97]. Auto-focus errors, residual lens aberrations, and resist thickness variations may also produce non-planar surfaces during lithography [Gry93, Ste97]. Planarization has its benefits at each level of

the MLM structure [Ols93]. Planarization of the pre-metal and interlevel dielectric improves the patternability of metal interconnects, decreases line resistance, and increases the reliability of the device. Also, as topography is minimized before ILD and metal deposition, the stack-up effect is reduced, which reduces the complexity of subsequent planarization steps. Along with the benefits of dielectric planarization, metal planarization results in an increase in step coverage, device speed and device yield, and a reduction in manufacturing cost.

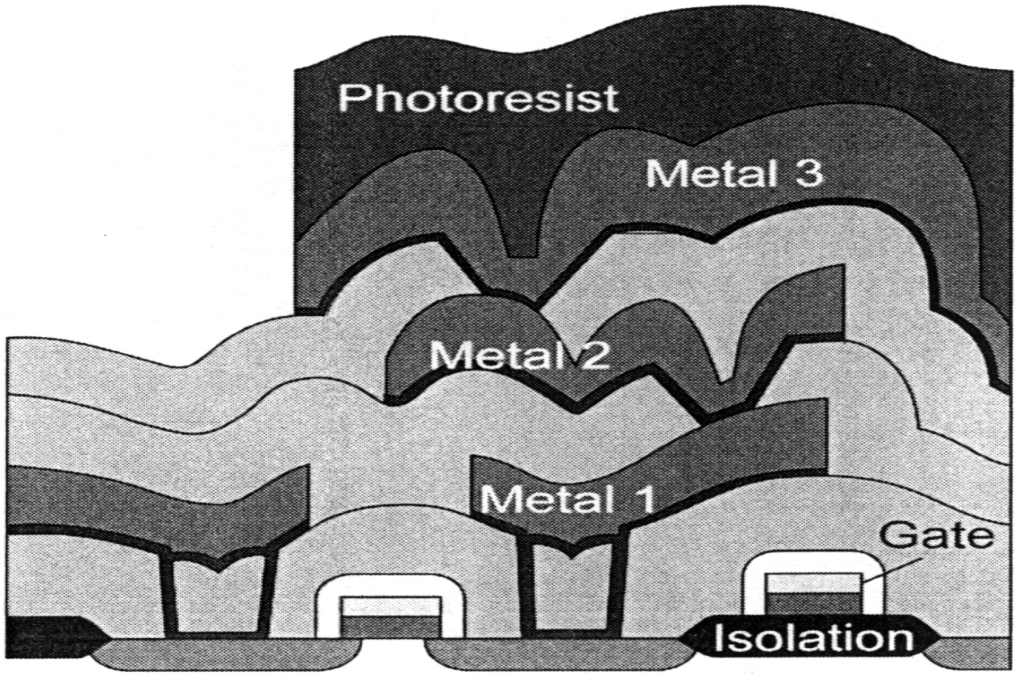

Figure 2-2 Schematic depiction of cumulative increase in topography for non-planar MLM structures [Vie01].

Several techniques capable of achieving some level of planarization exist. For example, thermal flow of BPSG films is used to planarize the pre-metal dielectric layer. After chemical vapor deposition (CVD) of the BPSG film, an anneal step is conducted to soften and flow the film over voids or thickness non-uniformities [Ols93]. This technique is not universally applicable because of the presence of metals with low melting

temperatures like Al. Resist etchback (REB) or reactive ion etching (RIE) uses a sacrificial spun-on material as a planarizing agent [Ols93, Ste97]. After dielectric deposition onto the interconnect, photoresist is spun onto the entire wafer. The smooth surface of the resist is transferred to the underlying dielectric layer by a non-selective blanket etchback process. The photoresist etch rate is selected to match that of the oxide etch rate so that the surface is removed uniformly. A second layer of dielectric is then deposited to achieve the desired dielectric thickness. This technique is undesirable because several attempts are necessary to achieve planarization and the plasma used for etching is composed of hazardous gases [Mur93]. Thermal flowing, reactive etching, and all other planarization techniques have one common flaw: none can produce universal globally planarized surfaces.

CMP Components

CMP is the only technique capable of producing global planarization. Figure 5.3 shows schematically the difference in planarization length for local and global planarization. Generally, CMP systems consist of only 3 main components, pad, slurry, and wafers. Currently, intense research is being conducted to understand the fundamentals of the process.

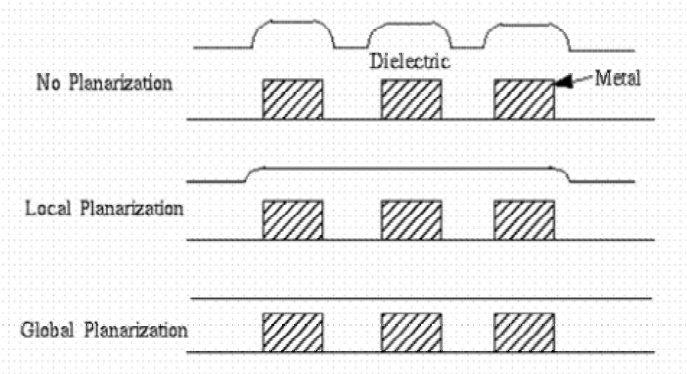

Figure 2-3 Schematic depiction of the degrees of planarization.

Polishing pad

Until recently, CMP polishing pads have received little attention. Although the polishing pad structure determines the polish rate and planarity of a CMP process, pad effects and properties are poorly understood. Generally, manufacturing processes for CMP pads are empirically derived. Because of the ability to control pad characteristics, polyurethane impregnated felts or cast polyurethane foams with filler materials are the most desirable materials for commercial CMP pads [Ste97, Jai94]. A hydroxyl-terminated resin known as polyol is reacted with di-isocyanate, in the presence of a catalyst and foaming agent to form polyurethane, a condensation polymer [Jai94]. Filler material may be added to achieve the desired mechanical properties.

During the CMP process, the pad has 3 functions [Ste97]. Pores in the bulk transport slurry to the pad–wafer interface, the pad asperities provide points of contact to form the abrasive–wafer interface, and the pad also transports abraded material away from the pad–particles–wafer interface. Appreciable removal rates are expected only when the abrasive particles are embedded in the CMP pad and slide against the wafer surface [Zha99]. The difficulty in engineering the performance of CMP pads is related to ambiguity on the effect of pad properties on the CMP performance. Specific gravity, compressibility, hardness, shear modulus, dynamic shear modulus, pad asperity height, width, and distribution, and pad roughness control planarization efficiency. To achieve planar surfaces, the pressure at high features should exceed the pressure at low features. Empirical results indicate hard pads with low compressibility are more effective in achieving planar surfaces, because they do not conform to wafer topography. However, considerable difficulty exists in determining what pad properties should be measured to determine pad hardness. The dynamic nature of the CMP process further complicates the

measurement. Through diffusion, water molecules break hydrogen bonds in the polyurethane structure, which leads to pad softening (figure 5.4) [Hog73]. The pad performance, in terms of planarity and removal rate, is dependent on the its modulus of elasticity (G) [Ste97]. To maintain the pressure differential at high and low features, high G values are desirable for CMP pads.

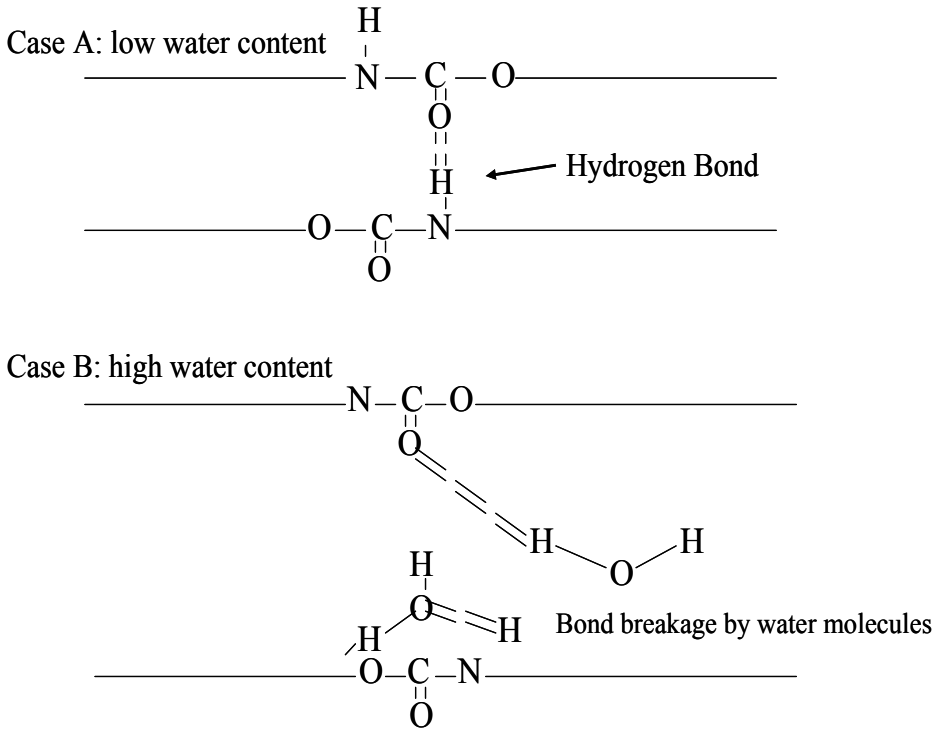

Figure 2-4 Schematic depicition of the effect of water on the mechanical properties of polyurethane chemistry adapted from [Hog73].

Polyurethane responds elastically and viscoelastically to shear stresses during CMP. CMP phenomena occur in short timeframes–approximately micro to milliseconds. Further insight into planarization behavior is possible by measuring the dynamic shear modulus (Ǵ) under periodic stress. Ǵ increases with measurement frequency. Planarity has also been shown to increase with pad rotation speed. At higher frequencies, the pad

has less time to deform, decreasing the pad sensitivity to wafer topography. Early measurements of pad properties were conducted in dry conditions. More recent measurements have shown a dependence of pad properties on water content, temperature, polishing cycles, and slurry chemistry [Ste97, Mur94, Jai94]. Water soaking and pad heating are known to lower the mechanical properties of the pad. Alteration of the pad properties leads to inconsistent CMP performance. To maintain reproducible conditions, CMP pads are conditioned between runs or during the process. In our studies, a diamond pad conditioner was used between CMP runs. The conditioner reproduces the original rough surface and also removes slurry particles from the previous CMP run. Conditioning extends pad lifetime and prevents glazing–plastic wear of the pad surface.

Fixed abrasive pads–wherein the pad is coated with slurry particles–are receiving increased attention. With fixed abrasive pads, slurry handling is no longer an issue. Fixed abrasive pads are also less sensitive to wafer topography, which may increase the planarization capability of the CMP process. Since slurry stability is not a concern, more diverse slurry chemistries may be investigated. Fixed abrasive pads are potentially applicable to STI [Gor03], Cu CMP [Ngu01], and MEMS [Kul04] fabrication processes where over-polishing, erosion, and pattern density effects complicate the conventional CMP process.

Wafer

Virtually all materials are candidates for planarization via CMP. Knowledge of the chemical, structural, and mechanical properties of the surfaces to be polished is key for designing materials-specific CMP processes. The mechanisms for dielectric and metal CMP differ significantly. Metal CMP may be considered a repetitive corrosion/erosion process [Ste97], wherein the slurry chemistry is tailored to form a modified surface layer

or oxide scale. This scale is then rapidly removed by repetitive abrasive contact. To control removal rate, planarity, defectivity, and selectivity considerable latitude exists in metal CMP processes. Several chemical additives are used in metal CMP slurries to control the kinetics of layer formation and the mechanical properties of the surface layer [Ste97, Sin02, Lee03]. Metal CMP slurries are more chemically active than dielectric slurries. Generally, dielectric CMP processes are based on dissolution of the substrate or wafer via slurry additives or abrasive particle indentation. Chemical processes in dielectric CMP are largely due to the presence of water. For example, little polishing is observed in oil or alcohol based slurries [Coo90] even with diamond abrasives [Ste97, Coo90].

Few techniques exist that are capable of measuring the modified surface layer properties in-situ. This problem is particularly glaring in dielectric CMP. However, for metal CMP, electrochemistry and surface sensitive thin-film techniques have been used to determine the properties of the metal surface layer. Bielmann demonstrated the active–passive behavior in W [Bie98] by measuring the current vs. time while rubbing a sphere against the W surface and while motionless. Also, x-ray photoelectron spectroscopy (XPS), chrono-amperometry, potentio-dynamic measurements, and x-ray reflectivity techniques were applied to Cu CMP system. To achieve planarization without contributing to surface topography, the CMP process must interact with only the topmost atomic layers. For dielectric CMP, and silica in particular, attempts to characterize surface layer or ‘gel’ layer formation are conducted ex-situ. Ellipsometry [Fran99], infrared reflectivity [Wal96], and atomic force microscopy (AFM) [Adl00] indicate the presence of a softened surface layer with thickness in the nanometer range.

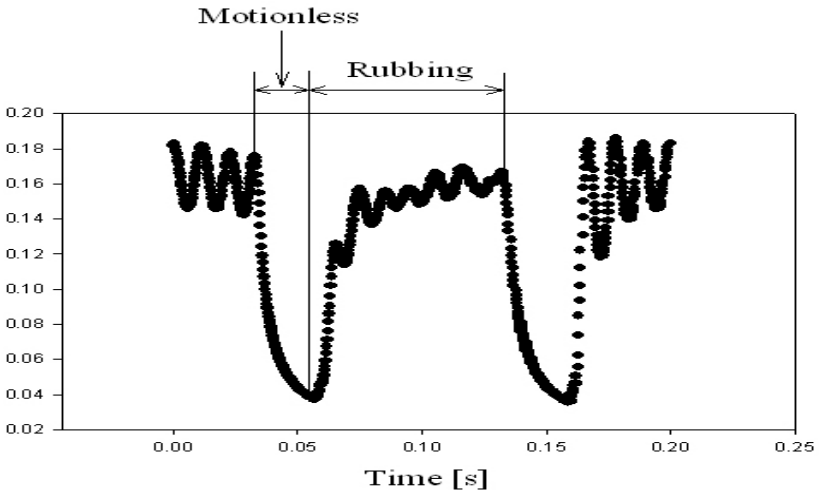

Figure 2-5. Current recorded for one stroke during tribological experiments on a tungsten substrate [Bie98].

Slurry

CMP slurries consist of abrasive particles 50-500nm in diameter suspended in de-ionized (DI) water. Abrasive particles in the slurry are responsible for mechanical abrasion, the M in CMP. Highly reactive particles like ceria (CeO_2) and zirconia (ZrO_2) may also contribute to the chemical component via particle–substrate bonding. The abrasive particles are also responsible for pad glazing during the actual CMP process. Residual particles must be removed between each CMP run. The abrasive particles may be characterized by measuring a variety of properties. The particle type, hardness, size, shape, isoelectric pH–the pH at which the surface is neutral–chemical reactivity, and solubility in the slurry environment all affect the planarization rate, surface finish, and defectivity of the process. The trend in slurry formulation is toward more 'gentle' CMP processes [Sin02]. Hard abrasives like alumina (Al_2O_3), which were originally used in W and Cu CMP are being replaced by ceria (limited cases), silica, or abrasive-free slurries that contain little to no particles. For dielectric CMP ceria is gaining widespread attention. Selectivity, enhanced removal rate, and improved surface finish are the factors

that have driven interest in ceria-based slurries. Oxidizers, corrosion inhibitors, complexing agents, stabilizers, dissolution agents, and surfactants are among the chemical additives found in CMP slurries [Sin02]. Dielectric CMP slurries tend to be less complex. Dispersants–to inhibit particle agglomeration dissolution agents–to enhance surface solubility and surfactants–to enhance polish selectivity tend to be the only additives in CMP slurries. Traditionally, slurries for silica CMP consisted of silica particles.

The most intense research efforts in CMP are in the areas of slurry formulation and particle properties. A tremendous potential for commercialization exists in CMP slurry manufacturing. In less than ten years the CMP slurry market has grown from non-existent to a billion dollar enterprise [Sin03]. Currently, the slurry market accounts for ~ 40% of the worldwide nano-particle market share. These facts are wonderful for industrial companies or the researcher who develops marketable CMP slurry. However, for the academic researcher, the tremendous profitability has led to reluctance to release proprietary information, which complicates efforts to understand CMP fundamentals. What is available in the open and patent literature does not sufficiently explain CMP mechanisms. Fundamental investigations into slurry properties are necessary, especially in a setting where a sustained effort can be maintained. Considerable room exists in the academic arena to contribute to the knowledge of CMP slurry development, particularly in areas like STI and MEMS that will be introduced in the near future.

Silica-Silica CMP Mechanisms

Aside from planarization of silicon wafers, the most fundamental studies in CMP exist in oxide CMP for back-end planarization after pre-metal and interlevel dielectric deposition [Ste97]. CMP of silica with silica abrasives is a mature process and may be

considered a model for other dielectric CMP processes. This section will cover the current understanding of silica–silica CMP fundamentals. Much of the knowledge in oxide CMP is based on over a century of glass finishing for optical lens applications [Cook90, Ste97, Kel98]. A significant amount of polishing data exists for many abrasive types - diamond and oxides of iron, cerium, chromium, silicon, zirconium, titanium, zinc, lanthanum, nickel, and aluminum [Cor63, Izu79, Izu84, Coo90, Ste97]. Therefore, it is worthwhile to begin this section of the review with glass polishing mechanisms. Although these glasses are not used in IC manufacturing, the variance in their physical properties is useful for understanding polishing mechanisms in glass, including that of silica for ILDs in IC manufacturing [Ste97]. Oxide CMP may be considered a specialized form of glass polishing.

Glass Polishing

The mechanisms for glass polishing may be grouped into three categories: wear, flow, and chemical [Hol64, Isu79]. The wear mechanism suggests surface smoothing is wholly mechanical because of increased contact at high points resulting in minimal wear at low points on the surface. The flow mechanism suggests the glass surface flows during polishing from peak to valley regions, until a smooth surface is achieved. Finally, glass polishing via a chemical mechanism is attributed to increased dissolution at high surface features because of the high pressures exerted by the abrasive particles. Izumitani determined the glass polishing mechanism by examining the polish rate as a function of glass hardness (bulk), softening point–a measure of a glass' resistance to flow, and chemical durability [Izu79]. Among the three, only chemical durability influenced the polish rate. The chemical durability of a glass is measured by the weight loss in water or dilute acids. Weight loss occurs because heavy modifier ions (Pb^{2+} and La^{+}) are leached

from the glass and replaced by lighter hydrogen ions [Ste97]. The influence of chemical durability on polish rate indicates that chemical reactions influence the glass polishing mechanism. Chemical modification of the glass surface alters the surface properties, including hardness. Izumitani measured the effect of leaching time on Vickers microhardness and polish rate versus surface hardness of glasses. Here the hardness was shown to decrease with leaching time and the polish rate correlated well with the surface hardness of the glass [Izu79]. Glass polishing is crucially dependent on the presence of water [Coo90]. Polishing rates are negligible in hydrocarbon liquids like kerosene [Izu84], paraffin [Cor63], or oil [Izu79], and non-hydroxyl containing liquids like formamide [Cor63]. Furthermore, the polish rate in dry conditions or oil solutions correlated with the bulk hardness of the glass [Izu79]. Surface modification is not expected in dry or oily conditions. In these conditions, wear dominates the glass polishing mechanism. The surface quality of glass polished in solutions other than water or in dry conditions was poor and polish rates were significantly lower. Therefore, optimum glass polishing occurs due to synergistic interactions between chemical and mechanical interactions.

Silica Hydrolysis

From the preceding discussion two points should be emphasized. First, water-based slurries are essential, both for effective planarization and desired surface finish. Second, during CMP the abrasive particles only interact with the topmost, chemically modified layers of the surface to be polished. In the case of silica, this modified layer results because of hydrolysis, which proceeds as follows [Ile79].

$$SiO_2 + 2H_2O \rightarrow (SiO_2)_{x-1} + Si(OH)_4 \qquad (2.4)$$

In the hydrolysis reaction, Equation 2.4, interactions between siloxane bonds (Si—O—Si) and water determine the behavior of silica during CMP. Budd described this reaction, in three stages, as the attack of the solvated hydrogen ion (H_3O^+) on the negative sites of silica [Bas02a, Bud61]. First, a water molecule from the environment attaches to the Si—O—Si) bond by forming a hydrogen bond between its hydrogen and the oxygen atom of the silica surface; lone pair orbitals of the oxygen from water interact with the Si atoms. Second, hydrogen bound to water transfers a proton to the oxygen of silica, while an electron is simultaneously transferred from the oxygen of water to the Si atom. Finally, two new bonds are formed (Si—O—H), by destroying the original siloxane bond. The dissolution of silica occurs if all four bridging oxygen bonds are hydrated, forming the solute species $Si(OH)_4$ (silanol) [Ile79, Coo90, Tro94]. The rate of this reaction is controlled by the diffusion of water into the silica surface, the pH of the polishing slurry, and the indent depth of the abrasive particle into the silica surface [Ile79, Coo90]. The dissolution rate of silica increases rapidly above pH 9.0. Therefore, formulating slurries in the basic pH regime enhances the removal rate and the surface finish [Cook90]. According to Budd, the OH^- ion acts a catalyst for water attack on the silica network [Bud61]. OH^- ions create excess electrons, resulting in higher negative surface potentials, which increases the affinity for attack by H_3O^+.

The diffusion of water is known to affect the surface hardness [Izu79, Hir87], fatigue [Han90, Han91], and structure of silica [Tro94, Dav96, Wal96, Adl01]. However, attempts to measure the properties, specifically the thickness and hardness, of the chemically modified layer on silica formed during CMP have been inconclusive. Trogolo and Rajan have reported, using transmission electron microscopy (TEM) and Fourier

transform infrared reflectivity (FTIR), the presence of two near-surface regions, 3 and 15-20 nm below the surface after CMP [Tro94]. The 3nm surface layer possessed density lower than the bulk value, with the 15-20 nm layer displaying an increased density with a gradual return to bulk values ~ 20nm below the surface. However, Wallace et al., using x-ray reflectivity, reported the opposite [Wal96]. According to their measurements, the near-surface region after CMP is compacted, resulting in an increased density. They further dispute the validity of a 20 nm region of increased density, because the accompanying increase in electron density due to water diffusion was not observed. Adler observed a short-range repulsion at the silica surface by direct measurement of surface forces with AFM [Adl01]. This behavior was attributed to the formation of a 'gel layer' because of swelling of the silica surface as a result of water diffusion. Since in-situ techniques capable of measuring these phenomena are not readily available, research efforts in oxide CMP have centered largely on particle effects. Fundamental observations have also been reported by measuring variations in the in-situ friction force during CMP conditions [Mah99a, Mah99b, Mah00, Cho03, Cho04a, Cho04b, Cho04c].

Silica CMP

In the last five to six years, considerable progress has been made in CMP research. Our group in the Particle Engineering Research Center (PERC) has been at the forefront, particularly in oxide CMP. The properties of the abrasive particles in CMP slurries have a significant impact on the polishing behavior. Alteration of the particle size, size distribution, and/or solids loading changes the number of abrasives available for polishing at the pad-wafer interface. This affects the polish rate and surface finish by modulating the load per abrasive particle. Therefore, the polishing behavior as a function

of particle size, size distribution, solids loading, and the contact characteristics at the pad–wafer interface should be understood.

The particle size effect has been studied by a number of researchers with conflicting results. Brown and Jairath reported an increase in polish rate with an increase in particle size [Bro81, Jai94]. Izumitani reported the opposite, a decrease in polish rate with an increase in particle size [Izu79]. In total disagreement, Cook and Sivaram concluded that the polish rate was not influenced by the particle size [Coo90, Siv92]. Despite the numerous studies on the effect of particle size in oxide CMP, considerable confusion remained. By studying the effect of particle size (0.2 μm-1.5 μm) and solids loading (0.2-15 wt%) simultaneously, Mahajan, a former member of the CMP group in the PERC, was able to clarify the particle size effects [Mah00]. According to his results, the polish rate was highest for larger particles at the lowest solids loadings. Except for 0.2 μm particles, the polish rate decreased with increasing solids loading (figure 5.5). Furthermore, silica surfaces polished with larger particles showed significant surface deformation, whereas, 0.2 μm abrasive particles produced smoother surfaces.

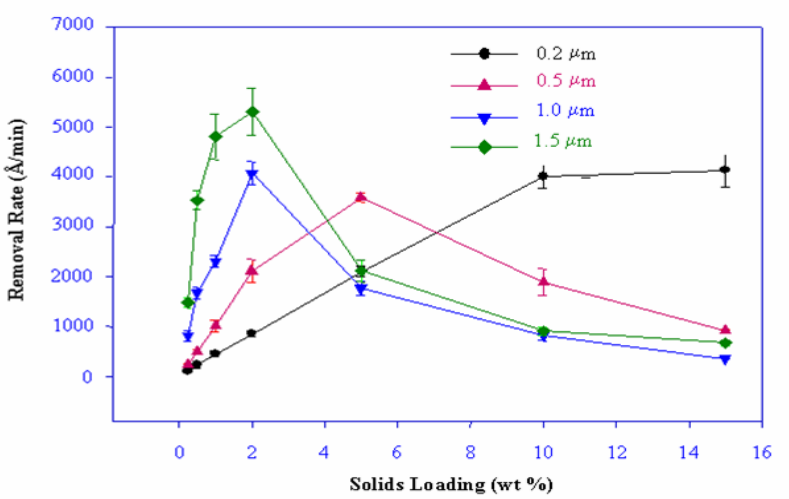

Figure 2-6 Material removal rate of silica as a function of the concentration of silica slurries for different particle sizes [Mah00].

To explain the CMP behavior as a function of particle size, two mechanisms were proposed [Bie98]. The first is a contact or surface area based mechanism, in which the polish rate depends on the total contact area between the abrasive particles and the surface undergoing CMP. The following expression gives the dependence of contact area on particle diameter:

$$A \propto C_0^{1/3} * \phi^{-1/3} \qquad (2.5)$$

where A is the contact area, C_0 is the abrasive concentration, and ϕ is the particle diameter. According to Equation 2.5, surface area controls the removal rate for smaller size particles. Also, more particles are available for polishing due to tighter packing at the pad–wafer interface. For the second, an indentation–based mechanism, polishing occurs due to penetration of the surface by the abrasive particles. The indent volume may be expressed as follows:

$$V \propto C_0^{-1/3} * \phi^{4/3} \qquad (2.6)$$

where V is the indent volume. Other results have also indicated that the indent depth increases with increasing abrasive particle size [Coo90, Qin04], figure 2-6.

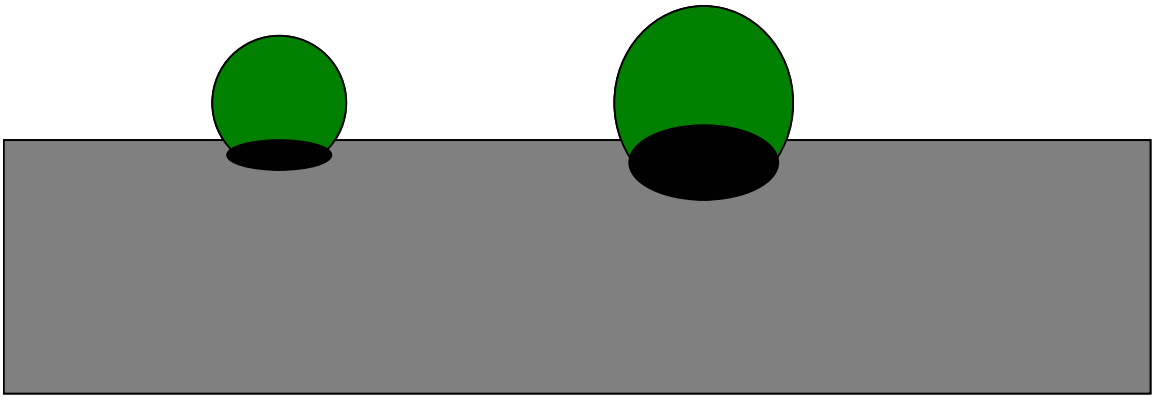

Figure 2-7 Schematic depiction of the indentation depth as a function of particle size.

CMP processes must produce planar surfaces with minimal surface deformation. Surface deformation or defectivity may be classified as scratches, pits, film delamination,

and/or chemical or particulate residue [Ste97]. The presence of microscratches has a deleterious effect on microprocessor performance [Sch95]. Earlier glass polishing experiments indicated that the surface deformation was less when slurries were formulated with monosized particles [Coo90]. A small percentage of oversized particles may be responsible for pitting or scratches after CMP. To determine the role of oversized particles during polishing, Basim formulated slurries with both hard and soft agglomerates for silica CMP [Bas02a]. The effect of hard agglomerates was studied by adding small amounts of oversized particles to the otherwise stable, monosized, and well-dispersed slurry [Bas00, Bas02a]. Soft agglomerates were grouped into 3 categories: 1) dry aggregates or partially dispersed slurries; 2) polymer flocculated slurries, which were created by adding 0.5 mg/g of polyethylene oxide (PEO); 3) coagulated slurries, which were produced by adding, 0.2M, 0.4M, and 0.6M NaCl [Bas02a, Bas02b].

In the case of hard agglomerates [Bas00, Bas02a], oversized particles were added to the slurry until the particle size measurement tool was able to detect their presence (~1.0 wt%). The baseline slurry consisted of 0.14 μm sized silica particles at 12 wt%. 0.5 μm, 1.0 μm, and 1.5 μm Geltech® particles were used to represent hard agglomerates. For all slurries except those spiked with 1.5 μm particles, the removal rate was less than that obtained using the baseline slurry. In all cases, the surface finish worsened when oversized particles were used. Scratches and pits were observed on the surface. Furthermore, surface deformation worsened as the concentration of coarse particles was increased. Basim explained these observations by considering the load distribution per particle. According to her results, coarse particles acts as pillars at the pad-wafer interface, decreasing the opportunity for smaller, primary slurry particles to participate in

the polishing process [Bas02a]. This assertion has two consequences: first, larger particles experience an increased load in comparison to smaller particles, and second, the total contact area at the pad–wafer interface decreases, which is because of a decrease in the effective number of abrasives at the pad–wafer interface. The pitting depth after CMP increased as the coarse particle size increased, because of the increased pressure and greater penetration depth of the larger particles [Bas02].

Hard agglomerates may be filtered as the slurry is pumped to the pad-wafer interface. However, even after filtering, defectivity may still be high [Ewa99]. Scratches or pits in this case may be attributed to transient or soft agglomerates formed during the CMP process [Bas02]. Van der Waals or weak physical bonds are responsible for aggregation in the case of dry agglomerates. Post–CMP particle size measurements indicate agglomerated particles are broken apart during the polishing process. During polishing, these interconnected particles experienced the majority of the load. Higher removal rates were obtained at the expense of surface quality. The effect of PEO addition was also studied for dispersed slurries, in which the polymer molecules are believed to completely surround each abrasive particle and flocculated slurries in which the mean particle size shifted to 5.82 μm from 0.20 μm. For flocculated slurries the polish rate slightly decreased with a significant increase in defectivity. However, for well–dispersed polymer containing slurries, surface deformation was comparable to the baseline values, with diminished removal rate. AFM force measurements indicated that the polymer acts as a lubricant at the pad–wafer interface, which is responsible for the removal rate decrease [Bas02a, Bas02b].

The effect of coagulation on slurry performance can be simulated by adding ionic salts to the slurry. In the studies of Basim, coagulated slurries were formulated by adding different concentrations of NaCl. Salts enhance dissolution of the silica surface [Hou92, Dov92] and increase electrostatic interactions at the pad-wafer interface by screening charge on the opposing surfaces [Mah99b, Bas02a]. For 0.2 M, the particle size was unchanged. However, the removal rate increased along with the maximum pitting depth. For 0.4 and 0.6 M solutions, irreversible coagulation ensued. The particle diameter increased in both cases along with an increase in root mean square roughness, and maximum pitting depth. Furthermore, the particle size before and after CMP was identical. Meaning, the particles remain coagulated during polishing, or re-coagulate after polishing in the post-CMP slurry.

To this point, the effect of particulate properties has been covered. The research reviewed, although beneficial, has not completely uncovered the oxide CMP mechanism. A precise description of how the abrasive particle interacts with the surface layer from the micro to the nano-scale is needed. In metal CMP, surface layer formation is easily quantifiable. The layer properties may even be tuned for the desired CMP application. In dielectric CMP, and oxide CMP in particular, it is extremely difficult to quantify the extent of surface modification that occurs in the CMP environment. Mechanistic investigations have instead focused on interfacial interactions. In-situ friction force measurements are the most widely used diagnostic tool for oxide CMP interfacial phenomena [Mah99a, Mah99b, Sik01, Hom03, Cho03, Cho04a, Cho04b, Cho04c].

From a micro and nano-scale viewpoint, the surface removal rate (RR) can be estimated by the following equation [Sin02]:

$$RR = K_c(\Delta x S_c P_c)V \qquad (2.7)$$

where K_c is a constant, Δx is the depth of indentation by a particle, S_c is the fraction of the pad surface covered by abrasive particles, P_c is the contact area of the pad on the surface (< 1% [Bas02a, Bas03]), and V is the linear velocity difference between the particle and the wafer. S_c is dependent on particle size, concentration, and the state of dispersion. P_c is a function of the applied pressure, relative velocity, and mechanical properties of the pad, including pad degradation. In-situ friction force measurements may be used to estimate S_c and P_c [Sin02].

Using a sapphire (Al_2O_3) substrate and silica abrasives Choi et al. attempted to measure the contact area as a function of particle size, down pressure, and particle concentration [Cho04b]. Sapphire, a hard, inert material, was used to determine the specifics of mechanical contact in the absence of surface roughness effects. The normalized fractional surface coverage (S_c) is a strong function of particle size. For smaller sized particles, the pad was almost completely covered with particles [Bas02, Cho03, Cho04b], which corresponds to a value for S_c near 1. S_c showed a weak dependence on concentration and no pressure or down load dependence. These measurements confirm Basim's assertion that oversized particles act as pillars at the pad-wafer interface [Bas00, Bas03]. By varying the particle size and particle concentration, Choi et al. confirmed early polishing results.

Friction force measurements showed analogous transitions from high to low friction (figure 2-7) [Cho03, Cho04c] as a function of particle size as the removal rate (figure 2-6). For 0.2 μm particles, the friction force steadily increased with particle concentration. However, larger sized particles 0.5 μm, 1.0 μm, and 1.5 μm showed a

transition from high to low friction as particle concentration increased. For larger particles, the transition occurred at lower particle concentrations. Increasing the particle concentration results in an increase in the number of abrasives available for polishing at the pad-wafer interface. For 0.2 μm particles, more efficient packing is achieved as evidenced by an increase in the fraction of the polishing pad covered by abrasive particles [Cho03, Cho04c]. As a result, pressure at the pad-wafer interface is more uniformly distributed. This assertion is confirmed by the reduction in the root mean square (RMS) surface roughness as a function of particle concentration after polishing. According to these results, 0.2 μm particles are completely embedded into the polishing pad and remove material by sliding on the wafer surface.

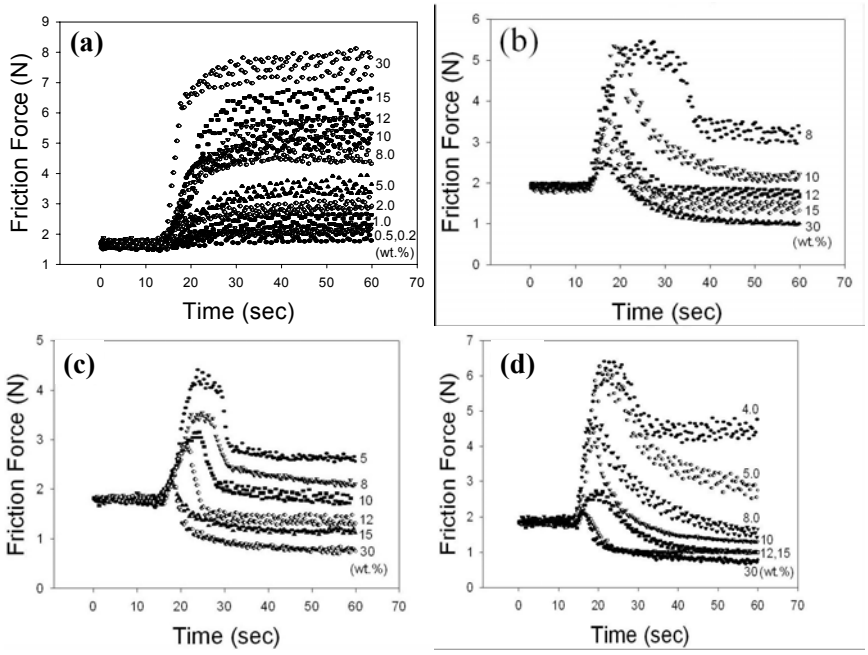

Figure 2-8 Dynamic particle motion as a function of silica particle size and concentration. As particle size increase, the sliding to rolling transition occurs at lower solids concentration. a) 0.2 μm - sliding motion, b) 0.5 μm sliding to rolling transition occurs at 8 wt%, c) 1.0 μm sliding to rolling transition occurs at 5 wt%, d) 1.5 μm sliding to rolling transition occurs at 4 wt% [Cho03, Cho04b].

In the particle size range (0.5-1.5 μm), the transition from high to low friction may be considered the boundary between predominantly sliding particle motion to

predominantly rolling motion [Cho04c]. Again the surface or contact area of the particles may be invoked to explain these phenomena. The decrease in surface area with increasing particle diameter results in less interaction area between particles and wafer. According to a CMP model proposed by Zhao and Shi [Zha99], the material removal mechanism is dependent on a threshold pressure (P_{th}). P_{th} marks the onset of sliding to rolling or vice versa. For $P < P_{th}$, material removal rates are expected to be negligible and polished surfaces will have a 'shot blast appearance'. Conversely, for $P > P_{th}$, the particles are embedded in the compliant CMP pad and surfaces with scratches are produced. Using in-situ friction force measurements, theoretical predictions of the existence of a threshold pressure were experimentally validated.

Introduction to Shallow Trench Isolation (STI)

The ability to produce surfaces with global planarity has resulted in the application of CMP in emerging technologies. Applications where the surface dominates device performance (i.e. optoelectronic devices, high k dielectrics, packaging, and flat panel displays) are candidates for CMP [Ste97]. Shallow trench isolation (STI) is critically dependent on the planarization capability of the CMP process.

The continued march down the International Technology Roadmap for Semiconductors (ITRS) has profound implications on materials selection, processing, and device architecture. Specifically, the demands for smaller geometry and higher circuit density require more effective isolation of active regions of complementary metal oxide semiconductor circuits [Lin99]. Traditionally, local oxidation of silicon (LOCOS) has been the method of choice for device isolation. In the LOCOS process, silicon nitride (Si_3N_4), a barrier to oxidation, is selectively deposited onto the sacrificial or pad oxide. The silicon substrate is then thermally oxidized in regions without Si_3N_4. After removal

of the Si_3N_4 by chemical etching, the thermal oxide provides electrical isolation by separating active regions of the device. LOCOS contributes to nonplanarity and reduces device packing density, which is unacceptable for device dimensions less than 0.5 μm [Ste97, Lin99, Sch99].

The STI process allows dense, more functional, high-speed devices to be fabricated at lower costs [Zha01]. Furthermore, the introduction of nonplanarity because of 'bird's beaks' associated with LOCOS is alleviated with STI (figure 2-9)**.** In the STI process, trenches are etched into the Si_3N_4 mask layer and the Si substrate. Chemical vapor deposition (CVD) or spin on glass (SOG) techniques are used to fill the trenches with SiO_2. CMP or a combination of RIE and CMP then remove the overlying oxide. The planarized trench-fill oxide isolates the device after removal of the Si_3N_4 mask. To reduce process complexity, single-step STI CMP processes are being developed [Zha01].

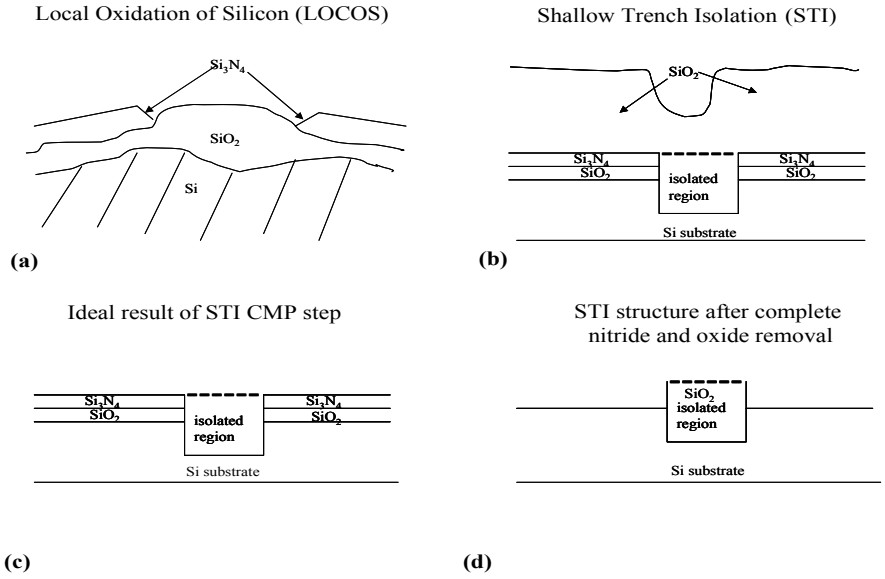

Figure 2-9 Schematic depiction of device isolation: a) LOCOS b) STI before CMP c) STI after CMP d) STI structure after nitride and oxide removal.

STI is not possible without CMP. An ideal STI CMP process stops at the nitride layer and requires uniform removal of the trench-fill oxide (figure 2-9c). Naturally, STI

CMP slurries must have high selectivity to oxide with respect to the nitride, and should leave the surface planar and defect-free. Over polishing of the nitride or erosion of the oxide causes damage to the active region and degrades isolation performance [Lin99]. Since STI CMP is a device level process, it must be more tightly controlled [Sch99]. Defectivity in the form of scratches, foreign contaminants, and particle residue should be suppressed. Traditional ILD consumables are not sufficient for the STI CMP process [Hos97, Sch99]. New slurry and pad chemistries with tunable properties are required to meet the stringent planarity, removal rate, and surface finish requirements of the STI process. For this application, ceria-based slurries outperform silica-based slurries. Ceria slurries preferentially remove the oxide layer with minimal polishing of the underlying nitride. To date, the ceria-silica polishing mechanism is unclear. Currently, the ceria CMP literature is applications oriented. In this study, ceria-silica polishing is studied to understand the fundamental interactions that lead to material removal. With this knowledge, the STI CMP process can be more effectively controlled.

Ceria-Silica CMP Mechanisms

The ceria based CMP literature is analogous to that of the silica based literature approximately 5 years ago. Rigorous fundamental investigations in the manner of silica-silica CMP experiments have not been conducted. Despite the relative immaturity of the ceria-silica CMP process, three competing mechanisms exist. The first two, ‘chemical tooth’ and a surface defect model, are based on results from glass polishing. The third, specifically for ceria-silica CMP, is more mechanical in nature. None of the models conclusively explain the particle-surface interactions during CMP that lead to surface removal.

Chemical Tooth

Why do ceria abrasives polish silica so much faster than silica-based slurries? This is the fundamental question in ceria-silica CMP. For STI applications, understanding the origins of preferential polishing of oxide to nitride surfaces is also important. The chemical tooth model is the most widely accepted explanation of the ceria-silica polishing mechanism. Much has been made of the enhanced chemical reactivity of ceria abrasives, hence the name chemical tooth. However, little experimental validation of this concept has been presented. According to the chemical tooth model, the material removal rate is controlled by the relative rates of [Coo90]:

1. water penetration into the surface layer
2. surface dissolution under particle load
3. adsorption of solute onto the abrasive particle surface
4. re-deposition of solute products onto surface
5. surface dissolution between particle impacts

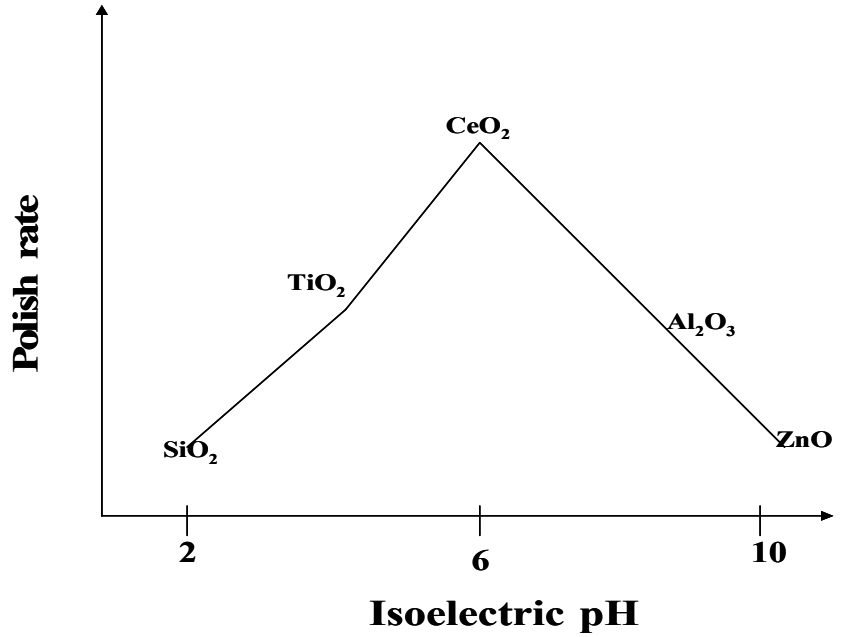

Figure 2-10 Glass polish rate versus IEP of common abrasive compounds [Coo90].

Ceria slurries, by far, are the most efficient in removing the glass or pure silica surface (figure 2-10). In fact, Cook estimated that one SiO_2 molecule is removed for every twenty-four collisions between the ceria abrasive and silica substrate, compared to five hundred million collisions for silica abrasives [Coo90]. Among the properties of abrasive particles (Gibbs free energy of formation, bond dissociation energy, metal–oxygen bond strength, aqueous solubility product, Z/R_{ionic}, Z/R_{eff}, pK^1, and isoelectric pH), only those related to surface charge, i.e. dissociation constant (pK), effective ionic field strength (Z–cationic charge/R_{eff}–separation distance between the cation and the adsorbed proton), and charge density, which is related to the coordination number correlated with polishing rates [Coo90]. Although a direct correlation was not found, the product of the log of the single oxide bond strength and the difference between IEP and slurry pH offers some predictive capability on polishing activity for prospective polishing compounds [Coo90].

The chemical tooth model depicts CMP as a molecular scale process in which material removal is achieved by displacing silica tetrahedra from the surface into the abrasive slurry. Net removal occurs if the solute products are bound by the abrasive or swept away by the turbulent motion of the flowing slurry. Otherwise, re-deposition may occur. Due to particle impact at the silica surface, water penetrates the silica network, equation 2.4 proceeds in the forward direction–creating solute species $Si(OH)_4$ (silicic acid), which is released into the solution, and hydroxylated surface species are created with one, two, or three remaining linkages to the silica network. This process is repeated as each abrasive particle traverses the pad-wafer interface. In the case of glass polishing and STI CMP, polishing is done near the isoelectric pH (point of zero charge) of ceria,

which is ~ 6-8. According to Cook, the extent of particle-surface bonding is controlled by a hydrolysis reaction of the form:

$$Si - O^- + Ce - OH \rightarrow Ce - O - Si + OH^- \qquad (2.8).$$

Silica, with an IEP ~ 2-3, remains negatively charged across the pH range. Because of its median IEP, ceria is amphoteric–able to adsorb positive and negative charges. As the particle moves away from the abrasive site, the Ce–O–Si bond, equation 2.8, is strained and finally ruptured. If the strength of the Ce–O > Si–O, silica accretion at the particle surface occurs and vice versa. This bond scission and release of surface species is expected to happen only when one Si–O bond remains of the tetrahedrally coordinated silica [Coo90]. The silicic acid molecule may re-bond to the glass surface, form a complex with active sites on the abrasive particle via hydroxyl exchange, or form colloids in the solution [Coo90, Oss02]. If particle-surface bonding indeed occurs, residual Ce–O bonding should be present on the silica surface, an important point reserved for further discussion. The chemical tooth model is based on interactions between surface functional groups at the particle and silica surface. Therefore, the nature of the abrasive-silica interactions should be strongly dependent on pH.

Osseo-Asare has examined the relationship between the silica removal rate and the IEP of the abrasive material [Oss02]. In this work, silica removal is achieved by surface complexation of the abrasive by silicic acid. Osseo-Asare stipulated that the slurry pH should be greater than the IEP of the silica surface and near the IEP of the abrasive particle. Furthermore, the IEP that demonstrates maximum silicate adsorption corresponds with the IEP for maximum polishing (ceria). The central feature of Osseo-Asare's theoretical formulation is the exchange of hydrogen and hydroxyl ions

(protonation and de-protonation) to form neutral hydroxyl groups at the abrasive surface. In the case of an abrasive particle with IEP < slurry pH (M-OH → $M\text{-}O^- + H^+$), there is a lower concentration of neutral sites. Conversely, when the abrasive particle IEP > slurry pH ($M\text{-}OH + H^+ \rightarrow M\text{-}OH_2^+$), there is also a lower concentration of neutral sites and the main reaction is the transfer of protons to the silica surface [Oss02]. Therefore, the most favorable conditions for maximum silicate removal by ceria particles occur at neutral pH, which is near the IEP of the ceria abrasives [Oss02].

Surface Defect

Nearly 50 years ago, a general model for glass polishing was proposed based on lattice defects (ionic vacancies) at the abrasive surface [Kal56a, Kal56b, Kal98]. Despite its longstanding presence in the literature, the defect-based glass polishing mechanism has been virtually disregarded in the literature [Kal98]. The central features of this theory are:

1. The abrasive should be softer than the surface to be polished
2. Minute bits of the abrasive are rubbed off during polishing
3. The abrasive hardness should exceed some minimum value to ensure that the particle is not pulverized during polishing.

According to Kaller, the abrasive particles are bound to the glass surface via a tribochemical reaction and movement of the polishing disk results in breakage of the solid bonds [Kal91]. Glass removal is expected to be a molecular-scale process. And similar to the chemical tooth theory, the removed glass bonds to the abrasive particles at high-energy defect sites [Kal91, Kal98]. At the time this theory was proposed, there was little opportunity for experimental validation because of the lack of sufficiently sensitive analytical techniques. Forty years later, Kaller presented milling and BET surface area

data as a function of time to prove the fractionization or creation of particle debris during the polishing process [Kal98]. In the surface-defect theory, intrinsic defects are considered to have a minimal effect on polishing. Defects or distortions may be created in a variety of ways: 1) reduction/oxidation reactions, i.e., Ce^{4+} to Ce^{3+}, incorporation of foreign metal ions or molecules (i.e., alloying of iron oxide with Ni^{2+}), 3) rapid quenching from high temperature during synthesis, and 4) freezing in of thermal vibrations after long dwell times at high temperature [Kal98]. These defects are expected to be responsible for the gripping or bonding of the abrasive particle to the surface. Furthermore, the defect density and hence the particle reactivity are expected to increase as the particle is abraded due to the exposure of freshly created, more reactive sites [Kal91, Kal98].

Particulate Generation

The first two ceria-silica mechanisms are general models for all metal oxide abrasive particles for glass polishing. The accelerated removal rates for ceria with respect to silica have been attributed to its median IEP [Cook90, Oss02] or multiple valence states [Kal91, Kal98]. The final model is based on more mechanical interactions and is proposed only for ceria-silica polishing as an alternative to the chemical tooth theory [Hos01]. In this model, silica particulates are cleaved from the surface during wear and bound by the abrasive particle. In support of this assertion, the particle size and composition of the post-CMP slurry was analyzed. Hoshino observed an increase in particle size from the original 80 nm to 600 nm lumps of a white paste-like substance. Inductively coupled plasma atomic emission spectroscopy, scanning electron microscopy, infrared spectroscopy, and x-ray microanalysis were conducted. According to their analysis, the large, irregularly shaped, white paste was SiO_2 cleaved from the surface. In

their opinion, if the chemical tooth mechanism was operative then silicic acid should be isolated in the post-CMP slurry. Since lumps of SiO_2 were present in the slurry they assumed they must have been directly cleaved from the surface.

The interpretation of Hoshino et al. is complicated by the presence of an organic surfactant, the slurry pH - pH 8, and the dynamics of colloidal silica stability in this pH regime. The presence of the surfactant likely complicates the analysis of the ceria-silica polishing mechanism, since surfactants have been demonstrated to change the characteristics of contact at the pad-particles-wafer interface [Bas02a, Sin02]. Also, at ~ pH 5 colloidal silica rapidly aggregates, with particle growth ensuing at ~ pH 7 [Ile79]. Recalling the formulation of Cook, in the post-CMP dispersion; the solute species, $Si(OH)_4$, is free to form a complex with the abrasive particle, which could change the shape of the original ceria particle or coalesce and form colloids, which may explain the growth of the silica particle.

To this point, three models with diverging mechanisms have been proposed. However, each has a central feature ceria-silica bonding that is believed to occur upon particle-wafer impact. Therefore, the surface chemistry of ceria should be considered in all proposed mechanisms for ceria-silica CMP.

Ceria Surface Chemistry

Cerium, atomic number 58, is one of the rare earth elements in the lanthanide series, which are characterized by the filling of 4f-orbitals [Sam73]. The chemistry of all lanthanides is similar. With the exception of cerium, the lanthanides have a valence of 3. However, cerium may also have a valence of 4, forming two oxides–Ce_2O_3 (cerrous oxide) and CeO_2 (ceric oxide). Ceria is an extremely efficient polisher of glass. A fact that has been ascribed to enhanced chemical reactivity between ceria and silica even in

the absence of chemical additives to the liquid portion of the slurry. Ceria has a fluorite crystal structure, with the oxygen atoms coordinated to four cerium atoms and the cerium atoms coordinated to eight oxygen atoms. The cerium atoms assume face-centered cubic (FCC) crystal symmetry with oxygen inserted into the eight tetrahedral spaces within the FCC unit cell (figure 2-11) [Eva04].

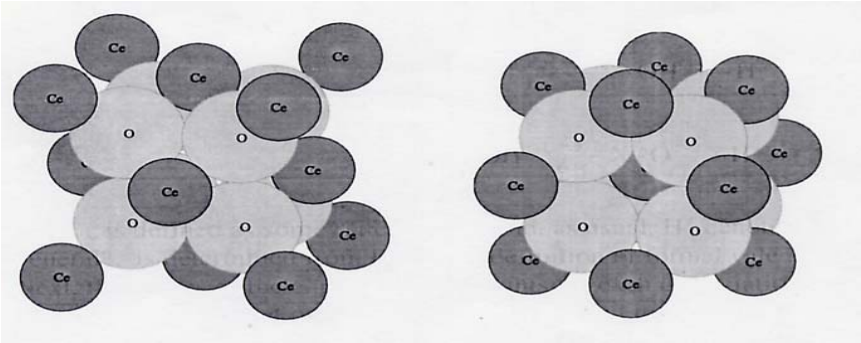

Figure 2-11 Ceria crystal structure normal view (left), displaced by one-half a lattice parameter (right) [Eva04].

The size of abrasive particles has continually decreased as more specialized CMP processes are introduced. Because of the high surface area of smaller particles, surface chemical effects are important for all CMP applications. This is especially true for such reactive abrasives as ceria. The transition to nanometer scale particles from the sub-micron regime has profound implications on the CMP process from slurry formulation, handling, and transport, to actual polishing, and finally post-CMP cleans. A thorough understanding of the abrasive surface chemistry allows tailoring of the surfaces for enhanced dispersion before use, reactivity and desired polishing during use, and efficient removal after use. Stable micron-sized dispersions may be obtained by simple manipulation of the pH. However, in the sub-micron to nanometer scales, dispersion agents like surfactants, polymers, or excess ions (electrolytes) are required [Nab93]. Nanosized particles, in particular, cannot be kept apart from each other through

electrostatic repulsions, because the interaction potentials are less than $15k_BT$ (Boltzmann's constant * temperature) [Nab93, Ver48], ~$8K_BT$ for ceria [Ver48]. Therefore, in water nano- particles will experience multiple collisions, which should result in aggregation due to particle-particle bonding [Nab93]. This is especially true for ceria, which demonstrates three states of stability based on the chemical treatment sequence [Nab93]. The loss of stability, i.e. agglomeration, has negative impacts on the particle's polishing capacity because of the reduction in surface area and loss of active sites.

Nabavi et al. have investigated the surface chemistry of ceria [Nab93]. Applying Pauling's definition of formal valence charge, the multi-site complexation or 'MUSIC' model was used to determine the acid-base behavior of surface hydroxyls [Nab93, Hie89]. In this treatment, atoms in an ionic crystal give each of its neighbors a number of electrons, v = Z/CN where z is the atomic number of the atom and CN equals the number of nearest neighbors. For n metals, a charge of Z = nv results. Its nearest neighbors in a bulk crystal compensate this charge. A hypothetical free surface may be created by splitting the crystal along a plane of oxygen atoms, creating dangling bonds. Surface passivation is achieved by adsorption of aqueous species (H^+, OH^-)–general protonation or de-protonation equilibria. Through such reactions an electric charge is acquired at the particle-liquid interface.

Additional complications arise when additional ions are present. This process is driven by the surface energy of the oxide in water. Ion adsorption may be hindered by steric repulsion or steric poisoning, which lowers the surface energy by binding of ions from the solution. In addition to chemical reactions at the surface, charge may be

acquired by isomorphous substition within the lattice (i.e., Si^{4+} replaced by Al^{3+}) and adsorption of a hydrophobic species or surfactant ions [Stu92]. Thus the electrical state of a surface depends on the spatial distribution of electronic or ionic charges in the near-surface region. Using the Gouy-Chapman model this concept is idealized as the electrical double layer. In this model, one layer is depicted as a region of fixed charge rigidly bound to the surface while the other layer is distributed more diffusively in the liquid in contact [Stu92]. The potential drop across the mobile portion of the double layer (figure 2-12)**,** zeta potential (ζ), is responsible for the electrokinetic phenomena, particle motion in the presence of an electric field, which may be related to dispersion stability.

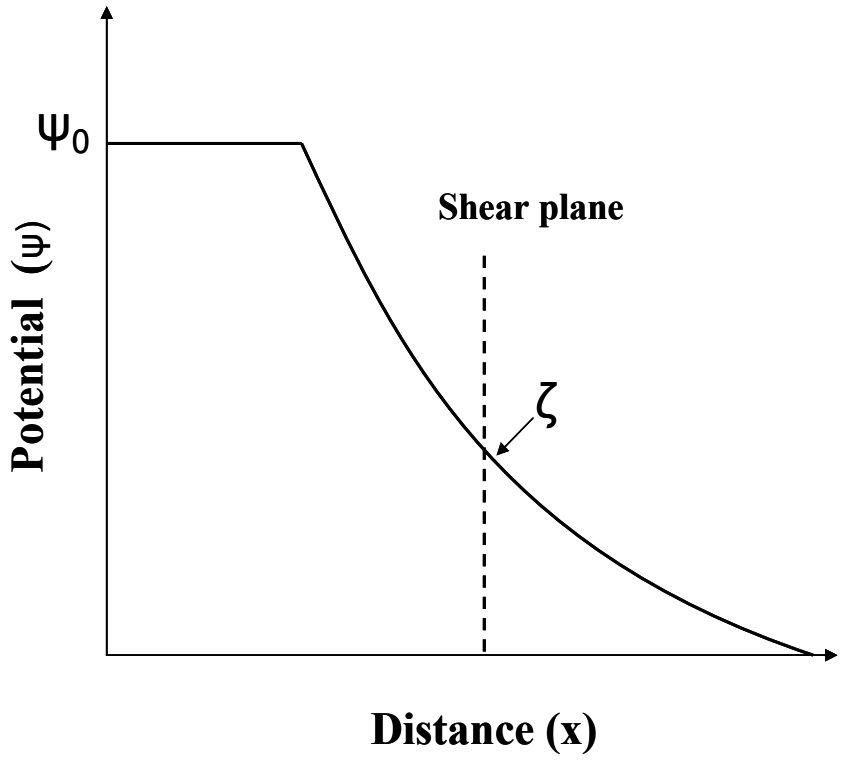

Figure 2-12 Potential versus distance for a charged surface [Stu73].

The surface chemistry of ceria and its effect on dispersion stability is particularly intriguing. In the work of Nabavi et al., nanosized ceria particles were obtained through precipitation of $Ce^{4+}(NO_3^-)_4$ salt of the form $CeO_2(HNO^3)_{0.5}(H_2O)_4$ at very low pH

[Nab93]. Simply raising the pH caused irreversible aggregation and transformation of the particle surfaces well below the predicted point of zero charge (pzc). Three dispersion states were obtained based on the affinity for proton (H^+) adsorption and also binding and release of nitrates present from the nitric acid based precursor solution. The acid-base equilibria at the ceria particle surfaces were investigated through titration of the surface groups with a base (NaOH) or acid ($HClO_4$). The pH was measured and he concentration of free nitrate ions (NO_3^-) at each step of the titration was also measured.

In Nabavi's work, the behavior of the dispersion was related to the difference in hydroxyl and proton consumption in dispersions of acidic and basic pH and the presence or lack of nitrates as counter-ions or covalently bound surface species [Nab93]. According to their results, titrating the dispersion above pH 5.0 results in a loss of active sites that is reflected in an excess amount of hydroxyl consumption with respect to proton consumption in the reverse cycle. The transition between different surface states occurred in narrow pH ranges, generating a hysteresis-type curve for pH versus volume of acid or base used (figure 2-13). The horizontal distance between the curves corresponds to an excess consumption of hydroxyl during the first part of cycle [Nab03]. According to their results, these phenomena may be explained as follows. The original dispersion contains a high concentration of nitrate ions as either counter-ions or strongly bound surface species. The counter-ions are released because charge is cancelled by a progressive release of protons and adsorption of hydroxyls. Covalently bound nitrates were released up to pH 6.0 in an exchange reaction of the form:

$$Ce\text{-}O\text{-}NO_2 + OH^- \rightarrow Ce\text{-}OH + NO_3^- \qquad (2.9).$$

Particle aggregation ensues, which results in a loss of surface. The remaining surface sites determine the electrical charge characteristics of the dispersion. This is reflected by a shift in the pzc from the theoretically predicted value of 7.9 to 10.0. Particle aggregation results in flocculation of the dispersion. The dispersion stability of nanoparticles ceria is thus related to the presence of strongly bound ionic surface species, which influences the ability to adsorb aqueous species from the liquid environment.

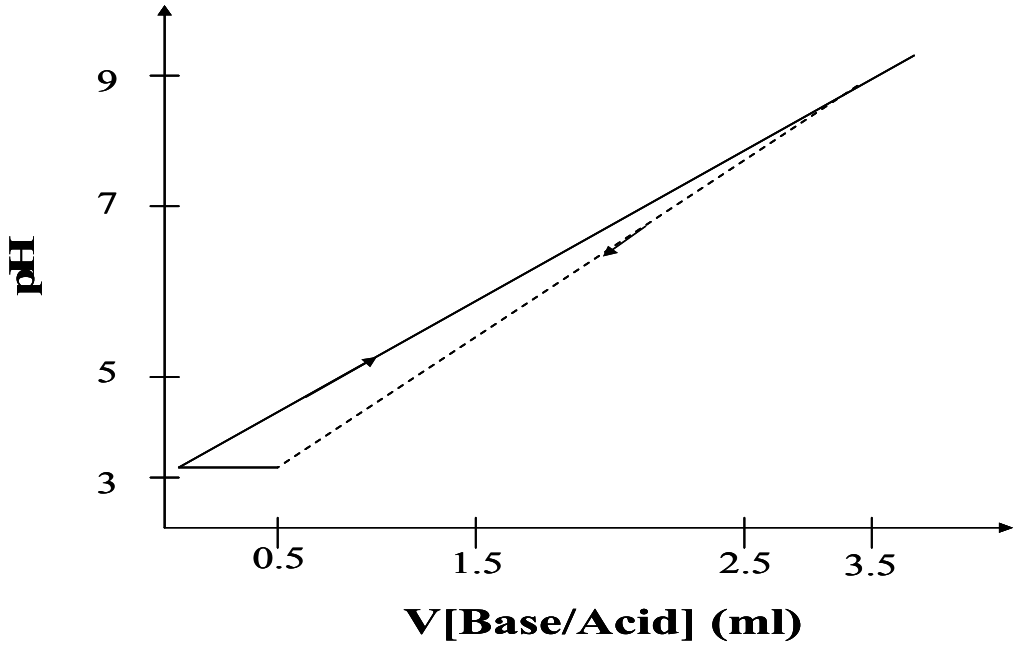

Figure 2-13 pH versus acid/base concentration. Horizontal distance between curves is related to excess consumption of OH- during acid to base cycle [Nab93].

These observations have wide-ranging implications for the various technological applications of ceria particles. For CMP in particular, irreversible changes in the particle dispersability, reactivity, and surface area should be reflected in the polishing behavior as a function of pH. Three major questions form the basis of this research.

4. Why does ceria polish so much faster than other abrasives especially silica?
5. Why does ceria preferentially polish oxides over other materials?

6. How can the polishing characteristics of ceria slurries be controlled for optimum STI polishing?

There are major gaps in the literature concerning ceria abrasives for silica CMP. As previously mentioned, too few studies have focused on the fundamental interactions between the ceria particle surface and the surface of the silica substrate. Most studies complicate mechanistic studies by including surfactants into the ceria-based slurries. However, recent publications indicate the focus is shifting towards more fundamental investigations. The surface structure of individual ceria particles has been studied by electron energy loss spectroscopy (EELS) [Gil04]. These measurements have confirmed the presence of Ce^{3+} at the surface of bulk CeO_2 particles. In this dissertation, ceria-silica interactions will be investigated, specifically surface interactions. To confirm the existence or absence of chemical reactions between the ceria particles and silica substrates extensive surface analysis has also been conducted. The major application of this research is in STI CMP. Therefore, general strategies for STI CMP are also proposed.

CHAPTER 3
MATERIALS AND METHODS

Introduction

This research involves polishing experiments using ceria-based slurries and a silica film. In-depth analysis of the effect of pH on ceria surface chemistry, silica removal rate, ceria-silica contact characteristics, ceria particle morphology, and silica surface morphology is discussed. The in-situ friction force is reported using a novel apparatus that was fitted to our tabletop polisher. Slurry stability, particle size, and zeta potential measurements are reported using a variety of light scattering instruments. Surface analysis using x-ray photoelectron spectroscopy, scanning electron microscopy, atomic force microscopy, and variable angle spectroscopic ellipsometry results are presented.

Samples

Silica Wafers

Silica (SiO_2) samples for all experiments had a nominal thickness of 2 μm. Plasma enhanced chemical vapor deposition (PECVD) was used to the deposit the oxide layers on 1 mm thick, p-type silicon substrates with (001) orientation. The silica wafers were obtained from Silicon Quest International.

Ceria Slurries

Ceria particles were obtained from Samsung/Corning. The slurries were dispersed in DI water at pH 4.5. KOH or HCL were used to adjust the pH to the desired value. The concentration of the particles in suspension was between 2 and 3wt%.

Ceria Thin Films

Ceria thin films were grown on Si substrates using pulsed laser deposition (PLD). The PLD ceria thin films were used to measure the force measurements with a 7.3 μm silica particle. The deposition was conducted at 700^0 C in 100 mtorr of O_2. A KrF laser of wavelength 248 nm was used. The laser energy was 500 mJ and the pulse rate was 5 Hz. During PLD, a pulsed laser strikes a solid target. Target materials are removed in the form of a plume. Substrates of choice may be coated by exposure to the plume, which is created by laser bombardment. The major advantages of PLD include; film stoichiometry close to that of the target, low contamination levels in deposited films, and high deposition rates.

Functionalized Cantilevers

Cantilever oxidation

Silicon tapping mode atomic force microscopy (AFM) cantilevers were functionalized by thermal oxidation at 1000^0 C for 2 hours in air. The cantilevers were furnace cooled. After oxidation, the cantilevers were used to abrade the ceria thin films at different pH values. The wear profile and cantilever composition was measured before and after the experiment with a scanning electron microscope.

Particle attachment

AFM cantilevers can be further functionalized by attaching a particle for force measurements. A micromanipulator fitted onto an optical microscope was used to attach a 7.3 μm silica to a silicon nitride contact mode AFM tip. The spring constant of the cantilever was 0.13.

CMP Equipment

CMP Tabletop Polishers

Polishing experiments were performed on a Struers® Rotopol 31 and TegraPol 35 tabletop polishers. The TegraPol 35 polisher allows control of platen velocity and pressure down to 2 psi. The ceria polishing slurry is delivered by a Struers® Multidoser unit that is connected to the polisher. The head and platen speed were 150 rpm and the center of the sample to be polished was placed at a distance of 8.9 cm from the center of the table. This setup leads to a linear velocity of 137.44cm/s. Perforated IC 1000/Suba IV (figure 3-1) stacked pads by Rodel Inc. and Rohm and Haas were used for all polishing tests. During polishing, the slurry is continuously stirred by a magnetic bar, and pumped to the pad-wafer interface at a flow rate of 100 mL/min by the Multidoser unit. The pad was conditioned before each polishing run with a grid-abrade diamond pad conditioner manufactured by TBW®. The diamond conditioner minimizes pad glazing (figure 3-1d) and ensures reproducible pad conditions for each polish run. The sample holder for the polishing experiments is a stainless steel cylinder 2.25 inches in diameter and 1.125 inches in height. The flat surface of the cylinder has a recessed, machined area of 1 $inch^2$ and 0.03 inches deep. The recessed area ensures the sample holder holds the wafer during polishing experiments. A porous carrier film supplied by Rodel slightly raises the wafer

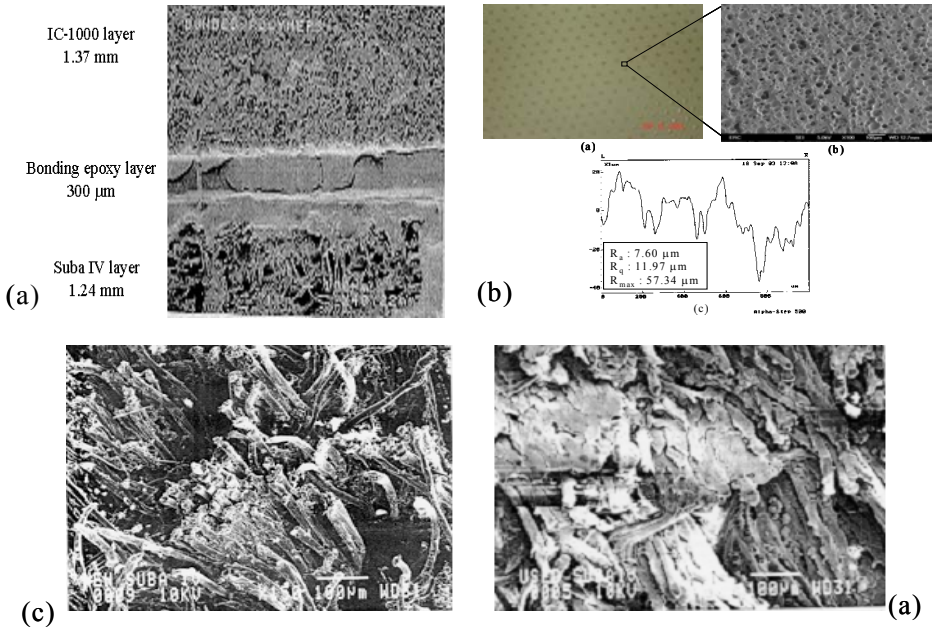

Figure 3-1 SEM analysis of CMP pad: a) cross-section of IC 1000/Suba IV stacked polishing pad (40 ×) [Obe98] b) Plane view image with profilometer scan showing pad roughness [Cho03] c) image of fresh pad [Ste97] d) image of used pad [Ste97].

over the recessed area. Additionally, when wet, the film ensures the wafer remains stationary during the experiment.

Friction Force Measurement Apparatus

The friction force studies were conducted using the tabletop Struers Rotopol 31 polisher. An apparatus, developed by us, was fitted to the polisher (figure 3-2). Glue was used to mount the silica samples (0.8 in^2) on a rectangular aluminum block. Circular washers were then loaded onto the block to achieve the desired down force. The entire assembly is then placed in a restraining fixture that ensures movement occurs only in one direction. During the experiments, the lateral force applied by the aluminum block on the restraining fixture is measured by a force transducer (Sensotec model 31 load cell). The load cell is connected to a data acquisition system. A data point was taken every 250 ms.

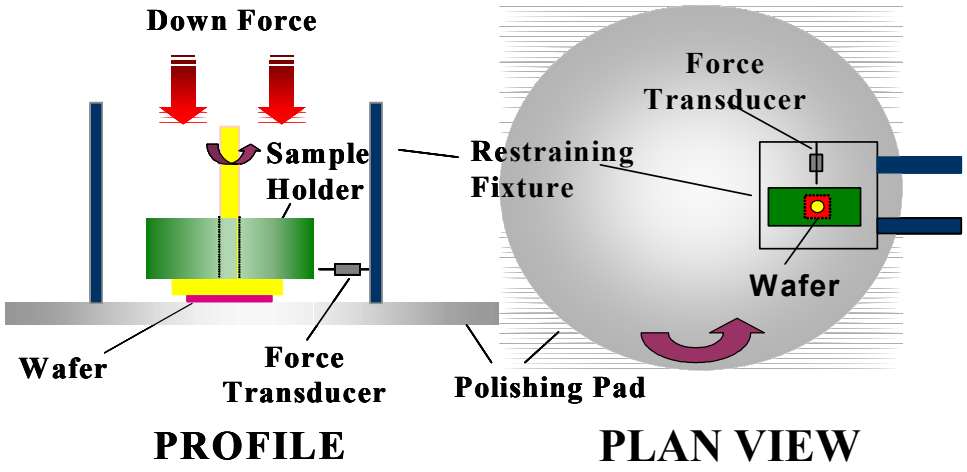

Figure 3-2 Schematic of in-situ friction force apparatus.

Particle Characterization

The particle size and surface charge are two properties that have a profound influence on the slurry stability and resultant polishing characteristics. Multiple light scattering techniques were used to measure the particle size and zeta potential, and to determine the stability of the ceria slurries.

Zeta Potential Measurement

Almost all solids acquire a surface charge in polar liquids like water. The various ways of charge accumulation have been covered in Chapter 2. The surface charge or surface charge density plays a crucial role in slurry stability. This is especially true for nano-sized particles. Because of dynamic motion and continuous particle-particle collisions, attractive forces are always present. These forces originate from the momentary, induced dipoles that arise when particles approach each other [Zeta]. London, van der Waals, and/or dispersion forces are common terms for these short-range attractive forces. To maintain slurry stability, electrostatic and/or steric repulsive forces

can be applied. Because of their surface charge, particles move with an average velocity (V) in an electric field (E), which is referred to as electrophoresis.

A Zeta potential analyzer manufactured by Brookhaven Instruments was used for zeta potential measurements as a function of ceria slurry pH. There is not an instrument that is capable of directly measuring the zeta potential. Instead, the velocity of the moving particles is measured. The electrophoretic mobility (μ_e) is then calculated as a function of velocity (V) and electric field (E).

$$\mu_e = V/E \qquad (3.1)$$

The particle, adsorbed ions, counter-ions, solvent molecules bound to ions on particle and/or counterions, and surfactants or polymers if any exist, may be considered a single unit. The velocity is measured experimentally as the charged particle is drawn to an oppositely charged electrode. The zeta potential is then calculated from the mobility.

The concept of surface charge density leads to a simplified model referred to as the electric double layer. In this approach, the particle surface is populated by counter-ions with opposite charge of the particle and co-ions that possess the same charge as that on the particle surface. Thermally driven collisions between particles and the solvent molecules cause continuous agitation of the adsorbed ions. This results in an electrostatic potential (Ψ) that decays exponentially for planes separated from the particle surface (figure 3-2).

$$\Psi = \Psi_o e^{-\kappa x} \qquad (3.2)$$

The electric double layer thickness (κ^{-1}), which is on the order of nanometers, determines the distance from the particle surface over which various electrical potentials are significant [Stu73]. This thickness is a function of temperature, fluid dielectric constant,

and the ionic strength or free ion concentration. For high ionic strength conditions, the electrical double layer is compressed and the particle-particle interactions are more attractive.

Thus the zeta potential is the potential between the bulk of the liquid and the surface of shear or shear plane that extends out from the surface of the particle. This potential is a direct measure of the repulsive force between two charged bodies. However, the zeta potential and mobility depends on the model chosen. For a particle of radius a, the Huckel limit is applied when $\kappa a << 1$. It is practically impossible to satisfy this limit for most particle systems. Therefore, the zeta potential analyzer utilizes the Smoluchowski limit for $\kappa a >> 1$, where zeta potential (ξ) is proportional to the product of the fluid viscosity (η) and the mobility divided by the dielectric constant (ε) of the fluid [Hun01].

$$\xi = \eta \mu e / \varepsilon \qquad (3.3)$$

Particles move in a direction perpendicular to the focused laser of wavelength 670 nm (red). The Doppler shift due to the scattering of the incident beam is determined and mobility and zeta potential are calculated as described above.

Particle Size Analysis

A Microtrac UPA 150 particle size analyzer manufactured by Honeywell was used to determine the average particle diameter as a function of pH. Particles were sonicated in solutions of pH 2.5-10.5. The background solution used in the particle size analyzer was of the same pH as the ceria slurry. This instrument also utilizes dynamic light scattering for measurement purposes. Again, the velocity and particle motion direction are randomized by collisions with solvent molecules. The velocity distribution of a large number of mono-sized particles will approach a well known functional form. After

compensating for thermal and viscosity effects, the velocity distribution becomes a unique function of the particle diameter.

The scattered light by moving particles is proportional to the particle velocity. A dispersion of particles will have a unique distribution of frequency shifts. Spectra from small particles have more high frequency components than spectra from large particles. Care must be taken to minimize thermal and fluid viscosity contributions. Both increased temperatures and decreased fluid viscosities will increase the high frequency components of the spectrum causing an underestimation of the particle size. The particle distribution is computed directly from the measured frequency spectrum obtained from the Doppler shifted scattered light.

Slurry Stability

Slurry stability is an anomalous property. CMP slurries must not only be stable at the point of use, but also must maintain stability during shipping and while on the shelf. In this work, a Hach model 2100AN laboratory turbidimeter is used to determine the stability of the slurries at different pH values. This instrument measures turbidity from 0-10,000 Nephelometric Turbidity Units (NTU). A tungsten filament lamp is used to provide the incident beam. Lenses and apertures focus the light. Four detectors are used: 90 degree, forward-scatter, transmitted, and back-scattered light detectors. In the Ratio On mode, mathematical calculations are used to average signals from each detector for improved linearity, calibration stability, and wider measuring range, and to perform measurements of colored solutions.

A nephelometer is an instrument that measures the amount of cloudiness in a dispersion. The intensity of scattered light changes as the particles settle out of solution.

High NTU values correspond to dispersed or cloudy solutions. Measurements with this instrument are presented as normalized NTU.

Characterization of Silica Surface Morphology

Atomic Force Microscopy (AFM)

Roughness is a surface property that affects device performance. Even well polished surfaces have topographical variations that can be considered surface roughness. Atomic force microscopy (AFM), a hybrid of scanning force microscopy allows imaging of surface topographical variations with sub-nanometer resolution [Ste92]. In this study, the topography after CMP was compared to as received samples using AFM. AFM, although time consuming, is a robust technique that allows characterization of insulating and conducting surfaces in liquids or in air.

AFM uses a sharp tip mounted on a flexible cantilever. Repulsive van der Waals forces between atoms on the tip and substrate cause deflection of the cantilever. The force between the tip and sample are a function of the separation distance. Therefore, surface topography is obtained by monitoring the cantilever deflection. Raster scanning during AFM is controlled by a piezoelectric tube, which maintains a constant separation between the tip and sample. Cantilever deflection due to surface topography is measured using light from a laser diode that reflects from the back of the cantilever to a position-sensitive photodiode (figure 3-3). The AFM image is generated by monitoring the position of the scanner.

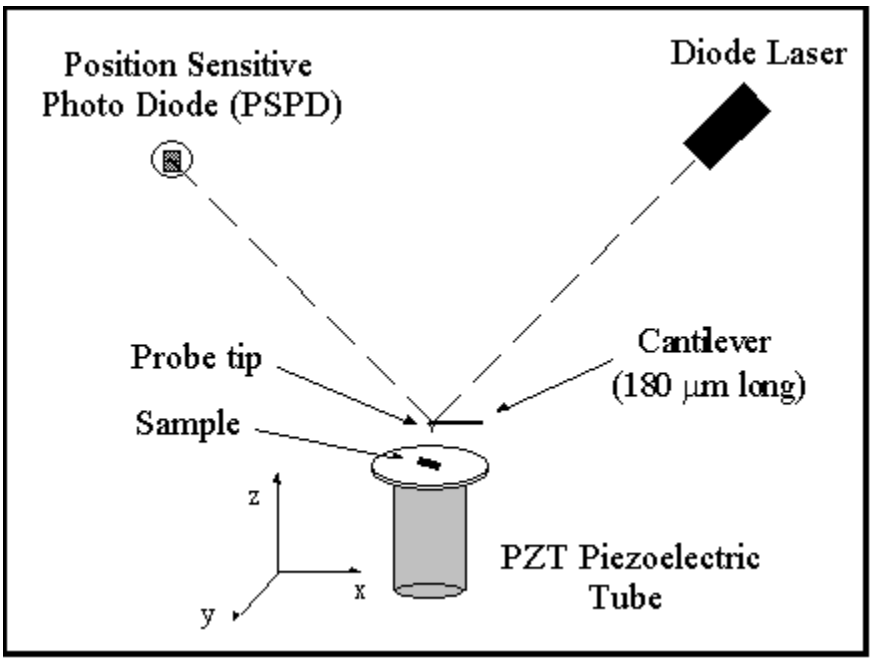

Figure 3-3 Schematic diagram of AFM apparatus.

In this study, a Digital Instruments Nanoscope III AFM apparatus was used. The measurements were conducted in contact mode. Contact mode tips have four Si_3N_4 cantilevers with spring constants that vary from 0.06 to 0.58 N/m. For topographical imaging, 10 μm scan sizes were used to quantify the extent of scratching and surface damage after CMP. The software bundled with the AFM calculates Root Mean Square (RMS), average (R_a), and peak-to-valley (R_{pv}) roughness values. The RMS roughness is used in this study.

$$RMS = (\sum(Y_i^2/N))^{1/2} \qquad (3.4)$$

$$R_a = \sum Y_i/N \qquad (3.5)$$

$$R_{pv} = R_{max} - R_{min} \qquad (3.6)$$

In all three equations, Y is the height value and N corresponds to the total number of measurements. For all scans, a plane fit and flatten data filter were applied to the AFM

images using the AFM software. With these filters, scanning artifacts can be removed and the image quality is improved for display purposes.

Force measurements are also possible using the AFM. They may be conducted with the standard AFM tip or with cantilevers that have been functionalized by attaching a micron-sized particle. In this study, a 7.3 μm diameter silica particle was used to measure the interaction force as a function of separation distance at various pH values using a ceria thin film. Further functionalization is possible using specialty coatings. To further study the ceria-silica mechanisms in the absence of particles, chemical vapor deposition was used to coat silicon tapping mode cantilevers with a 100 nm thick silica layer. Tip wear against a ceria surface was compared at different pH values.

Scanning Electron Microscopy

Scanning electron microscopy (SEM) provides a highly magnified image of the surface of a material that is similar to what one would expect if one could actually see the surface. SEM provides both topographical and elemental composition. Resolution down to a few nanometers is possible with magnification of ~300,000X.

During SEM analysis, electrons are flooded onto the specimen surface with a variety of output signals. Electrons with energies of ~ 50 eV are called secondary electrons [Bin92]. Secondary electrons result from inelastic scattering between the primary electron beam and atomic electrons of the specimen [Bin92]. The surface sensitivity of SEM is due to the shallow escape depth of secondary electrons. Inelastic scattering in the specimen bulk results in electrons with insufficient energy to escape from depths greater than a few nanometers. Backscattered electrons, including characteristic Auger electrons, have energies in excess of 50 eV [Bin92]. Backscattered electrons result from elastic scattering of the primary electron beam. A further utility of

the backscattered electron signal is composition mapping. The backscattered electron intensity increases with atomic number, yielding brighter images [Bin92]. Characteristic x-rays are also emitted as an excited atom decays to its ground state. The x-ray emission single can be sorted by energy or wavelength in an energy dispersive or wavelength dispersive x-ray detector. The distribution of energies or wavelengths is characteristic of the elements that produce them.

There are three types of emission capable of producing beams for SEM analysis: thermionic, LaB_6, and field emission. Field emission provides the brightest emitted beam with the sharpest electron energies, which limits chromatic aberrations of magnetic defocusing lens [Bin92]. Field emission SEMs offer enhanced resolution at lower applied voltages. In this study, a SEM equipped with a field emission gun (JEOL JSM 6335F) will be utilized along with the energy dispersive x-ray detector (EDX) for compositional analysis of the polished surfaces.

SEM analysis can be limited by the sample properties. To minimize charging, insulating samples must be imaged at voltages below 2 keV or a thin (< 10 nm) conductive coating must be applied. Also, the specimen should be stable at high vacuum and be of appropriate size for the sample holder.

X-ray Photoelectron Spectroscopy

X-ray photoelectron spectroscopy (XPS)is based on the photoelectric effect explained by Einstein in 1905 [Bru92]. High-energy x-rays ionize an atom producing free photoelectrons.

$$KE = h\upsilon - BE \qquad (3.7)$$

Since the energy of the incoming photons is known, by measuring the kinetic energy (KE) of the ejected electron, the binding energy (BE) of the electron to the

particular atom can be determined. The binding energy of the electron is sensitive to the chemical state of the atom. Therefore, XPS is a powerful surface analysis tool that provides semi-quantitative elemental composition information. Since XPS peaks are due to the ionization of core level electrons, they can be used to detect all elements except hydrogen and helium. Liquids, gases, and solids can be analyzed. Generally, XPS spectra give information from the topmost atomic layers (2-20) [Bru92].

The number of peaks in an XPS spectrum corresponds to the number of occupied energy levels in the ionized atoms whose binding energy is lower than the energy ($h\upsilon$) of the incident radiation. The peak position determines the respective binding energies of the electrons in subatomic orbitals and provides a means of identifying atoms present in the specimen. Additional features in the spectrum are due to the involvement of passive electrons (non-photoelectrons) [Bru92].

Unlike valence electrons, core level electrons do not participate in chemical bonding. Therefore, the elemental binding energies have characteristic values that provide unique signatures of elements. Quantitative analysis (at%) of the relative amounts of elements present is possible by comparing the relative peak intensities. This requires knowledge of the photoionization cross section for each element and control of experimental artifacts that affect peak intensities [Bru92]. XPS provides only semi-quantitative elemental composition information because of: variations in peak widths and peak line shapes, incorrect background subtraction, and instrumental artifacts. Coupled, these factors introduce an uncertainty in the measurement that may be as high as 30%. However, for well characterized XPS peaks with well known standards the uncertainty may be reduced to only a few at. %.

In addition to quantitative analysis, the chemical environment of the ejected photoelectrons may be determined as well. Slight shifts in the binding energy of XPS peaks may be related to the respective chemical environment. In general, differences in the binding energy are seldom more than a few electron volts. Other features of the XPS spectrum may also be utilized to identify elements in the specimen. Shake-up satellites are created because valence electrons may be excited to empty orbital levels during relaxation. This results in photoelectrons of diminished energy, hence, a shift to higher binding energy. Since valence electrons participate in chemical bonding, additional chemical state information is obtained. Auger electrons are also generated when an electron from a higher energy level fills the core hole left by the ejected photoelectron. By changing the radiation source, overlapping XPS and Auger peaks may be resolved.

The primary use of XPS is for surface analysis. Electrons travel short distances before losing energy in collisions with atoms of the specimen. Therefore, only near surface photoelectrons contribute to XPS peaks. The background in a XPS spectrum may be attributed to electrons from the bulk that have lost energy due to inelastic collisions. Additional surface sensitivity is possible by utilizing a grazing incidence angle, which further minimizes the escape depth of elastically scattered electrons. The XPS system used in these experiments is a Perkin-Elmer PHI 5100 manufactured by Physical Electronics.

Spectroscopic Ellipsometry (VASE)

Spectroscopic ellipsometry is a surface sensitive thin-film measurement technique that measures changes in the polarization state of light after reflection or transmission from a surface of interest. Large amounts of data may be obtained using probe beams of various wavelengths and angles of incidence. A broad range of sample materials and

structures are suitable for this technique. As with all optical techniques the property of interest (in this case film thickness) is not measured directly.

Ellipsometers measure the change in the polarization state (Ψ and Δ) of the light reflected from the specimen surface. The parameters may be related to the Fresnel reflection coefficients (R_p, R_s).

$$\rho = R_p/R_s = \tan(\Psi)\, e^{i\Delta} \qquad (3.8)$$

Ellipsometry is a very precise and reproducible technique since it measures the ratio of two values. The sensitivity of the measurement is enhanced by the complex component of equation 3.6 that gives phase information.

Initially, the ellipsometer measures the reflected or transmitted intensity or the polarization state of the reflected light. A model is developed based on the probe wavelength, polarization state, angle of incidence, thickness, and optical constants. Next, the model is fitted to the experimental data by varying physical parameters and calculating data that closely matches the measured optical data. The ellipsometer in our lab, manufactured by J. A. Woollam Co. Inc., uses the Levenberg-Marquardt multivariate regression algorithm. Finally, the best-fit model should be evaluated to ensure the fit is unique and is physically reasonable. This is achieved by monitoring the MSE value. For a unique, reasonable fit the MSE value tends towards some unique minimum value that approaches zero.

Although ellipsometry is a robust technique that requires very little sample preparation, measurements should be made with caution. The roughness of the measured spot of the specimen should be less than 10% of the beam's wavelength. Also, the thickness of the film should vary no more than 10% over the width of the beam spot. The

presence of adsorbed contamination layers may slightly affect the measurement. Angstrom level measurements should also be made with care since the optical constants of thin films rarely are identical to bulk values.

CHAPTER 4
THE EFFECT OF PRESSURE, PH, AND VELOCITY ON THE SILICA REMOVAL RATE AND SURFACE FINISH: A STATISTICAL DESIGN OF EXPERIMENTS

Introduction

Chemical Mechanical Polishing (CMP) began as a proprietary process at IBM [Bey00]. Initially used for planarization of silicon, the CMP process has been successfully applied to all steps in integrated circuit manufacturing. In fact, CMP is an enabling technology for multilevel, interconnected structures that have allowed the continued shrinkage of microelectronic devices [Ste97]. Because of its ability to produce globally planar surfaces, CMP is being implemented in a number of emerging technologies. Although CMP is simple to perform, designing an optimum process for a new set of materials is not a trivial task. Often, conventional CMP consumables (pads, slurries, equipment) are not applicable to the new application. Furthermore, the use of CMP in new applications is complicated by the lack of fundamental understanding of general CMP processes that have been in use for well over a decade. Hence, conventional CMP processes can not be strictly relied upon when developing strategies for novel CMP applications.

Lacking a defined starting point for new CMP applications, fundamental investigations of the nature of those reviewed in Chapter 2 for silica-silica CMP are often necessary to develop an efficient, reliable CMP process. Singh et al have identified over forty variables micro- and nano-scale effects, and output parameters that control the CMP process [Sin02]. Common CMP experiments investigate the effects of only a few

variables at a time by varying one parameter while all others remain fixed. After an optimum response is received at one level, another parameter is varied and so on until the desired polish rate, surface finish, planarity, and/or selectivity are achieved. A thorough investigation of the influence of each variable and its effect on the respective output parameters is impossible using the one variable at a time experimental approach. Statistically designed experiments are an attractive alternative to testing one variable at a time.

Statistical methods are crucial tools for industrial CMP practitioners [Par04]. The competitiveness of the microelectronics fabrication industry requires that resources be used efficiently, that processes are reproducible with minimal lot-to-lot variation, and that manufacturing delays be minimized to ensure maximum profit. Statistically designed experiments based on sound scientific and engineering principles allow companies like chip manufacturers to continually increase production at lower costs, resulting in higher profits. In laboratory testing, statistical methods are usually applied only in data analysis (i.e. measurement average and standard deviation from measurement average). CMP research, with its many variables and inter-related interactions, is a prime area for implementation of statistically designed experiments.

The basic principle of statistically designed experiments is that all measurements are subject to variation [Mas89]. Variations in measurements may be because of experimenter bias, changes in the experimental ambient, or measurement error. Failure to minimize error can often result in the wrong interpretation of data. For example, if an output parameter has a large variation about the measurement mean it is not clear that the observations are significant, which results in the obscuring of the true effects of the

variables in question. Statistical experimental designs are effective in eliminating bias, ensuring the measured output is gained from the experiment, and conservation of resources. Each observation generally provides information on all the factors of interest in the experiment. Conventional laboratory procedures limit the number of variables that may be studied. Also, since only one variable is changed at a time, the evaluation of the effect of interactions among experimental variables is not possible. Statistical designs allow for the estimation of the magnitude of uncontrollable variation, and modeling of relationships between measurements of interest and variables believed to influence these measurements [Mas89].

Selecting a Statistical Design

Mason, Gunst, and Hess identified five statistical design criteria: 1) consideration of objectives, 2) factor effects [Appendix A], 3) precision, 4) efficiency and 5) randomization [Mas89]. While formulating the objectives of the experiment the nature of the anticipated conclusions, the manner in which concepts are defined, and the manner in which observations are measured and reported should be considered. For factor effects, systematic errors should be eliminated, covariates should be measured [Appendix A], variable relationships should be identified, and the entire experimental range should be explored to ensure a meaningful experimental design is produced. Precise experiments include an estimation of inherent uncertainty associated with the experiment, replication of experimental runs, adjustment for covariates, and blocking [Appendix A]. Precise experimental designs also ensure that the detail of the response and its relationship to the factors is clear. Efficient experiments are characterized by the examination of multiple factors with screening designs. Finally, the experiments should be randomized.

Randomization protects against unknown sources of bias like instrumental drift and helps validate assumptions required to apply certain statistical techniques [Mas89].

Statistically based experimentation is widely practiced in various fields. Basim et al investigated the effect of particle size, applied load, and particle concentration on the silica-silica CMP removal rate and surface finish using a central composite design with three factors at five levels [Bas03b]. Park used three designs: a nested design, a completely randomized block design, and a factorial design to analyze gate polysilicon critical dimensions for integrated circuit devices [Par03]. Martin et al used a fractional factorial design to optimize cryo-preservation conditions for rat liver slices and to evaluate the day-to-day variation in the levels of cryo-preservation [Mar03]. Tye has reviewed the applications of statistical design of experiments in drug discovery [Tye04]. Finally, Zaman et al. used the Box-Behnken method to investigate the solubility of metal ions dissolved from kaolin in the presence of different anionic dispersing agents [Zam03].

Role of Pressure, Velocity, and pH in Silica CMP

Contact mechanics, wherein the polishing process is believed to occur because of wear due to direct wafer-particle contact, are most commonly utilized to explain the CMP process. In fact, most mathematical CMP models are based on an empirical relationship (equation 4.1) initially proposed for glass polishing [Pre27]:

$$RR = K_p PV \qquad (4.1)$$

where RR is the material removal rate, P is the applied pressure, V is the relative velocity between the wafer and the pad, and Kp is a process dependent constant [Coo90, Bas02a, Qin04]. Hence, the pressure and velocity are the most studied variables in CMP experiments. As the applied pressure is increased, the contact area at the pad-wafer

interface increases. The increase in pad-wafer contact results in an increase in the number of abrasives available for polishing. Particles not embedded in the polishing pad have a negligible effect on the material removal rate [Zha99]. According to Basim, a decrease in particle size or an increase in solids loading results in a significant increase in the removal rate while an increase in the applied pressure does not significantly impact the removal rate [Bas02a]. Due to the viscoelastic response of the polishing pad to applied loads, the actual contact pressure at the particle-wafer interface is not changed significantly. Improvements in surface quality were predicted for smaller particles, lower solids loadings, and lower applied pressures.

The removal rate and surface finish are also affected by the relative velocity between the pad and wafer. The pad-wafer contact area is influenced by the rotational velocity. Using in-situ friction force measurements, Choi investigated the effect of velocity on the pad-wafer contact area [Cho03]. According to his results, at low solids loading (< 5 wt%) the pad-particle contact area is greater than the particle-wafer contact area, which results in a decrease in friction force with increasing velocity. However, the increase of friction force with platen velocity when the solids loading exceeded 5 wt% was attributed to increased shear as the number of particles at the pad-wafer interface increased. Choi's analysis did not consider the mechanical properties of the pad in his analysis.

Generally, CMP pads are made of polyurethane or polyurethane impregnated felts [Ste97]. Therefore, the response to an applied load is time-dependent. For maximum pad-wafer contact ~1% of the pad asperities are actually in contact with the wafer [Bas03]. As the velocity is increased, the pad response time may affect the pad-wafer contact area.

This may be noticeable in particle-free and low solids loading conditions. There may not be sufficient pad asperities in contact with the wafer to ensure sufficient abrasives are available for polishing. However, as the number of particles at the pad-wafer interface increases, the viscoelasticity of the pad may have less of an effect on the pad-wafer contact area since sufficient particles may be present.

The pH also has an effect on the silica removal rate and surface finish. However, in the pH regime of this study (2-6), the pH effects on the silica surface properties should be negligible. As reviewed in Chapter 2, the pH has a significant effect on the ceria surface chemistry, which controls the stability and reactivity of the abrasive particle. Above pH 6, rapid agglomeration ensues, which results in a reduction in the total ceria surface area. This results in a decrease in the density of reactive sites on the ceria particle surface, which lowers the chemical reactivity of the abrasive particles. Generally, shallow trench isolation (STI) CMP is conducted below pH 7. Therefore, this study is restricted to the pH regime in which the ceria slurry should be stable.

Experimental

My Design Expert software version 6.0.5 was used for statistical modeling of the effect of pressure, pH, and velocity on the removal rate and surface finish during CMP of silica with ceria abrasives. To formulate an effective statistical design, the general outcome should be known. Therefore, an initial study of the effect of pH was conducted at a fixed pressure and velocity. The Box Behnken method was used for this three factor design (pressure, velocity, and pH). Box Behnken designs are alternatives to 3^k factorials (figure 4-1c, which are a combination of the central composite (figure 4-1a)and Box Behnken designs (figure 4-1b) [Mas89]. Box Behnken designs for 3 factors are efficient, rotatable [Appendix A], and require fewer runs than central composite or fractional

factorial designs. For three factors, only fifteen experiments are required by the Box Behnken method compared to 17 for central composite designs and 27 for a 3^3 factorial design [Mas89]. In the Box Behnken design, all points may be envisioned as occupying a sphere. Extreme edges of the cube created by two level factorial designs are not considered [Box78]. The experimental design for this study, which uses the Box Behnken method is shown in Appendix B.

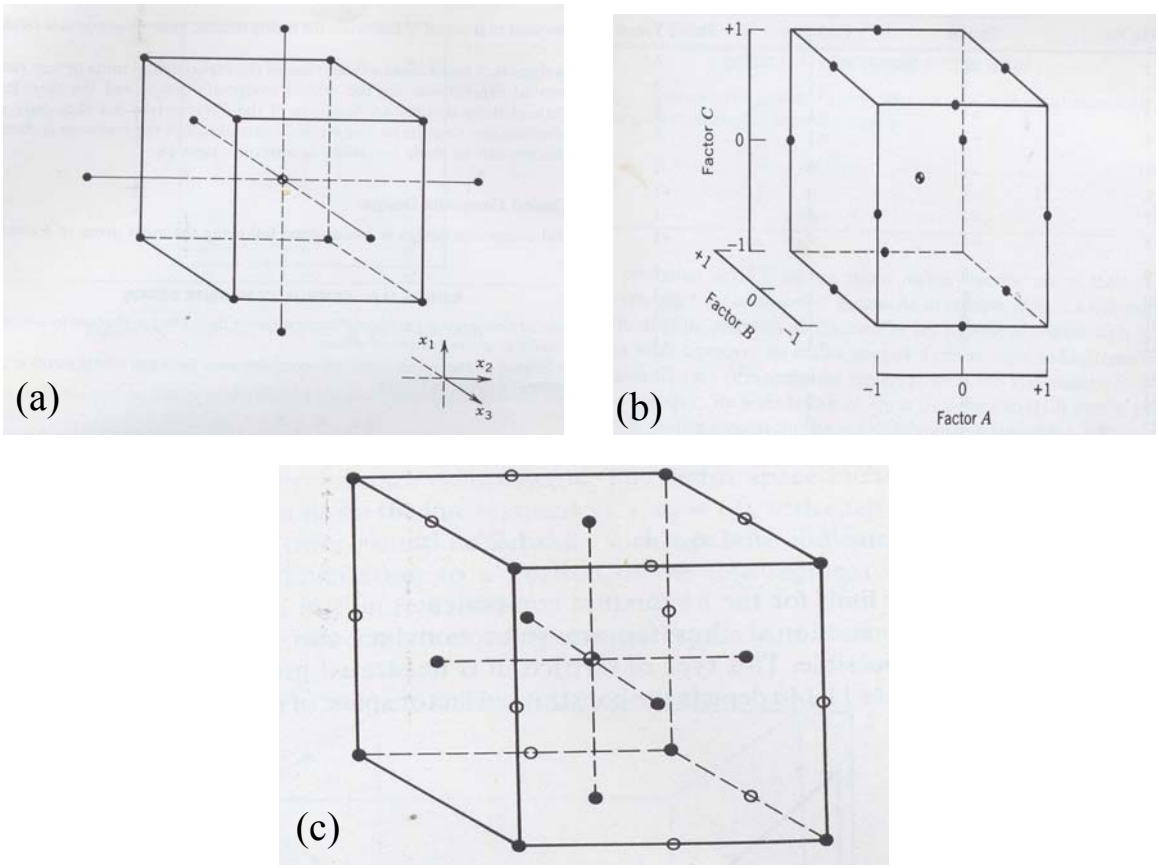

Figure 4-1 Factor space for different statistical designs: a) central composite b) Box-Behnken c) fractional factorial [Mas89].

Results and Discussion

Removal Rate Response

Scientific problems are usually expressed as relations of one or more variables (i.e. material removal rate = f(pressure, pH, velocity)). Using statistical design methodology,

this is accomplished by an empirically derived response function (Appendix A). `Generally, knowledge of the form of the response function (f) is obtained by fitting models to data obtained from the statistical design. Response functions are important for multiple reasons [Mas89]:

1. The function is characterized in the region of interest to the experimenter.
2. They are used to model the relationship between factors and observations.
3. Gives concise summary of experiment.
4. Statistical inferences can be made on the sensitivity of responses to factors of interest.
5. Factor levels can be determined for which response variable is optimum.
6. Factor levels can be determined that simultaneously optimize several responses.

Contour plots are a popular graphical representation of a response surface that can be fitted to a statistical design. For simple response functions, contour plots are generated by plotting one factor versus the other (two level experiment) and fixing the response. When the response function is more complex, matrices of the response variables are calculated and the numerical values of the response are plotted as a function of the factors. The optimum response can then be located by fixing the experimental variables to the desired values.

Figures 4-2 (a-c) shows the contour plots for pH versus pressure at 75, 112.5, and 150 RPM, respectively. At 75 RPM figure 4-2a, the region that predicts the highest removal rate is at ~ 6 psi and pH values less than 3. The silica removal rate should be in the range of 200-800 nm/min. This criterion is only met for low pH values and applied pressures in

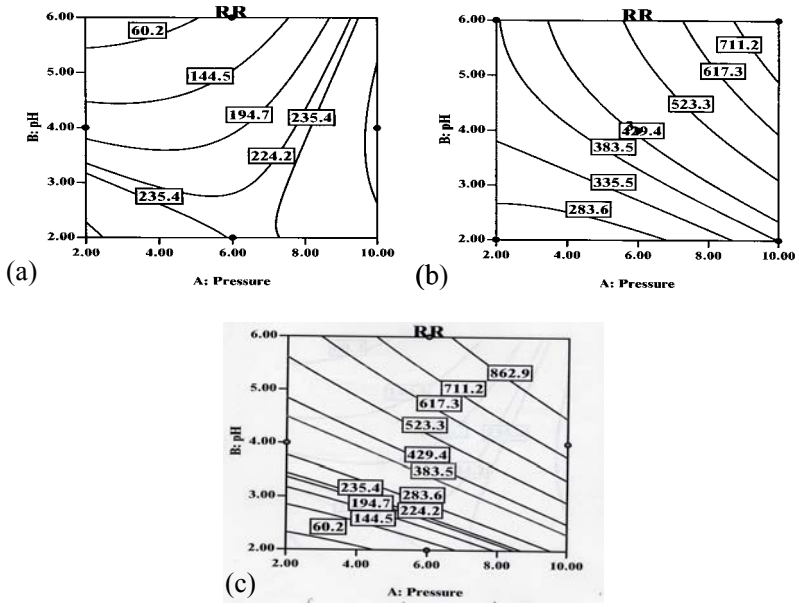

Figure 4-2 Predictions of removal rate as a function of pressure and pH at: a) 75 RPM b) 112.5 RPM c) 150 RPM.

low to mid-pressure regimes < 6 psi at 75 RPM. At 112.5 RPM, the contour plot for pH versus pressure changes, figure 4-2b. The removal rate is predicted to increase uniformly as the pH and pressure increases. In contrast to the 75 RPM case, at 112.5 RPM the minimum removal rate criteria is achievable at all values of pressure and pH. Figure 4-2c (150 RPM) shows a similar trend to that predicted in Figure 4-2b. However, pH values in excess of 3 are required to achieve the minimum removal rate criterion. If we compare figures 4-2a-c, the optimum region for removal rate as function of pressure and pH is clear only in figure 4-2a. However, in figures 4-2b and 4-2c, the removal rate increases in the same direction (increasing pH and pressure). The lack of a contour with a maximum response indicates the optimum removal rate is outside of the experimental region of figures 4-2b and 4-2c for the respective experimental designs.

Figures 4-3 (a-c) are the interaction profiles for the variables under investigation. Pressure increases at pH 6.0 have a more pronounced effect on the removal rate than at

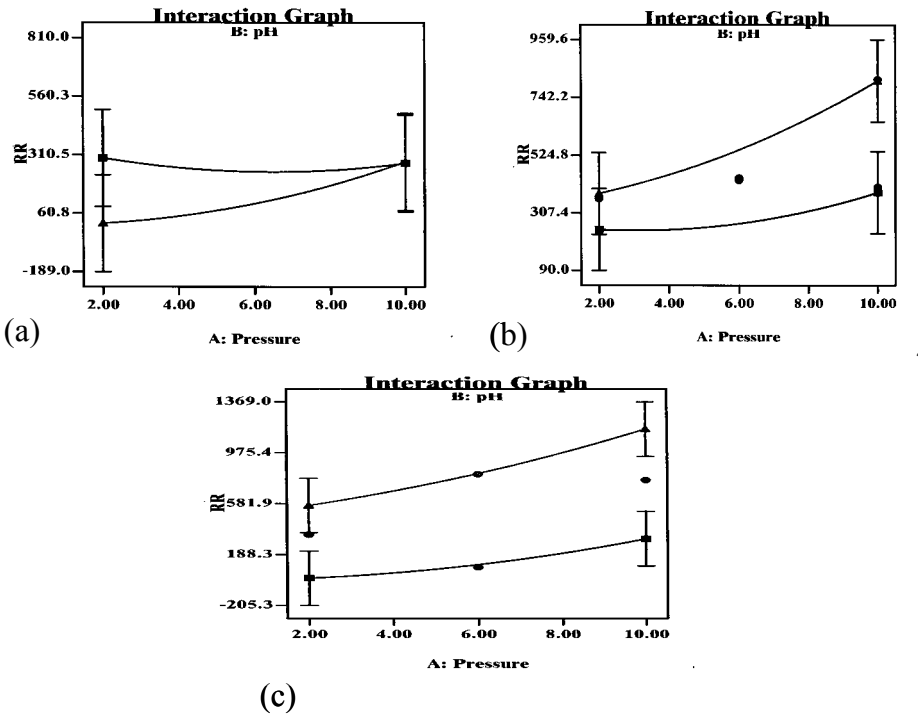

Figure 4-3 Interaction profiles for removal rate as a function of pressure and pH at: a) 75 RPM b) 112.5 RPM c) 150 RPM.

pH 2.0 for the velocity range in this study. From 2-10 psi, the removal rate increases five-fold at 75 RPM (figure 4-3a) and two-fold at 112.5 (figure 4-3b) and 150 RPM (figure 4-3c) at pH 6.0. An increase in applied pressure only results in a slight enhancement of the removal rate at pH 2.0 for all velocities. To understand this behavior, the actual contact pressure at the pad-wafer interface should be considered. For slurry pH values << than the IEP of ceria (~ 6.1-6.3 for these slurries), the particle size remains unchanged. However, as the slurry pH approaches the IEP of the ceria abrasives, the effective particle diameter increases because of agglomeration, which occurs as particle-particle repulsive forces are reduced. Now, as the applied pressure increases, the number of particles at the pad-wafer interface and the pad-wafer contact area increases. For smaller particles (low pH case), the fraction of the pad that is covered with abrasives or fractional surface coverage increases [Cho04b]. In this case, the actual contact pressure at the pad-particles-

wafer interface only slightly increases. However, in the case of pH 6.0 large agglomerates are formed, the fractional surface coverage is less [Cho04b]. Hence the actual contact pressure or load per particle is higher in the high pH case, which is evidenced by the removal rate response as a function of applied pressure.

Figure 4-4 shows the predicted removal rate response for all three variables (pressure (A), pH (B), and velocity (C)). A negative sign on the factor or variable corresponds to the minimum variable in the range, with positive signs being used for the maximum value. The numerical values are the removal rate responses for the respective combinations of pressure, pH, and velocity. The maximum removal rate should be reached for high pressure, pH, and velocity values (10 psi, pH 6.0, and 150 RPM).

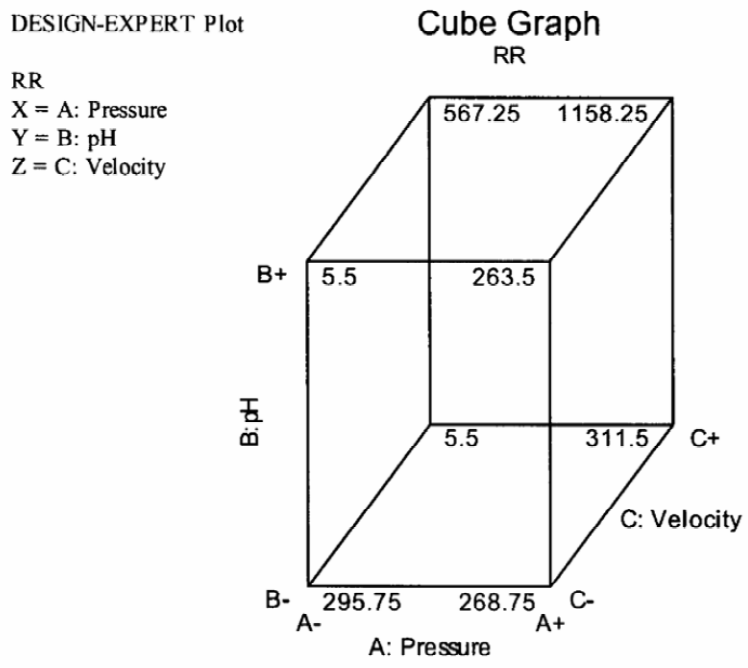

Figure 4-4 Predicted removal rate as a function of pressure, pH, and velocity.

Surface Finish Response

A successful CMP process requires more than just a high removal rate. Among the many parameters that may be considered, surface finish is perhaps second in importance only to the removal rate. For integrated circuit manufacturing, the surface roughness or topographical variations must be minimized to ensure conformal deposition of successive materials and error-free lithography [Wil93]. In STI CMP for DRAM structures, the surface roughness must be minimized to ensure the read-write heads of recording media do not crash into the storage material.

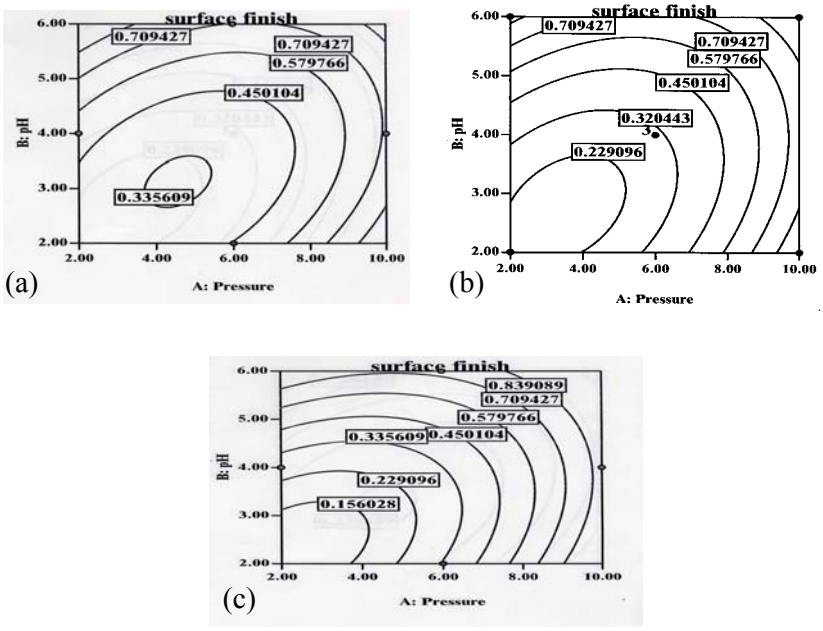

Figure 4-5 Predictions of RMS roughness as a function of pressure and pH at: a) 75 RPM b) 112.5 RPM c) 150 RPM

Figures 4-5 (a-c), show the predicted root mean square (RMS) roughness in nanometers as a function of pressure and pH for 75, 112.5, and 150 RPM respectively. For the 75 RPM case (figure 4-5a), the lowest roughness values are achieved for pH 3.0 and when the applied pressure ~ 4.0 psi. An increase in the velocity to 112.5 RPM (figure 4-5b) results in a further decrease in the lowest predicted roughness. Again this optimum

region is located at low pH (< 4.0) and low pressure (< 5 psi). Further improvements in surface finish are predicted as the velocity is increased to 150 RPM, figure 4-5c. This optimum region is also located at low pH (< 4.0) and low pressure (< 4 psi). As the rotational velocity is increased, the regions of factor space that predict the lowest RMS roughness values are found at increasingly lower pH and pressure values. The indentation depth of a single particle is proportional to the applied pressure and the particle diameter [Coo90]. An increase in pressure, pH, or both in tandem, results in deeper penetration into the silica surface. The interaction profiles for the surface roughness predictions, figures 4-6 (a-c), show that there is a strong interaction between the experimental variables at low velocities (figure 4-6a). The mutual effects weaken as the rotational velocity is increased (figure 4-6c and 4-6c). According to this design planarity should increase with velocity.

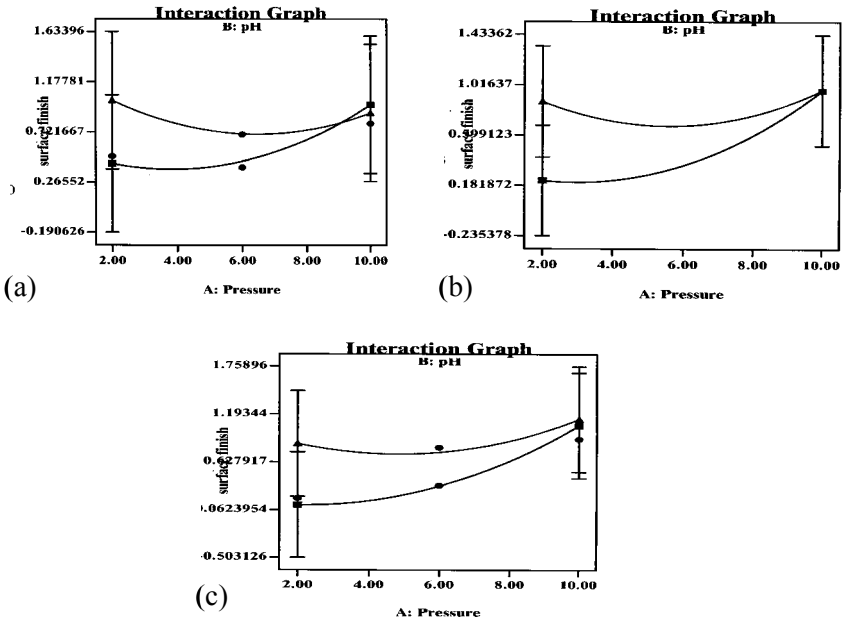

Figure 4-6 Interaction profiles for RMS roughness as a function of pressure and pH at: a) 75 RPM b) 112.5 RPM c) 150 RPM

Figure 4-7 shows the predicted surface finish as a function of pressure (A), pH (B), and velocity (C). The optimum regions that produce minimal surface deformation occur at low pressure and pH values and high rotational velocities. The statistical results have been explained using actual CMP phenomena. Hence, this statistical model accurately predicts the effect of pressure, pH, and velocity on the removal rate and surface finish for ceria-silica CMP.

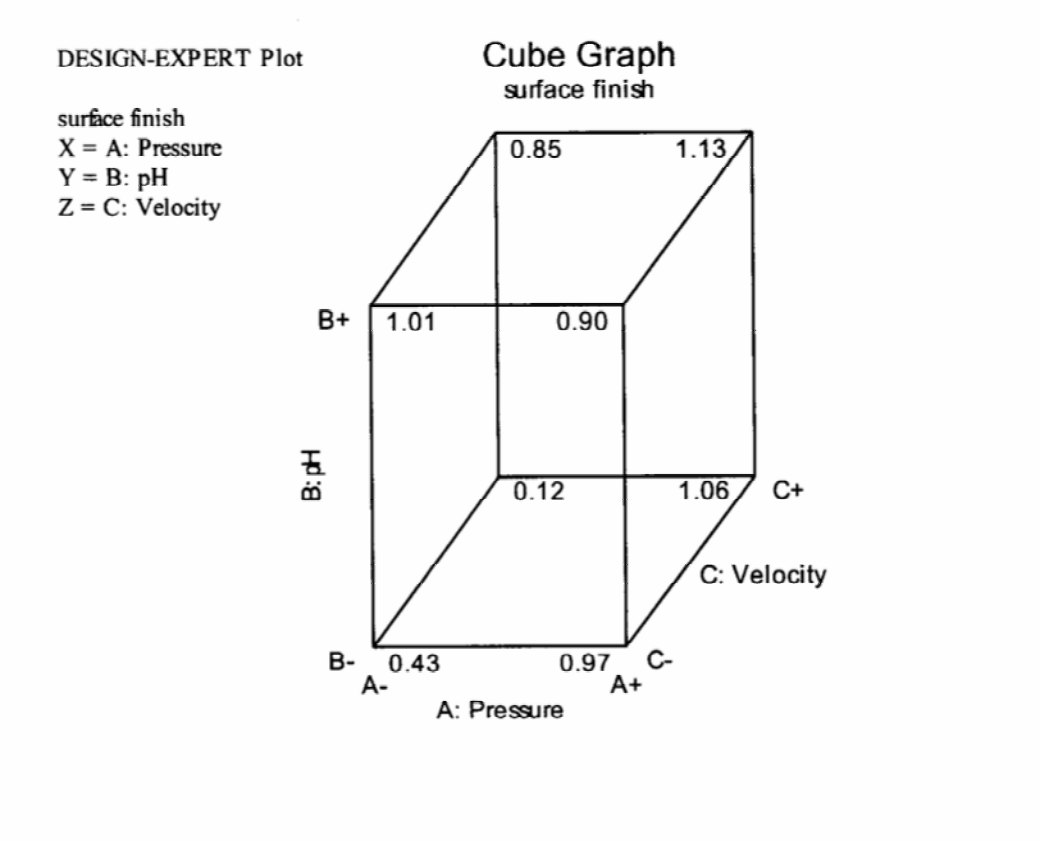

Figure 4-7 Predicted removal rate as a function of pressure, pH, and velocity.

Summary

A statistical design based on the Box Behnken method was used to predict the removal rate and RMS roughness after CMP as a function of pressure, pH, and velocity. Both the removal rate and surface finish are predicted to be strongly pH and velocity dependent. The applied pressure is expected to have only a slight effect on the material

removal rate for most of the experimental conditions examined. However, the surface roughness does depend strongly on the applied pressure, since the indentation or particle penetration depth is proportional to the applied pressure. Using statistical methodology, the isolated and joint effects of three variables were simultaneously investigated.

Statistical designs are a powerful means of process optimization. However, the goal of this study is to understand the mechanisms of the ceria-silica interactions during CMP that lead to material removal. Therefore, the remainder of this study will focus on the fundamentals at the ceria particle silica wafer interface. In the next chapter, chemical and surface chemical effects are investigated.

CHAPTER 5
THE EFFECT OF CERIA SLURRY PH ON THE SILICA REMOVAL RATE, FRICTION FORCE, AND SURFACE MORHOLOGY DURING CHEMICAL MECHANICAL POLISHING

Introduction

A statistical design based on the Box Behnken method was used in Chapter 4 to predict the effect of pressure, pH, and velocity on the silica removal rate and surface finish after CMP with ceria slurries. Statistical designs are important methods for process optimization or materials selection. However, statistical methods are limited in usage by the depth of knowledge of the system under investigation. Furthermore, mathematical rather than statistical models are required for articulating the materialistic responses based on the properties of the components of the system in question (i.e. surface layer hardness, particle hardness, pad hardness, etc.). Hence, fundamental experiments are required and the one-factor-at-a-time laboratory testing technique is unavoidable.

The rapid growth of the semiconductor industry is made possible by a combination of innovative device integration schemes, technological advances, and judicious materials selection. The continued scaling of microelectronic devices has resulted in unprecedented improvements in microprocessor performance and an increased density of memory chips. The advances in device integration and the introduction of new materials to integrated circuit manufacturing have also driven the development of novel processing techniques. Vertically stacked or hierarchal type structures that are critically dependent on global planarity are utilized in a variety of manufacturing techniques.

Hence, CMP is increasingly relevant and has stimulated significant research interest in the academic arena.

Shallow trench isolation (STI) is an example of a novel manufacturing technique that is critically reliant upon CMP. Traditionally, silica-based slurries were used for the interlevel dielectric CMP step during IC fabrication. The popularity of STI has driven the interest in new CMP consumables (pads, slurries, and slurry additives), to meet the stringent planarity, removal rate, selectivity, and surface finish requirements. Significant improvements in device characteristics are realized by replacing conventional isolation techniques with STI. However, STI CMP is much more complex. For a successful STI CMP process, the oxide to nitride polish selectivity, oxide erosion or dishing, and nitride loss must be controlled. Ideally, the STI CMP process will come to a halt immediately as the oxide is cleared and the nitride is exposed. Ceria-based slurries are promising for high selectivity polishing as they intrinsically polish oxides faster than nitrides or bare silicon [Eva04]. The CMP process should also result in uniform removal of the trench oxide. Deviations in oxide thickness in excess of 3%, trench oxide erosion greater than 50 nm, and nitride overpolishing may cause damage to the underlying silicon substrate [Sch99, Zha01]; all are deleterious to device performance.

The “holy grail” of sorts in STI CMP is an appropriately high selectivity, i.e. high oxide polish rate with little to no nitride removal. If the selectivity is low, nitride loss may occur. However, if the selectivity is too high, the oxide removal rate is uncontrollable and oxide erosion results. To achieve the desired oxide to nitride selectivity (> 100:1), two methods have been adopted. In the first method, surfactants (anionic, nonionic, or a mixture of the two) are used to passivate or lubricate the nitride surface. In the case

where the slurry pH is less than the IEP of the silicon nitride surface, an anionic surfactant in the ceria-based slurry is expected to selectively adsorb on the nitride surface. The mechanisms of the adsorption are not understood, but electrostatic attraction because of opposite charge at the nitride and surfactant surfaces is expected to play a role. Tseng, S-D Kim, Katoh, and Park have studied the effect of surfactants on the silica removal rate for high selectivity polishing [Tse01, Kim02, Kat03, Par04b]. Fixed abrasive pads are used in the second approach [Sim01, Gag02, Kul04].

Surfactant Based STI CMP

Tseng et al. studied the effect of two nonionic surfactants with similar molecular weights: SHE, which has a siloxane head group, and CHE, which has a methyl methacrylate head group [Tse01]. Silica-based slurries were used for the studies. The superior polish rate of CHE-based slurries was attributed to an acceleration of chemical processes during polishing. The results of Tseng and co-workers are insufficient for the STI CMP process. The maximum removal rate of the surfactant based slurries was less than that for silica-based slurries with no additives. Since the oxide removal rate is not accelerated, the oxide to nitride selectivity should remain low. Using atomic force microscopy, Basim determined that the addition of surfactants lowers the removal rate because of increased lubrication at the pad-wafer interface [Bas02a].

S-D Kim et al compared chip scale and wafer-to-wafer thickness variations for a ceria-based high selectivity slurry (selectivity values were not given) and a silica-based low selectivity slurry [Kim02]. According to their results, CMP with the conventional silica slurry resulted in greater nitride overpolishing and oxide erosion. An in-situ filter was required for the high selectivity slurry to minimize scratches on the polished surfaces. Katoh et al. studied the effect of surfactant concentration and ceria particle size

on the oxide and nitride removal rate [Kat03, Par04b]. For larger particles (120 nm), the polish rate without surfactant was twice that of the smaller particles (50 nm) for both oxide and nitride polishing. However, as the acrylic acid (water-soluble surfactant) concentration was increased to 0.10 wt%, the nitride polish rate rapidly saturated at ~ 5 nm/min, for the 120 nm and 50 nm (primary particle size) slurries. The oxide polish rate was not affected until the surfactant concentration reached 0.40 wt% for the 120 nm particles. The smaller particles showed similar polishing behavior for oxide and nitride surfaces. These observations were attributed to the difference in particle velocity in the viscous surfactant as a function of particle size. In their interpretation abrasive particles freely move through the fluid film, impinge on the surface, and remove material. According to their conclusions, the velocity of larger particles remains significant enough to reach the surface until a critical fluid thickness is reached at higher surfactant concentrations.

This assertion is problematic for several reasons. First, free-flowing particles that are not embedded in the pad are not believed to contribute to the material removal rate [Zha99]. Second, the suppression of the nitride removal rate for 120 nm at 0.10 wt% acrylic acid does not agree with the proposed explanation. Finally, because of agglomeration, the average particle size was nearly identical up to 0.4 wt% acrylic acid, negating particle size effects. It is more likely that the acrylic acid passivates the nitride surface resulting in a saturation of the nitride removal rate at very low surfactant concentrations. For the oxide CMP case, the enhanced removal rate for larger particles may occur because of the greater penetration depth of abrasive particles embedded into the polishing pad. An interesting aspect of this study by Katoh and co-workers is the

possibility of nitride passivation using acrylic acid, which results in enhanced oxide to nitride selectivity.

Fixed Abrasive Pads for STI CMP

STI CMP with high selectivity slurries is problematic because of increased oxide erosion. Robust endpoint detection schemes are needed to stop polishing as the nitride is exposed [Sim01]. Fixed abrasive (FA) pads are a revolutionary approach to STI CMP [Sim01]. Using FA pads, problematic issues associated with particle-based slurries such as handling, lifetime, and stability may be alleviated. Generally, FA CMP slurries consist of pH-adjusted water and a separate chemical for enhanced selectivity. A further complication of STI CMP with particle-based slurries is the requirement of an initial etch step to minimize difficult-to-polish topography [Ste97]. CMP with FA pads allows direct polishing and the additional advantage of reduced oxide erosion [Sim01]. The FA pad is a composite of ceria abrasives and a resin binder supported by polymer backing (figure 5-1). The composites have a well-defined shape and are regularly spaced to ensure transport of the liquid slurry and polish debris. The planarization efficiency is a function of the morphology of the composite.

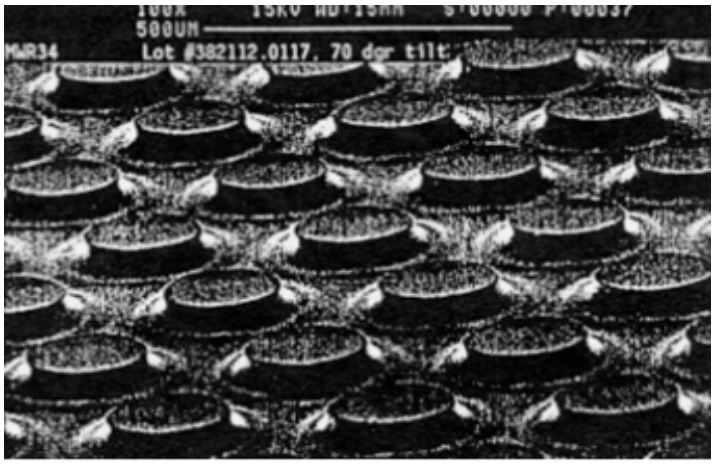

Figure 5-1 SEM micrograph of fixed abrasive pad surface (200x) [Vel00].

Simpson et al. studied three different fixed abrasive pads supplied by 3M that were classified as slow, medium, or fast according to their respective oxide removal rates [Sim01]. The slow pad consisted of cylindrically shaped ceria/polymer composite structures. The oxide removal rate for the slow pad was less than 10 nm/min. Hence, this pad was deemed suitable for CMP of thin oxide overfills of less than 20 nm [Sim01]. Simpson and co-workers characterized this pad as tough, meaning micro-scale topography was required to initiate polishing. The slow pad showed high selectivity to topography, which means the removal rate at low areas was negligible. Oxide dishing was eliminated with an overall improvement in oxide and nitride uniformity after CMP. The polishing capability of the slow pad was critically dependent on the quality of the oxide deposition [Sim01]. The pad classified as medium was structurally similar to the slow pad except that it releases more cerium during polishing [Sim01]. The medium pad also produced very low oxide removal rates (~20 nm/min). Unlike the slow pad, the medium pad did not provide a suitable overpolish process window (excessive oxide dishing), but may be applicable to borophosphosilicate glass polishing [Sim01]. The fast polishing pad was used for isolation trenches with thick overlying oxide layers. The oxide polish rate was significantly higher (> 200 nm/min). The fast pad produced poor oxide to nitride selectivity and excessive oxide dishing, and, was therefore deemed unsuitable for STI CMP.

Gagliardi et al have also studied FA CMP for STI. L-Proline, an amino acid, was used to tailor the oxide-to-nitride polish selectivity, eliminate nitride erosion, and oxide dishing [Gag02]. In their study the polishing tool was specifically configured for the FA study. A roll of fixed abrasive was loaded onto the CMP machine. After polishing a

wafer, the FA pad is moved ~ 3 mm. After a certain number of wafers are polished, each subsequent wafer is exposed to an abrasive surface that has been used in an identical manner [Gag02]. The abrasives were shaped like pyramids and were 63 μm tall and 125 μm wide. The combination of FA pad and L-Proline yielded a robust CMP process with well-defined polish characteristics. The oxide and nitride removal rates were controlled by the addition of L-Proline. An oxide to nitride selectivity in excess of 100 was obtained for a variety of pH conditions and amino acid concentrations.

For precise process control of particle-based and fixed abrasive STI CMP solutions, a fundamental understanding of the ceria-silica interactions is necessary. However, very few investigators have focused on the mechanisms of the ceria-silica CMP process. In chapter 2, the current understanding of the ceria-silica polishing process was reviewed. Despite the lack of fundamental ceria-silica CMP investigations, three models can be found in the glass polishing and CMP literature.

The chemical tooth model is most widely relied upon for explanations of the ceria-silica CMP mechanism. However, nothing in the manner of experimental proof has been extended to validate the proposed theory. Two other less-referenced models are also available. One, which I have termed the particulate generation model, depicts the ceria-silica polishing mechanism as more mechanical in nature. The other, which I have termed surface defects model, stipulates that efficient polishing compounds must have surface defects for desired polishing. Initial ceria-silica reactions are a central theme of all three proposed models. In Chapter 2, the effect of pH on the ceria surface chemistry was reviewed. Since the ceria polish rate is believed to be enhanced by its intrinsic chemical reactivity and the solution pH affects the ceria surface chemistry and chemical reactivity;

the CMP performance should be strongly pH dependent. In this chapter, the effect of the ceria slurry pH on the silica removal rate, friction force at the pad-ceria-silica interface, and silica surface morphology is presented.

Experimental

All polishing slurries contained ceria and DI water only. To adjust the pH to desired values (2-6.5), HCl and KOH were used. The slurry was delivered at a constant rate of 100 ml/min. In-situ lateral friction force measurements and polishing experiments were conducted on a Struers Rotopol 31 tabletop polisher. A more complete description of the CMP polisher and friction force apparatus may be found in Chapter 3. The sample size for polishing and friction tests was 1.0 x 1.0 in., and the samples were ~2 μm thick oxides deposited on p-type silicon (100) by chemical vapor deposition. The down pressures for polishing experiments and friction force measurements were 8.8 and 3.5 psi, respectively. All samples were polished for 30s. Slurry samples were collected at pH 2.0 and 6.0 during experimental runs. Rodel IC 1000/ Suba IV stacked pads were used for all experiments. To ensure reproducible conditions, a Grid-Abrade diamond pad conditioner was used to roughen the polishing pad before each run.

Dynamic light scattering techniques were used to measure the ceria particle size, zeta potential, and stability. A scanning electron microscope (SEM) equipped with a field emission gun was also used for particle size measurements. A Microtrac® UPA 150 particle size analyzer was used to measure the particle size before and after CMP. A turbidimeter Model 2100AN manufactured by Hach Company was used to assess the slurry stability at pH 2.0, 6.0, 6.5, and 10.5. Zeta potential measurements on the slurries before and after CMP were performed on an apparatus manufactured by Brookhaven Instruments. Material removal rates were calculated by measuring the oxide thickness

before and after CMP with a variable angle spectroscopic ellipsometer. AFM was used to characterize the morphology of the polished surfaces after CMP.

Results and Discussion

Ceria Slurry Characterization

In the pH range studied, the silica substrate possesses a predominantly negative charge because of deprotonation of surface hydroxyls.

$$Si\text{-}OH \leftrightarrow Si\text{-}O^{-} + H^{+} \qquad (5.1)$$

Conversely, the ceria abrasives go from predominantly positive to mostly neutral as the pH of the slurry approaches its isoelectric point.

$$Ce\text{-}OH_2^{+} \leftrightarrow Ce\text{-}OH + H^{+} \qquad (5.2)$$

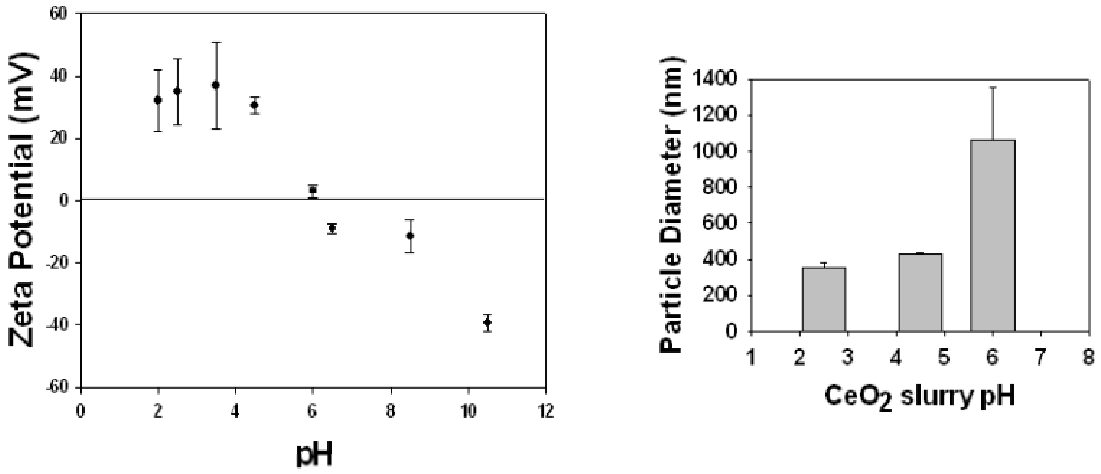

Figure 5-2 Ceria slurry characteristics as a function of pH a) zeta potential b) particle diameter.

The IEP for silica is between pH 2-3 and pH 6-7 for ceria [Coo90]. The effect of pH on the ceria slurry properties is shown in Figures 5-2a and 5-2b**.** In the absence of surfactants or other dispersing agents, electrostatic means are solely responsible for the dispersion state of the slurry. Figure 5-2a indicates the IEP of the ceria abrasives used is ~ pH 6.0. As the pH is increased from 2-6.5, the electrostatic interactions become less repulsive. As

expected, slurry agglomeration ensues, resulting in an increase in abrasive size and a decrease in slurry stability (Figures 5-2b and 5-3)**.** Even at pH 10.5, the ceria slurry remains unstable with the particles rapidly settling out of solution in less than 10 minutes. Since direct imaging is possible, SEM measurements were conducted, (figure 5-4). The primary particle size as determined by SEM is ~ 60 nm. The particle size values determined by light scattering should be considered the secondary or agglomerated particle size. The particle size measurements via light scattering were consistent even after sonication.

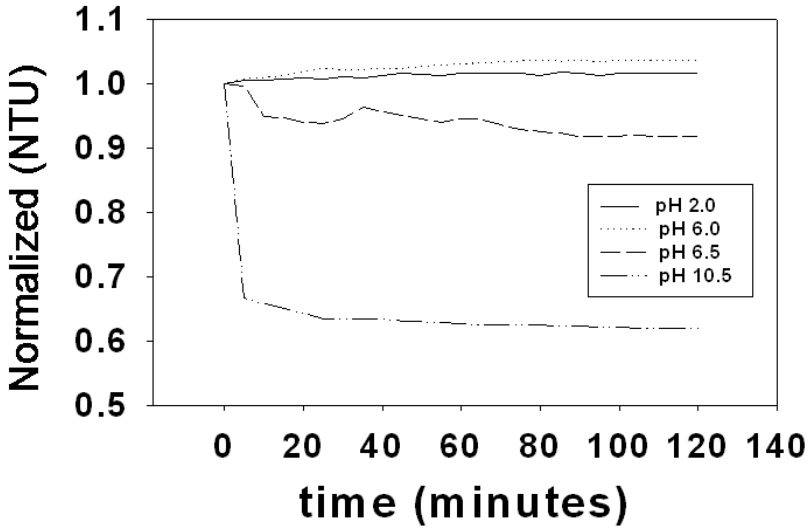

Figure 5-3 Stability of the ceria slurry as a function of time for different pH values. Vertical axis is displayed as normalized nephelometric turbidity units (NTU).

The lack of ceria stability at pH 10.5 is unexpected, especially in light of the zeta potential measurements. At pH 10.5, the zeta potential is ~ -40 mV, approximately equal in magnitude to the low pH case. Therefore, it is not unreasonable to expect that ceria dispersions at pH 10.5 should be as stable as dispersions at pH 2.5. The actual state of the dispersions used for turbidity and zeta potential measurements and surface chemistry of

ceria as studied by Nabavi et al. [Nab93] may shed some light on these contradictory observations.

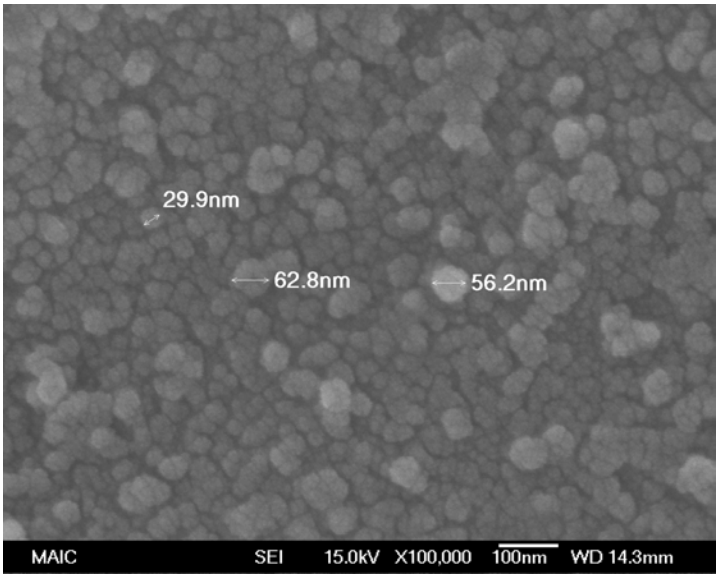

Figure 5-4 FE-SEM image of ceria particles.

The dispersions for zeta potential measurements are much more dilute than for turbidity measurements. For turbidity measurements, the ceria slurry is added to the turbidity cell as is, since the concentration is less than 3 wt%. However, for zeta potential measurements the specimen holder was initially filled with pH 10.5 DI water and then a drop of the ceria slurry was added to the specimen. The inter-particle spacing is greater for the dilute suspension and the likelihood of particle-particle collision diminishes as the concentration of the dispersion decreases. The samples for turbidity measurements are more representative of the actual slurries used for the CMP experiments. The zeta potential is directly related to the density of charged sites at the abrasive particle surface. Nabavi's investigation of the ceria surface chemistry as a function of pH is relevant to this discussion.

Nabavi demonstrated that stable ceria dispersions could only be obtained in certain pH ranges [Nab93]. Originally, Nabavi and co-workers set out to measure the surface charge of the nanoscale ceria particles through titration of the surface groups with either a base or acid. Surprisingly, it was found that titrations in the pH range where charge reversal was expected could not be performed as cycles, because the dispersion did not return to its original state. This behavior is demonstrated by an excess consumption of hydroxyls (OH^-) in acid to base titration as compared to the consumption of protons (H^+) in the reverse cycle. According to their results, three ranges of pH were identified that correspond to three unique dispersion characteristics (figure 2-10).

Range A extends up to ~ pH 5. The titration cycles in this range were completely reversible and the dispersion remained stable, which indicates the surface charge is constant. Range B extends from pH 7 to 10. Dispersions titrated from pH 3.4 to any pH in this range back to pH 3.4 resulted in an excess hydroxyl consumption of 40 [Nab93]. Flocculation ensued as the boundary between range A and B was crossed. The dispersions remained unstable even after titrating back to pH 3.4. Interestingly, successive titration cycles from range A to B and back did not show the hysteresis (excess hydroxyl consumption), which indicates the number of sites able to consume a hydroxyl ion is: 1) different from the original dispersion and 2) stabilized after the initial titration cycle. Range C extends beyond pH 10. The initial titration cycle in this range resulted in an excess consumption of 50 hydroxyl ions [Nab93]. The step at pH 10 was sharp for slow titrations. Nabavi et al suggested that the excess use of hydroxyls above pH 10 is associated with the kinetics of a slow reaction, which suggests a more stable dispersion may be obtainable at pH 10 if the liquid environment was changed rapidly

from acidic (pH < 5) to basic pH (> 10). The dispersions in ranges B and C remained unstable even after returning to the original acidic pH for 40 days. At pH 2, re-dispersion took 2 days and at pH 0.5, re-dispersion occurred immediately. This agglomeration was attributed to particle-particle condensation reactions that result in a loss of surface area [Nab93].

In light of this discussion, it is more reasonable to assume that the surface chemistry instead of the solids concentration is responsible for the lack of stability at pH 10.5 as measured by the turbidimeter. The ceria slurry was received in an aqueous dispersion at pH 4. To adjust the pH, KOH or HCl was added drop by drop until the desired pH value was reached. Since, the ceria slurries did not require significant dilution to perform the turbidity tests there was sufficient time for the condensation reaction to occur as the pH was adjusted from 4 to 10.5. However, for the zeta potential measurements a small amount of the slurry was immediately exposed to a pH 10.5 environment, which prevented particle-particle bonding and is evidenced by the appreciable zeta potential value. It should be noted that it may be possible to temporarily disperse the flocculated slurries using an ultrasonic bath.

Silica Removal Rate

Figure 5-5 shows the removal rate as a function of slurry pH. During CMP, a magnetic stirrer is used to counteract slurry settling, which makes it possible to polish wafers with unstable slurries. From pH 2.0 to 6.0 there is a five-fold increase in the removal rate. The silica polish rate continually decreases from pH 2.5 to the maximum value at pH 6. At pH 6.5, the removal rate begins to decrease. According to the chemical tooth theory as interpreted by Osseo-Asare [Oss02] the silica removal rate should be

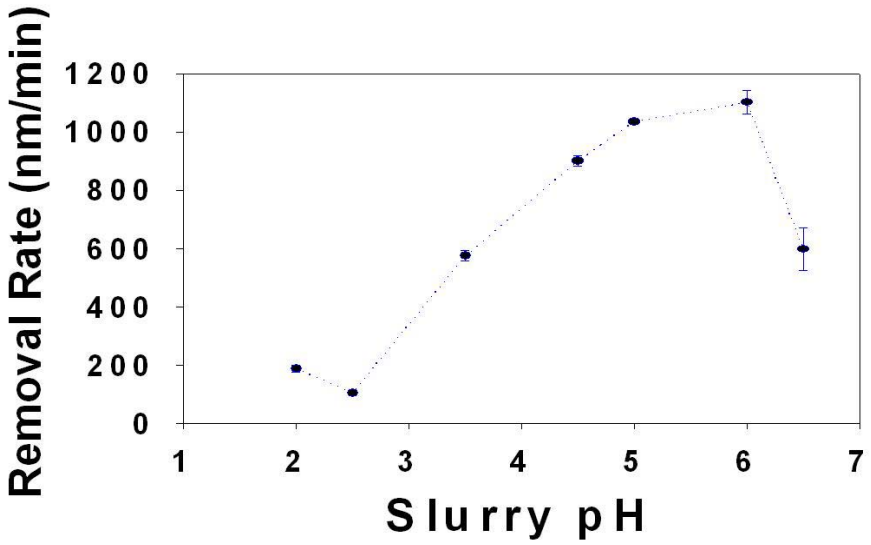

Figure 5-5 Silica removal rate as a function of ceria slurry pH.

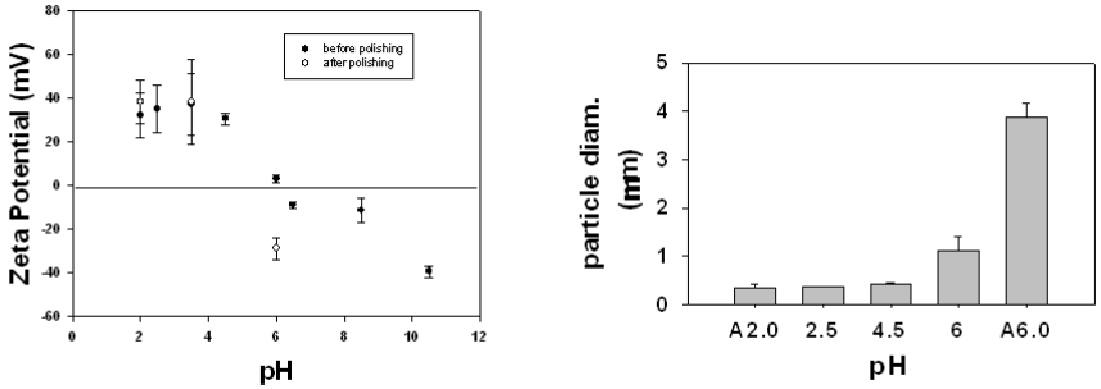

Figure 5-6 Post-CMP slurry characteristics as a function of pH a) zeta potential and b) particle size.

highest at the IEP of the abrasive particles. The chemical tooth theory depicts silica polishing as an adsorptive removal process, which is controlled by the interactions between surface functional groups [Coo90, Oss02]. If the ceria particles adsorb silicate species during polishing; the particle size and zeta potential of the post CMP slurry

should be significantly changed. The ceria slurry was collected during CMP at pH 2.0 and 6.0, and the zeta potential (circular data points) and particle size (A2.0 and A6.0) were re-measured (Figures 5-6a and 5-6b). After CMP at pH 6.0 the particle size increased significantly. Also, the zeta potential is much more negative than if ceria alone was present in the slurry. At pH 6.0 the zeta potential on the ceria and silica surfaces is expected to be approximately 10 mV and -60mV respectively. The measurements of particle size and zeta potential after CMP indicate the abrasive particle adsorbs silica during polishing or that the silica coats the ceria particle while in solution. The zeta potential of co-dispersions of ceria and silica has been reported [Eva04], figure 5-7**.** Mixtures of ceria and silica in an aqueous environment seem to behave like pure silica, which indicates that the ceria particle forms the core and the silica is the shell of the ceria-silica composite.

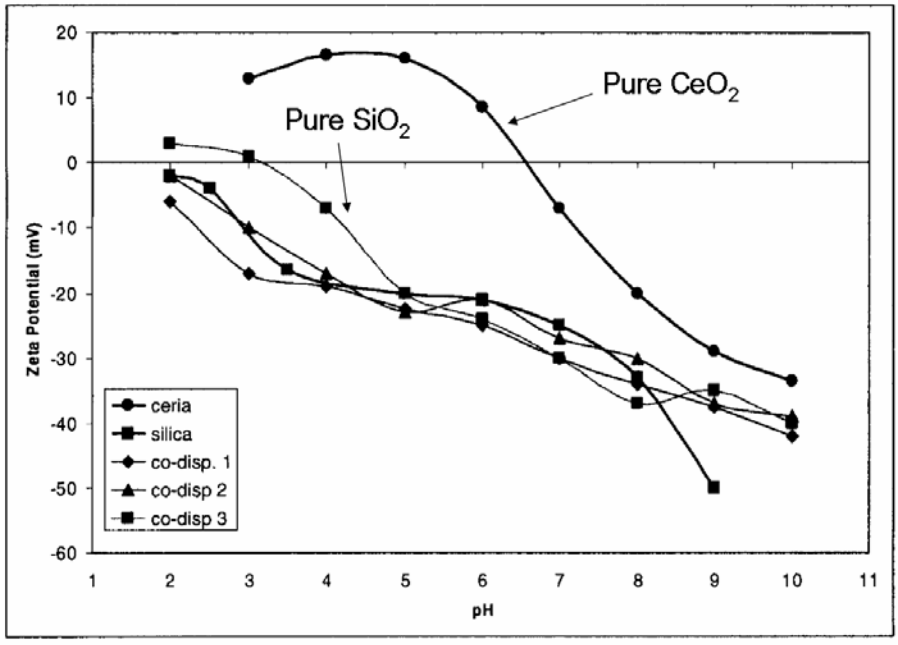

Figure 5-7 Zeta potential versus pH for ceria, silica, and co-dispersions [Eva04].

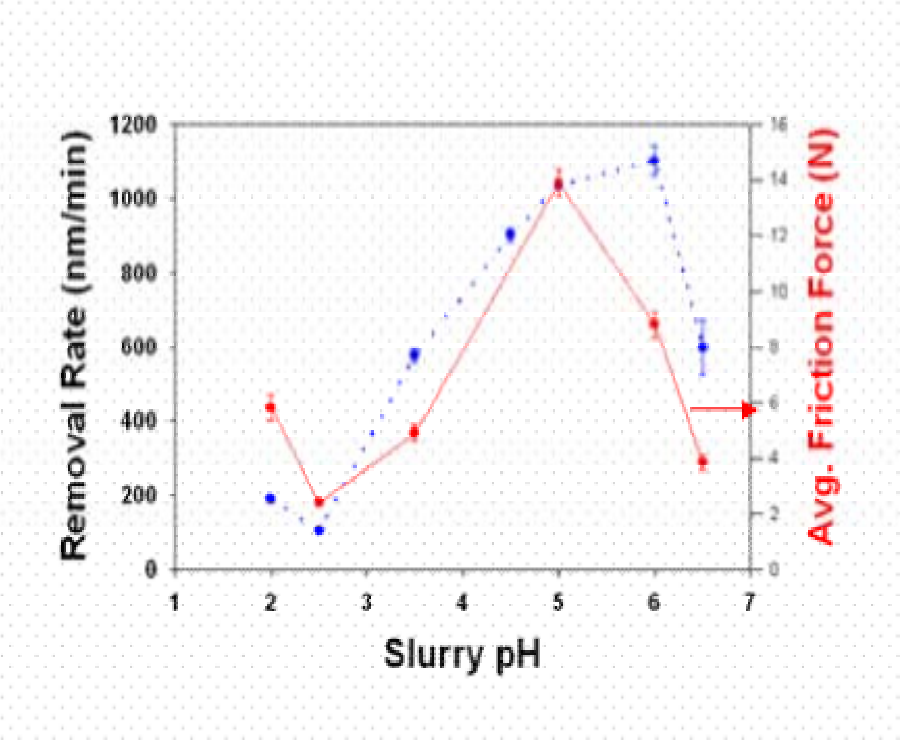

Figure 5-8 Friction force (right axis) and removal rate (left) at pad-ceria particles-silica wafer interface.

Friction at the Ceria-Silica Interface

In-situ friction force measurements have been used extensively to understand silica-silica CMP mechanisms [Mah99a, Mah99b, Cho01, Cho03, Cho04a, Cho04b, Cho04c]. The friction force is known to be strongly dependent on interfacial electrostatic interactions, dynamic surface conditions, properties of the opposing surfaces, and the abrasive particle size, which all influence the contact area between the opposing surfaces. Figure 5-8 shows the in-situ friction force at the pad-particles-wafer interface along with the material removal rate as a function of pH. The maximum in the friction force is highest near pH 5.0. Changing the slurry pH not only influences the slurry stability; the extent of the electrostatic interactions between the abrasives and the silica substrate are also affected. The electrostatic interaction between two surfaces is proportional to the product of the charge on each surface ($F \sim q_1 * q_2$), where F is the electrostatic force and q

is the charge on the opposing surfaces. Therefore, the product of the zeta potential on the ceria abrasive and silica substrate as a function of pH may be used as an indicator of the magnitude of the electrostatic interactions (Figure 5-9). Chen has demonstrated the validity of this assumption using the linear superposition approximation (LSA) for calculation of the electrical interaction energy (ΔG_E) between a silicon plate and a spherical particle [Chen00, Chen03]. The LSA states that the potential distribution (Φ) in overlapping double layers is just the summation of potential distributions in two isolated double layers [Chen03].

$$\Phi = \Phi_1 \exp(-\kappa x) + (\Phi_2 \exp[-\kappa(d-x)] \qquad (5.3)$$

Where κ is the inverse of the electrical double thickness, x is the position of surface 1, and d is the separation distance between surfaces 1 and 2. Chen adopted the method of Derjaguin [Der87] to derive the expression for electrical interaction energy:

$$\Delta G_E = 4\pi\varepsilon a \Phi_1 \Phi_2 \exp(-\kappa x) \qquad (5.4)$$

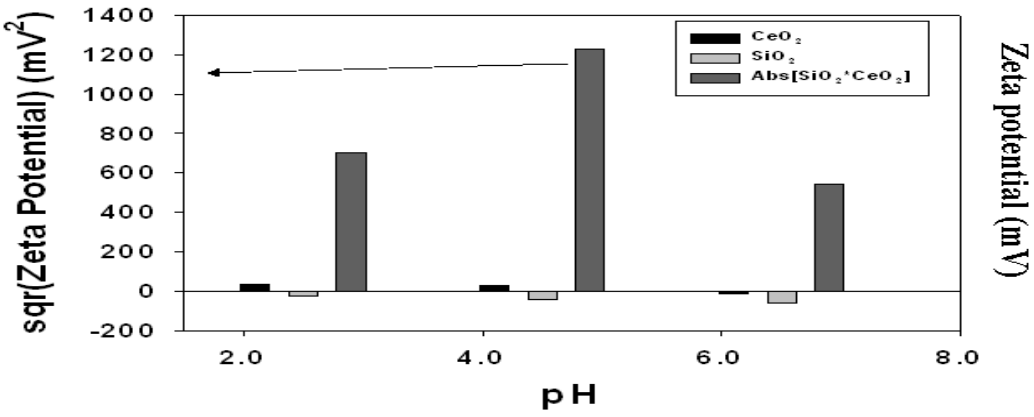

Figure 5-9 Qualitative comparison of the extent of the electrostatic interactions using the product of the zeta potential on the ceria and silica surfaces.

where ε is the dielectric constant of the liquid media and a is the particle diameter. The extent of the electrostatic interactions can be crudely estimated by examining the product of the zeta potential on the silica wafer and the ceria particles. In the pH range studied, ceria-silica interactions are predominantly attractive with a maximum at the apex of the friction force vs. pH curve. The particle size increase and the reduction in electrostatic attraction between the silica and ceria surfaces, which reduces the contact area, may be responsible for the decrease in the friction force above pH 5, whereas the removal rate increases up to pH 6. An additional contributing factor may be operational at pH 6.0 other than mechanically controlled wear.

Surface Morphology

The result of AFM analysis of the polished silica surface is depicted in Figure 4- Root mean square (RMS) roughness values were below 1 nm for the as-received silica samples and polished surfaces. The RMS roughness was nearly identical after polishing at pH 2.0 and 4.5. Because of slurry agglomeration, the RMS roughness of silica polished at pH 6.0 was nearly identical to that of the as-received samples. Therefore, if ceria slurries are required at pH 6.0, a smaller particle size is needed to improve the silica surface quality.

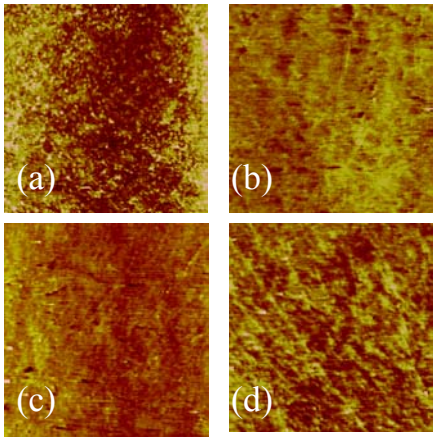

Figure 5-10 AFM topographical analysis of silica wafers a) no polishing b) polished at pH 2.0 c) polished at pH 4.5, and d) polished at pH 6.0.

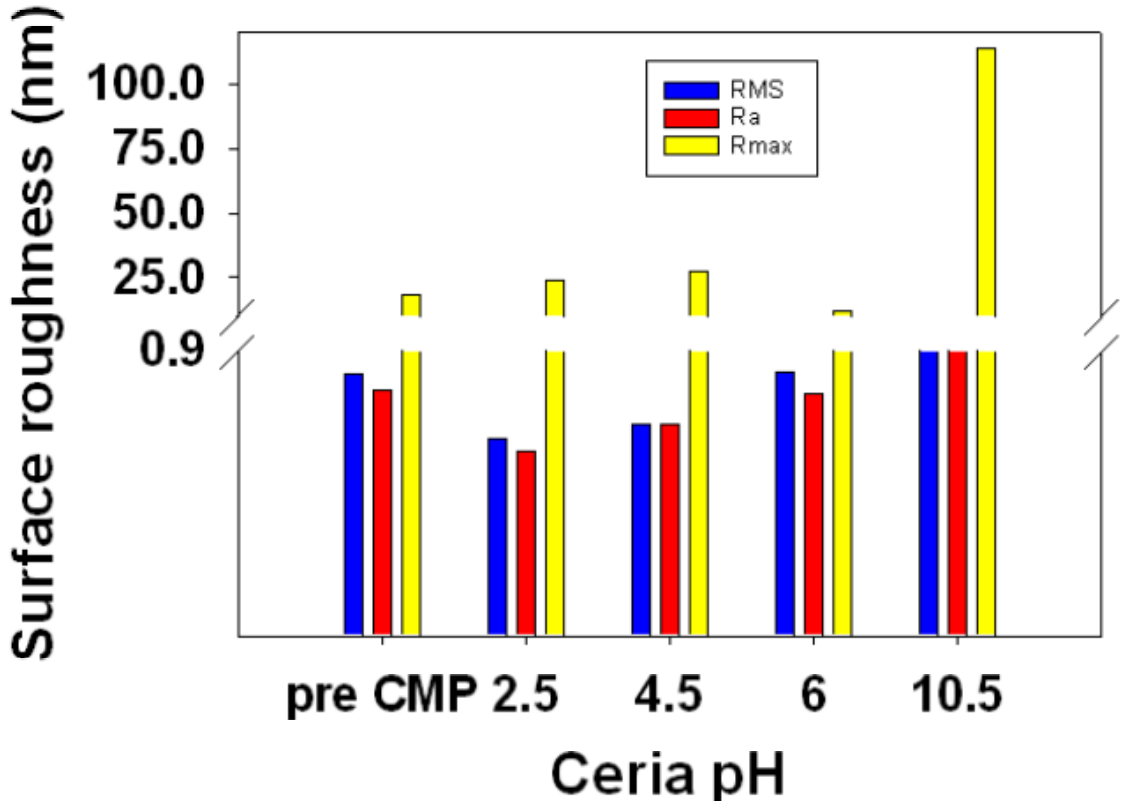

Figure 5-11 RMS roughness of silica wafers as a function of slurry pH.

Comparison of pH Effects of Ceria-Silica to Silica-Silica CMP

Silica-silica CMP may be considered a model system for other dielectric CMP processes. The chemical effects during silica-silica CMP are also pH-dependent. In silica-silica CMP, the primary chemical contribution to the polishing process is hydrolysis and dissolution of the uppermost silica layers (equation 2.4). Since silica-silica CMP provides the foundation for dielectric CMP processes, it is worthwhile to discuss the effect of pH on silica-silica interactions in light of the results of this chapter.

Mahajan measured the in-situ friction force and silica removal rate as a function of pH for abrasive-free slurries [Mah99b, Mah00]. The slurry pH was adjusted to 3.0, 7.0, and 11.0. In these findings, the frictional forces at the pad-wafer interface were highest

for the acidic pH condition. Mahajan attributed these results to electrostatic interactions between the pad and wafer. Since the polishing pad has an IEP near that of silica, increasing the slurry pH results in an increase in repulsive forces at the pad-wafer interface. Since no particles were used in these experiments, the silica removal rate as a function of pH was very low and relatively constant except for very basic pH conditions. Contrary to friction force measurements, the silica removal rate increased at pH 11. As reviewed in chapter 2, the solubility of silica increases rather rapidly above pH 9.0 [Ile79, Coo90]. According to Mahajan, the increased dissolution of the silica network at high pH was responsible for the enhanced polishing.

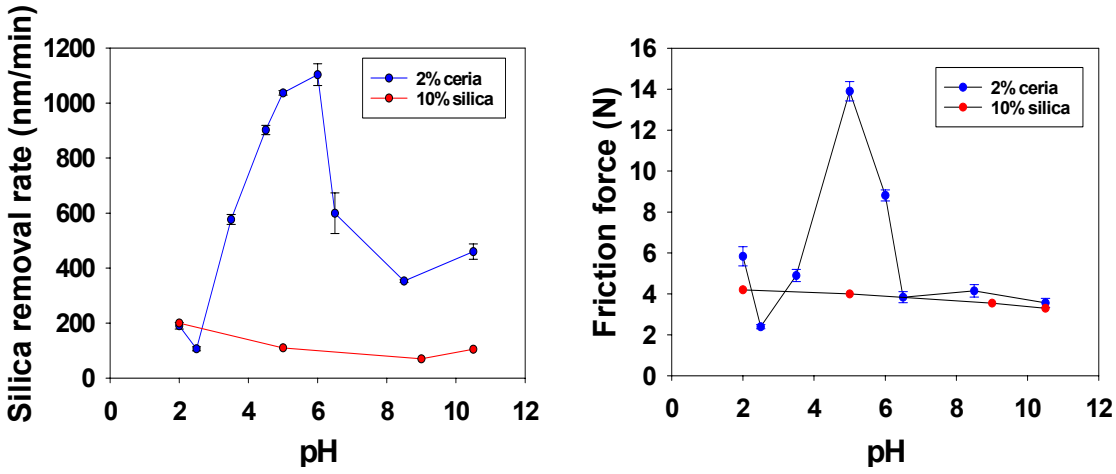

Figure 5-12 pH dependent ceria-silica and silica-silica [Cho03, Cho04d] interactions a) removal rate versus pH for 2 wt% ceria slurry at 8.8 psi and 10 wt% silica slurry at 10.5 psi and b) friction force versus pH both measurements conducted at 3.5 psi.

Choi studied the effect of pH on silica-silica polishing and measured the friction force for particle-based slurries [Cho03, Cho04d]. These results are presented in figure 5-12 along with the silica removal rate and frictional forces for ceria-based slurries. In figure 5-12a, the silica removal rate as a function of pH is plotted for silica and ceria slurries. For a true comparison, the results of figure 5-5 have been extended to pH 10.5.

For the pH range displayed, the silica particle size is constant. The removal rate for the silica slurries is much lower than that obtainable with ceria slurries. Also, the transition from high to low removal is fairly shallow, with the difference being approximately ~150 nm/min from pH 2.0 to pH 10.5. In contrast, the silica removal rate for ceria polishing increases from a minimum of < 200 nm/min to a maximum of over 1 μm/min at pH 6.0. The removal rate further decreases as the slurry pH is increased. At pH 10.5, a slight increase is seen.

For ceria-silica polishing, three distinct regions are present in the removal rate versus pH curves. The first, from pH 2.5-6.0 shows a steady increase in the polish rate with increasing pH. The second, pH 6.5-8.5 shows a decrease in the polish rate with increasing pH. Finally, the polish rate increases at pH 10.5. For silica-silica polishing, only two distinct regions are present. Initially, the polish rate steadily decreases with increasing pH. As in the ceria-silica case, an increase is seen at pH 10.5, which may be attributed to the enhanced silica dissolution kinetics in very basic media. Both Mahajan and Choi suggested the dominant interactions during silica-silica polishing are electrostatic in acidic to neutral pH conditions and enhanced indentation of the softened silica surface because of increased dissolution in basic pH conditions. Figure 5-12a clearly shows that ceria abrasives even at lower solids loading and applied pressure; possess some intrinsic properties that contribute to enhanced ceria-silica interactions that result in increased silica removal.

Figure 5-12b shows the measured friction force at the pad-wafer interface for both ceria and silica slurries. The silica data was obtained from Choi et al [Cho03, Cho04d]. Since, the silica particle size remains constant over the entire pH range, the silica-silica

in-situ friction force measurements are controlled by the electrostatic interactions and the dissolution of the silica surface. However, the ceria particles aggregate as the slurry pH approaches the IEP of ceria. Therefore, along with electrostatic interactions, silica surface dissolution, and the proposed ceria-silica chemical reaction; the change in particle size must be considered. The effect of particle agglomeration on the ceria-silica frictional forces was discussed earlier in this chapter. Perhaps the most interesting feature of figure 5-12b is the difference in the magnitude of the ceria and silica frictional forces at pH 5-6. The friction force value for ceria slurries is about 3 times that for silica slurries for pH 5-6. Frictional forces are a function of the contact area at the interface between the two opposing surfaces. If ceria-silica bonding does occur, the frictional forces should be enhanced. In fact, Cook suggested that frictional forces should be proportional to the fraction of the contact area in which bonding occurs [Coo90].

Summary

Ceria-silica interactions during CMP are strongly pH dependent. The rate of chemical reaction between the abrasives and the substrate, electrostatic interactions, the abrasive size because of agglomeration, and silica adsorption via ceria surface complexation may contribute separately or jointly to the observations in this work. The abrasive particle size along with the extent of electrostatic interactions between the abrasives and the silica surface affects the contact area. In-situ friction force measurements have demonstrated the effect of pH on both. Additionally, particle size and zeta potential measurements indicate dissolved silica is indeed adsorbed onto the abrasives during polishing. Furthermore, the additional chemical contribution for ceria slurries was demonstrated by comparing the silica removal rates and in-situ friction force responses as a function of slurry pH.

The results in this chapter may be interpreted as experimental proof of the validity of a portion of the chemical tooth theory that was first proposed for glass polishing [Coo90] and adapted to ceria-silica CMP [Oss02]. In accordance with prediction, the material removal rate is highest near the IEP of the abrasive particles. To this point, the central facet of all ceria polishing theories, the proposed particle-surface reaction, has not been verified. To determine the extent of the chemical reaction between ceria and silica and provide further interpretation of the results in this chapter, the next chapter's focus is silica surface analysis after CMP.

CHAPTER 6
NEAR SURFACE ANALYSIS OF POLISHED SILICA: CHARACTERIZATION OF THE CERIA-SILICA CHEMICAL REACTION

Introduction

Ceria CMP Models

A major feature of all ceria-silica chemical mechanical polishing (CMP) models: surface defect, chemical tooth, and particulate generation, is the belief in the existence of a chemical reaction between the ceria particle and the silica wafer [Coo90, Kal91, Kal98, Hos01]. The difference in the mechanisms is in the processes after ceria-silica contact. For the polishing model based on surface defects, Kaller stipulated that [Kal91, Kal98]:

1. The abrasive particles should be softer than the substrate
2. The abrasive is slightly worn away, which exposes high-energy defect sites abrasive-substrate bonding occurs
3. Material is removed on a molecular scale because of movement of the workpiece and subsequent rupture of the particle-substrate bonds
4. Portions of the substrate removed during CMP remain on the abrasive surface.

In his formulation, Kaller suggested intrinsic defects like oxygen vacancies did not contribute to the chemical reactivity of the abrasive particles; hence, their effect on the polishing process is negligible.

According to the chemical tooth model proposed by Cook [Coo90] and further developed by Osseo-Asare [Oss02], material removal during polishing is controlled by the interactions between surface functional groups at the abrasive and substrate surfaces. The relevant features of the chemical tooth model are:

1. Water initially penetrates the silica network.
2. Surface dissolution occurs because of simultaneous synergistic actions of hydrolysis and particle indentation.
3. The abrasive particle adsorbs the silica solute species.
4. The entire process is controlled by the respective surface charges.

Osseo-Asare further stipulated that the most favorable conditions for silica removal by ceria are met when the slurry pH is near the ceria IEP.

In the particulate generation model proposed by Hoshino et al, the ceria particles remove silica as discrete lumps or particulates. Infrared spectroscopy, electron microscopy, and x-ray microanalysis were used to characterize the size, shape, and chemical composition of the post-CMP slurry. According to the size analysis, 80 nm ceria particles and a 600 nm lump of silica was present after CMP. Additionally, the pH shifted from a pre-CMP value of 8 to 7.4 after CMP.

In the previous chapter the silica removal rate, friction force, and surface finish was shown to be strongly dependent on the ceria slurry pH. Also, the properties of the ceria dispersion are strongly pH dependent. The surface chemistry of ceria was correlated with the characteristics of the slurry (i.e. particle size, slurry stability, and zeta potential). To further develop our understanding of the ceria-silica polishing process, the surface chemical effects as a function of pH will be discussed in light of spectroscopic and microscopic analysis of polished substrates.

Recent Progress

There are few fundamental investigations into the properties of ceria for CMP applications. However, the increasing popularity of shallow trench isolation (STI) has stimulated interest in the fundamental polishing mechanisms. Also, re-examination of

earlier investigations from glass polishing have contributed to the understanding of ceria-silica interactions and are helpful in understanding the CMP mechanisms.

Sabia and Stevens determined separately the respective chemical, mechanical, and the chemical mechanical contributions to glass polishing using ceria abrasives [Sab00]. Sabia and Stevens assumed the material remove rate is just the summation of the respective contributions from the mechanical, chemical, and chemical mechanical portions. The chemical effect was studied by performing corrosion tests for 24 hours at 95^0C. The dissolved species from ceria slurries was used as a corrosive agent. No glass weight loss was detectable; therefore, Sabia and Stevens assumed there is no purely chemical contribution during ceria-silica polishing [Sab00]. The mechanical component of polishing was studied using ethanol-based ceria slurries. Ethanol has a similar viscosity (1.078 cP at room temperature) and dispersion performance as water. Substituting ethanol for water, Sabia was able to isolate the mechanical nature of the abrasive particles. The processing history (thermal treatments, milling, etc.) of the ceria abrasives significantly affected the mechanical interactions during polishing. According to their results, the particle size did not affect the mechanical interactions. The chemical mechanical component was extracted by subtracting the removal rate in the non-aqueous solution from the removal rate in water. Particle-substrate attraction dominated the chemical mechanical component of the overall polishing process [Sab00]. Sabia and Stevens concluded that contributions to the chemical mechanical component of polishing not related to surface charge or solubility are associated with mechanically induced particle-substrate interactions and interfacial chemical reactions [Sab00].

Kelsall [Kel98] and Sabia [Sab00] predicted that redox (reduction/oxidation) processes at the ceria particle surface contribute to the chemical reactivity of the ceria particles. CeO_2 has been shown to be thermodynamically unstable in aqueous environments [Pour66]. In light of Pourbaix's description, Kelsall predicted that ceria particles can be considered mixtures of the dominant Ce^{4+} and the reduced Ce^{3+} [Kel98]. Using electron energy-loss spectroscopy (EELS) in a field emission gun, scanning transmission electron microscope (FE-STEM), Gilliss et al. determined the valence state for single nanosized ceria particles [Gil04] by measuring several points from the center to the surface of the particle. The oxidation state of the cerium ion was determined from the ratio of the cerium white-line intensity (Ce M_5/M_4). The white-line intensity ratio of the Ce M_5/M_4 peaks was determined by taking the ratio of the sum of the intensities of the M_5 and M_4 white lines. The measurements (figure 6-1) show a gradual increase of the Ce M_5/M_4 ratio, from 0.85 to 1.1, with increasing distance from the particle center. The Ce $M_{4,5}$ edge occurs at the ionization threshold, which is approximately the binding energy of the 3d shell [Gil04]. These core-loss peaks are a result of the $3d^{10}4f^n \rightarrow 3d^9 4f^{n+1}$ transitions. CeO_2 (Ce^{4+}) is characterized by unfilled 4f states. The transition to Ce_2O_3 (Ce^{3+}) occurs with the production of oxygen vacancies and the localization of an electron in the 4f state [Sko02]. Therefore, during CMP, ceria particles should not be considered pure, stoichiometric CeO_2. Rather, the ceria particles consist of a mixed valence state of predominantly Ce^{4+} in the interior and Ce^{3+} at the surface.

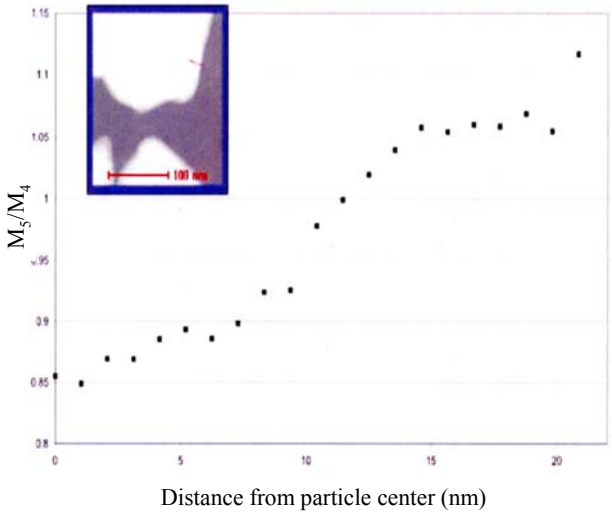

Figure 6-1 Ratio of Ce M_5/M_4 white lines versus position [Gil04].

Recently, Chandrasekaran reported the results of x-ray photoelectron spectroscopy (XPS) analysis of ceria particles after STI CMP of silica (SiO_2) and silicon nitride (Si_3N_4) wafers [Chan04]. The elemental composition before CMP and after CMP of oxide and nitride wafers was obtained from XPS data. As expected, no silicon was detected on the ceria particles before CMP. However, after oxide CMP, considerable Si was present (~ 14 at%). After 5 nanometers of sputtering, the silicon content decreased to ~ 12.20 at%, approximately equal to the cerium content (12.80 at%). Perhaps most interesting, was the XPS analysis of the ceria particles after nitride CMP. No silicon was detected after nitride CMP, even though the silicon to nitride ratio is 3:4.

Until recently, very little was known about the ceria-silica interactions that lead to material removal during CMP. In the past, the proposed chemical reaction between ceria and silica was supported by circumstantial evidence, at best. To understand the ceria-silica polishing mechanism, considerable attention has been focused on the ceria particles

themselves. For a complete understanding of the ceria-silica CMP process, it is necessary to understand the morphological changes of the substrate after polishing.

Experimental

The development of surface analytical tools with nanometer to atomic scale resolution has revolutionized materials characterization. Now, with these powerful techniques, theories originally proposed decades ago can be tested from a materialistic aspect. In this chapter, a combination of surface analytical methods was applied, in conjunction, to interpret the observations in Chapter 5. The characteristics of each measurement technique were described in detail in Chapter 3. If ceria-silica bonding is a reality, as many have asserted for years and recent results indicate; the silica surface should contain some residual cerium. Therefore, after CMP, XPS was used to analyze the silica substrates that were polished at pH 2.5, 3.5, and 6.0. The minimum and maximum removal rates and the silica and ceria IEP is near pH 2.5 and 6.0, respectively. An aluminum anode (1483.6 eV), was used for x-ray generation. To ensure the XPS results were not distorted because of residual ceria particles, field emission scanning electron microscopy (FE-SEM) was conducted.

The atomic force microscope (AFM) may be used for topographical, force, and wear measurements. The AFM can be further functionalized by depositing desired coatings on the atomically sharp cantilevers. Tapping mode cantilevers fabricated from silicon and supplied by Digital Instruments were thermally oxidized. The oxidation was conducted at 1000^0 C for 2 hours. The cantilevers were then furnace cooled. The silica-coated cantilevers abraded the ceria film for 30 minutes at pH 2.5, 4.5, 6.0, and 11.0. To minimize the sliding speed and to avoid re-tracing of the wear track, a 50 μm scan size was used and the scan rate was 0.1 Hz. The interaction force was measured using a 7.3

μm silica particle and a ceria thin film that was deposited using pulsed laser deposition (PLD). The silica particle was attached to the long, thick silicon nitride cantilever (spring constant k = 0.13). The silicon nitride cantilevers are commonly used for contact mode topographical imaging. Further confirmation of the friction force and zeta potential measurements was obtained via AFM

Results and Discussion

Interaction Force Measurements

The forces relevant to AFM are ultimately of electromagnetic origin [Gar02]. In the case of CMP, different inter-particle, surface, and environmental effects give rise to specific interactions that are strongly distance dependent. The sum of the forces (F_{total}) acting on an AFM tip or particle in this case is the summation of the long-range and short-range interactions [Gar02].

$$F_{total} = F_{electrostatic} + F_{van\ der\ Waals} + F_{chemical} \qquad (6.1)$$

Where $F_{electrostatic}$ refers to the long range interactions related to charge on the opposing surfaces, $F_{van\ der\ Waals}$ refers to bonding that occurs because of interactions of fluctuating dipoles, and $F_{chemical}$ refers to the short-range binding forces typical of chemical bonds. Using a liquid cell filled with a solution of desired chemistry, non-contact AFM force measurements are possible. DI water solutions were formulated at the desired pH values using KOH and HCl. Interaction forces are measured by monitoring the displacement of the AFM cantilever as it approaches the surface. For strongly adhering surfaces, hysteresis is seen in the approaching and attracting force versus distance curves.

Figure 6-1 shows the force versus distance curves for the respective pH conditions (2.5, 4.5, 6.0, and 10.5). The force was normalized by the particle radius. At pH 2.5 there is only a slight, short range attraction that occurs at separation distances less than 5 nm.

As expected, the dominant interaction between the silica particle and the ceria thin film is electrostatic and occurs at pH 4.5. This measurement agrees well with the zeta potential, friction force, and qualitative estimation of the extent of the electrostatic interactions via the product of the ceria and silica zeta potentials discussed in Chapter 5. A moderate attraction also exists at pH 6.0. In basic pH conditions the ceria-silica electrostatic interactions are entirely repulsive.

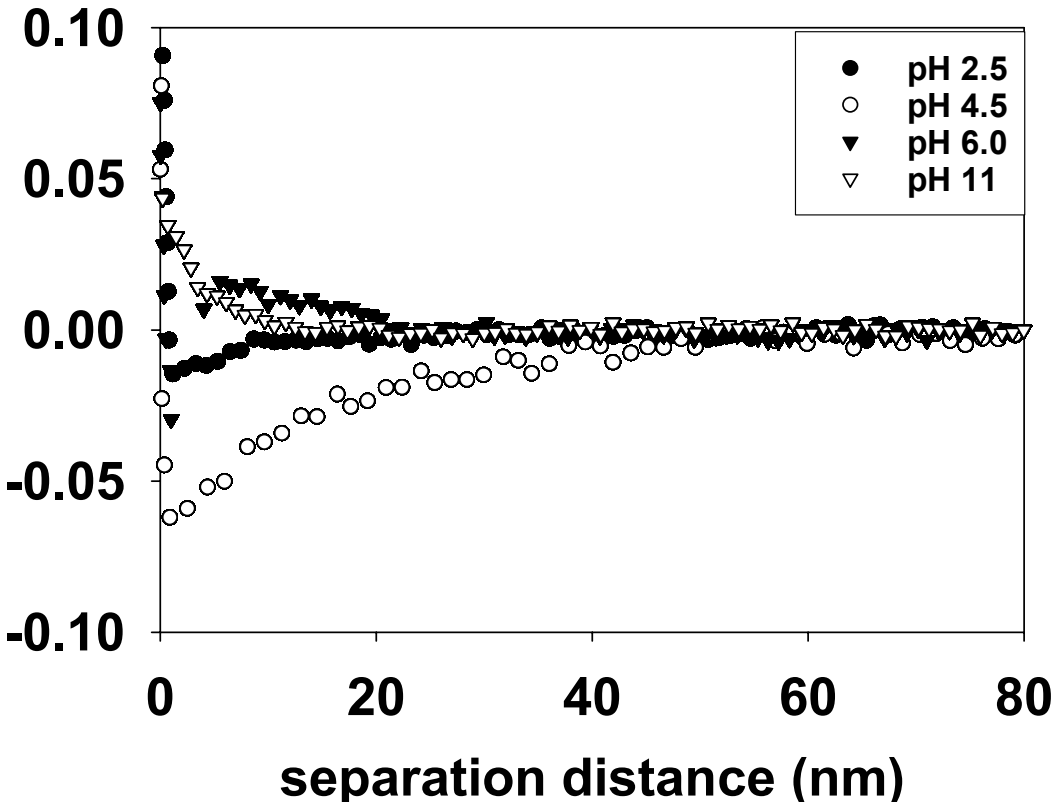

Figure 6-2 Interaction force measurements, the retracting portion of the curve: force versus separation distance for a ceria thin film and silica particle at different pH values.

XPS Analysis

Because of its sensitivity to local atomic bonding, XPS was used to probe the surface region of the polished substrates. The surface sensitivity of XPS is due to the shallow

escape depth of the photoelectrons. Information is obtained from only the first few atomic layers. The concentration of chemical species on the surface may be determined by comparing the relative peak intensities of the constituent elements at their respective atomic binding energies. The as-received silica sample shows the presence of Si, C, and O atoms (figure 6-3a). The adventitious C 1s peak can be used for calibration of the atomic binding energies, i.e. for correction of peak shifting because of charging. Figure 6-3b shows a typical XPS spectrum of the silica substrate after polishing at pH 6.0 along with a plot of Ce content (at%) versus polish pH (6-3c). The Ce 3d peak after polishing at pH 6.0 is also presented (figure 6-3d). In comparison to the Si, C, and O photoelectron peaks, the Ce peak is relatively broad and of low intensity. The most intense Ce photoelectron peak is expected at 882 eV for Ce $3d^5$. The atomic bonding energies of Si $2p^3$, Si 2s, C 1s, O 1s, Ce $3d^5$, and Ce $3d^3$ are: 107.5, 158.5, 289, 537, 889, and 907.5. Ce (< 1 at %) is detected on all silica samples analyzed with XPS (pH 2.5, 3.5, and 6.0).

Table 6-1 shows the binding energies for the XPS peaks as a function of polishing condition. As shown in figure 6-3c, silica polished at pH 6.0 contained the most residual cerium. In the as received silica sample, the C 1s peak is shifted more than 3 eV. With a correction for charging, the XPS peaks for the as received silica samples are in agreement with well-known standards [Mou95]. The XPS peaks for the samples polished with ceria slurries at different pH values are shown in table 6-1. The binding energies of the peaks of interest occur at virtually identical positions for the samples polished at pH 2.5, 3.5, and 6.0. However, a difference of 1-1.5 eV exists in the binding energy of the Si $2p^3$ peak for the as received and polished silica samples. This discrepancy may be attributed to increased charging of the polished silica samples, which is confirmed by the higher

binding energy of the C 1s peak for samples after CMP. The 3d peak (figure 6-3d), the most intense in the Ce series, was the only XPS peak attributed to cerium surface species. If we assume uniform charging, the actual position of the Ce $3d^5$ peak is 884-885 eV, which is still considerably higher than the expected position for CeO_2. The closest matching ceria peak occurs at 883.6 for Ce_2O_3, which suggests the cerium compound is a reduced form of ceria. So, is this surface species particle contamination or a layer of ceria that has formed during polishing?

Table 6-1 XPS binding energies for silica samples before and after polishing with ceria slurries at different pH.

XPS peaks	As received	pH 2.5	pH 3.5	pH 6.0	Standard
Si $2p^3$	106.55	107.5	108	107.5	103.3, 103.6 ***SiO_2***
C 1s	288	288.5	289.5	289	284.6
O 1s	536	536.5	537	536	529.2 ***CeO_2*** 532.5 ***SiO_2***
Ce $3d^5$	_____	889	888.5	889	881.8, 882.4 ***CeO_2***

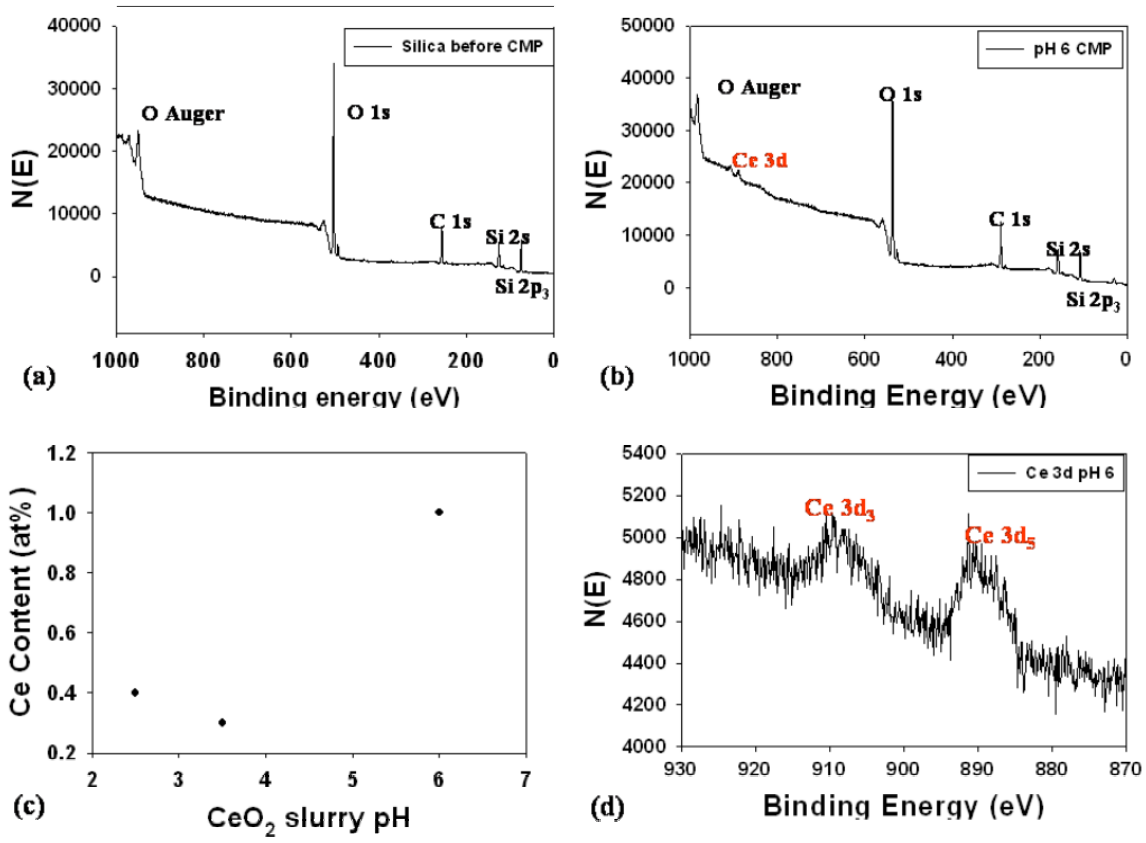

Figure 6-3 XPS analysis: a) silica before CMP b) silica after polishing at pH 6.0 c) Ce content versus polish pH d) Ce 3d peak after polishing at pH 6.0.

FE-SEM Analysis

To answer this question a FE-SEM equipped with an energy dispersive spectrometer (EDS) for chemical analysis was used to image the surfaces polished at pH 2.5 and 6.0. In figure 6-4a, what have been termed cerium rich 'island' type structures are clearly evident. EDS confirms that the "islands" are actually cerium-rich, figure 6-4b. Particle contamination was not detected at pH 6.0. However, at pH 2.5, figure 6-4a shows an interconnected network of particles on the silica surface. The island-like cerium-rich regions were also found on the silica substrate polished at pH 2.5. The EDS spectrum at pH 2.5 confirms the particles are ceria, figure 6-5b. The IEP of silica is near pH 2.5. Therefore, the silica surface is predominantly neutral. This may indicate adsorption as

predicted by Osseo-Asare. However, in this case the silica surface serves as the adsorbent and the abrasive particle is the adsorbate. Interestingly, a non-uniform coating, which may be dissolved silica, is present on the abrasive particles (Figure 6-5b). EDS results indicate only a small amount of cerium can be found on the surfaces of the polished substrates for both pH conditions, which is in agreement with the XPS elemental analysis.

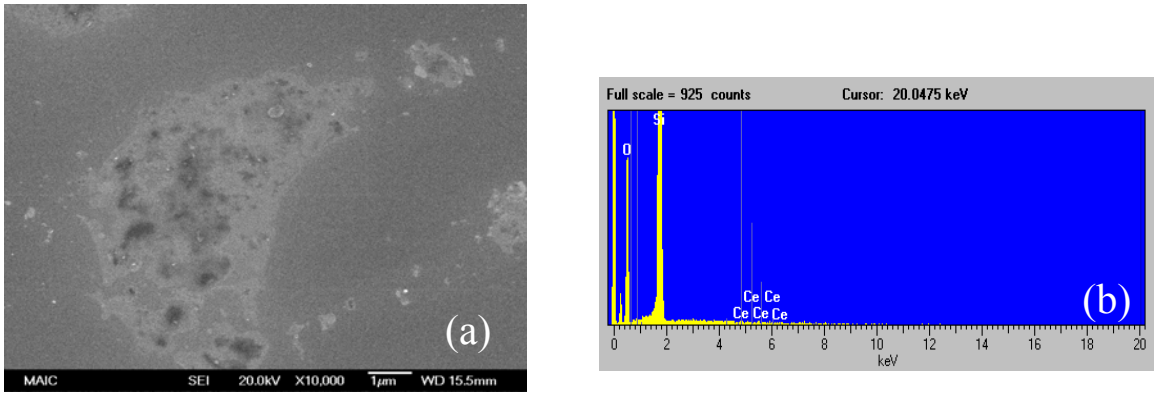

Figure 6-4 FE-SEM analysis of silica polished at pH 6.0: a) SEM image showing Ce-rich 'islands' b) EDS spectrum.

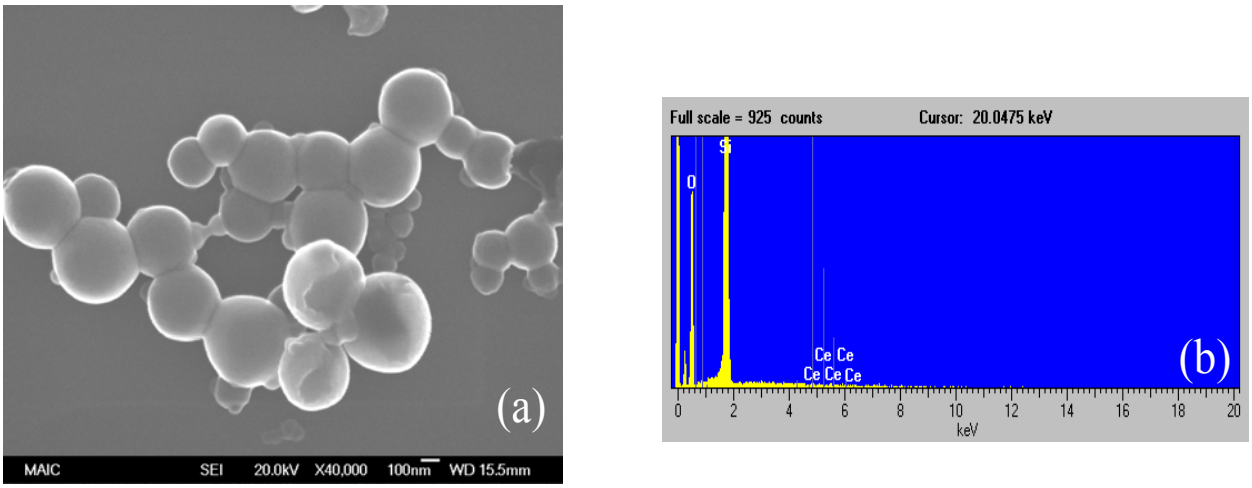

Figure 6-5 FE-SEM analysis of silica polished at pH 2.5: a) SEM image showing CeO_2 agglomerates b) EDS spectrum.

Wear with Silica-Coated AFM Cantilevers

During CMP, there are many complicated phenomena that determine the overall CMP performance. This is especially true for CMP using ceria-based slurries. Mechanistic studies to elucidate CMP polishing fundamentals are simplified when issues like slurry dispersion and polishing pad effects can be isolated. To further understand the silica-ceria CMP mechanism, wear measurements were conducted at several pH values using silica coated cantilevers and a ceria thin film. SEM image and compositional analysis was conducted before and after wear of each tip at every pH condition. With this approach, the ceria-silica interactions can be studied in the absence of complicating factors that are inherent to the CMP process. Figure 6-6 (a-d) shows the result of wear experiments conducted at pH 2.5. Figure 6-6a shows the silicon cantilever after thermal oxidation and 6.6b is an SEM image after wear for 30 minutes. Figures 6-6c and 6-6d are the EDS spectra before and after wear at pH 2.5. The tip shape is distinctly changed by the cantilever-film abrasion. The tip shape has changed from extremely sharp to blunted, which indicates the silica coating was worn away during abrasion. This is confirmed by EDS, which shows the O to Si ratio is decreased from stoichiometric silica to a nearly 1:1 ratio.

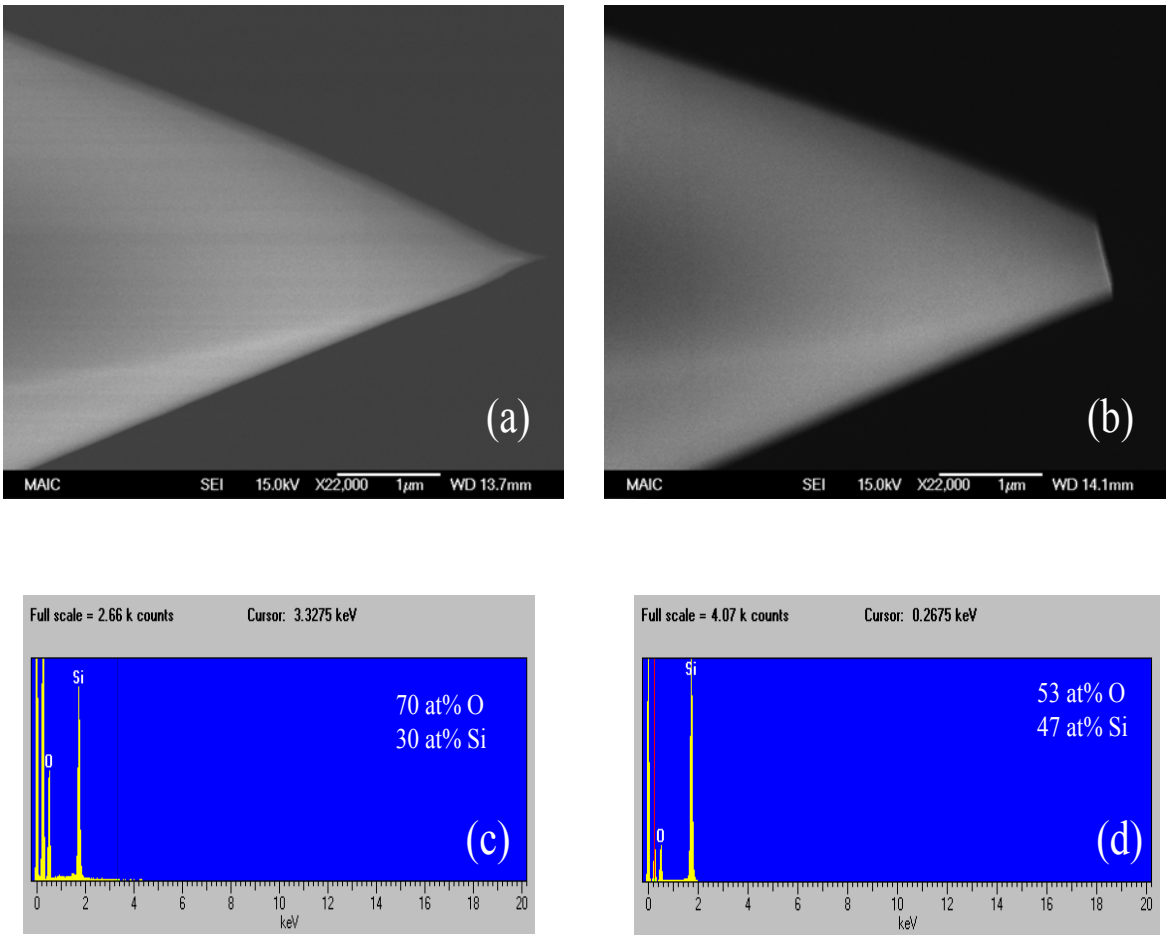

Figure 6-6 Cantilever-film wear at pH 2.5 a) tip after thermal oxidation b) tip after wear against ceria thin film c) EDS spectra of oxidized tip before wear d) EDS spectrum of oxidized tip after wear.

Figure 6-7 (a-b) shows the silicon cantilever before and after wear at pH 4.5 along with the respective EDS spectra (figure 6-7c and 6-7d). Similar to the pH 2.5 case, the tip is blunted after wear at pH 4.5. However, the EDS spectra are significantly different. After wear at pH 2.5, the O content decreased and the Si content increased, which indicates the oxide layer is being removed exposing the Si cantilever. However, after wear at pH 4.5 the Si content decreased and the O content increased (figure 6-7d). Visual inspection of figures 6-6b and 6-7b indicate that wear at pH 4.5 is greater than at pH 2.5, despite the EDS results. This result is in quantitative agreement with the polishing results discussed in chapter 5. The removal rate increases significantly

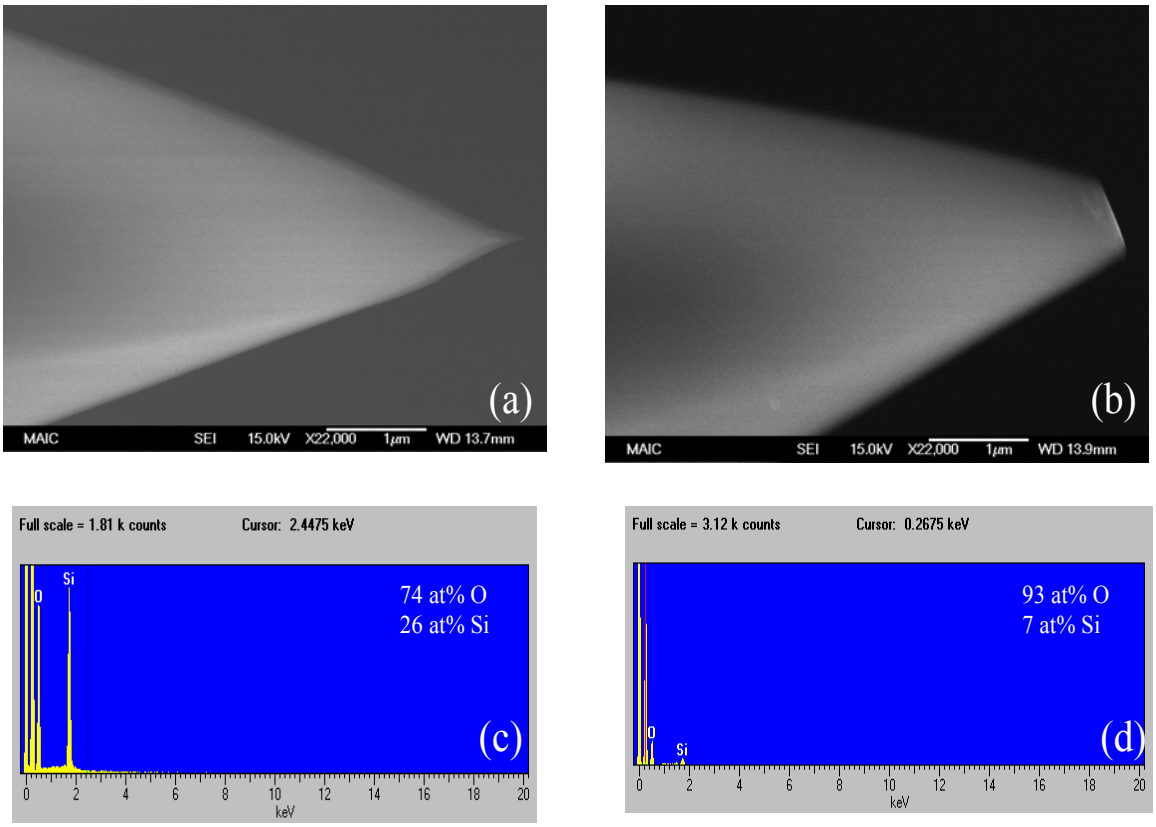

Figure 6-7 Cantilever-film wear at pH 4.5 a) tip after thermal oxidation b) tip after wear against ceria thin film c) EDS spectra of oxidized tip before wear d) EDS spectrum of oxidized tip after wear.

Figure 6-8 (a-d) shows the result of image and compositional analysis after wear at pH 6.0. Again, tip blunting is observed. The EDS spectrum in this case shows a considerable amount of cerium after wear (figure 6-8d). Also, debris or what appear to be particulates are present after abrasion (figure 6-8b). Hence, the ceria-silica reaction is unambiguously confirmed. The ceria thin film is the only source of Ce. Figure 6-9 shows the wear result for pH 11. Similar to the pH 4.5 result, the O content increased while the silicon content decreased after wear. Tip wear at pH 11 is most extensive. This may be because of the enhanced silica dissolution in highly basic pH conditions.

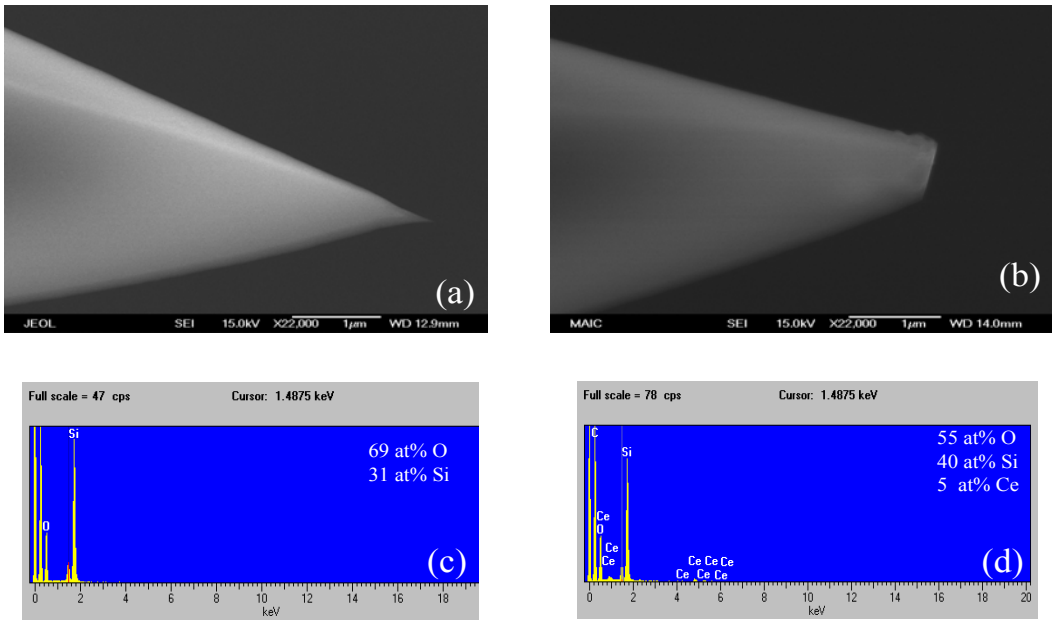

Figure 6-8 Cantilever-film wear at pH 6.0 a) tip after thermal oxidation b) tip after wear against ceria thin film c) EDS spectra of oxidized tip before wear d) EDS spectrum of oxidized tip after wear.

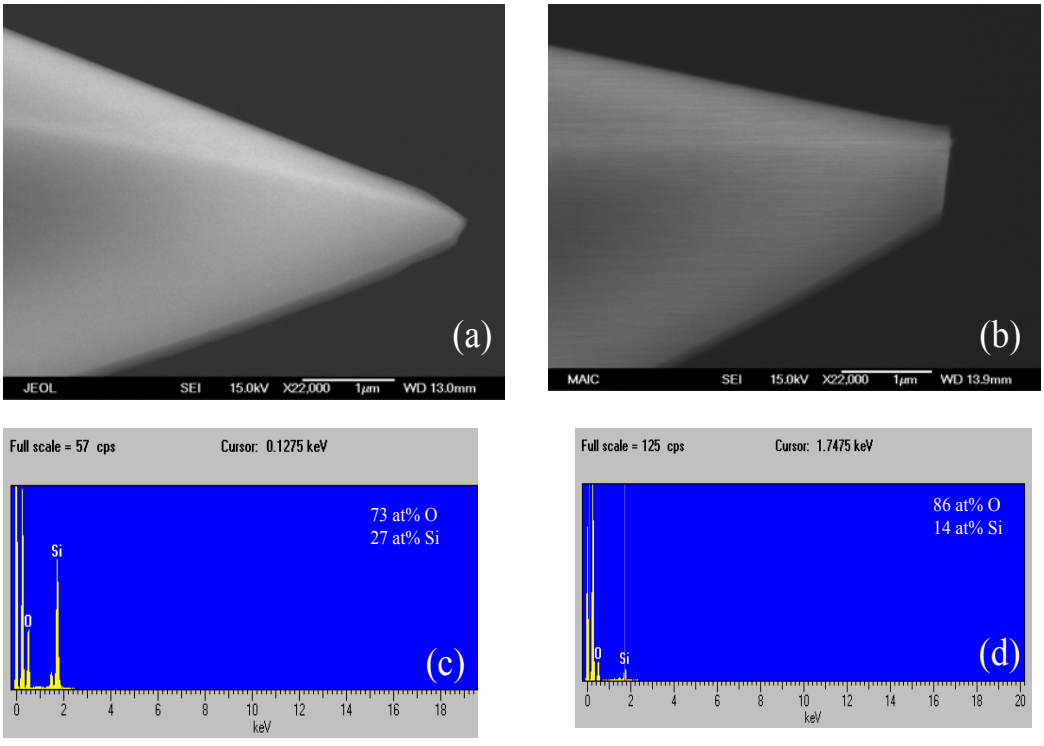

Figure 6-9 Cantilever-film wear at pH 11.0 a) tip after thermal oxidation b) tip after wear against ceria thin film c) EDS spectrum of oxidized tip before wear d) EDS spectrum of oxidized tip after wear.

Figure 6-10 (a-c) shows the tip wear against silica substrates under the same experimental conditions as the ceria-silica wear. This result demonstrates the effect of pH on silica dissolution. The debris present in figure 6-10a is likely dust or some other contaminant, compositional analysis indicated that no silicon or cerium species were present. The silica-silica wear changes from mechanical to chemical plus mechanical as the pH is increased. The wear at pH 11 is significantly greater than in the acidic pH regimes. As in the ceria-silica case the highest wear occurs at pH 11.

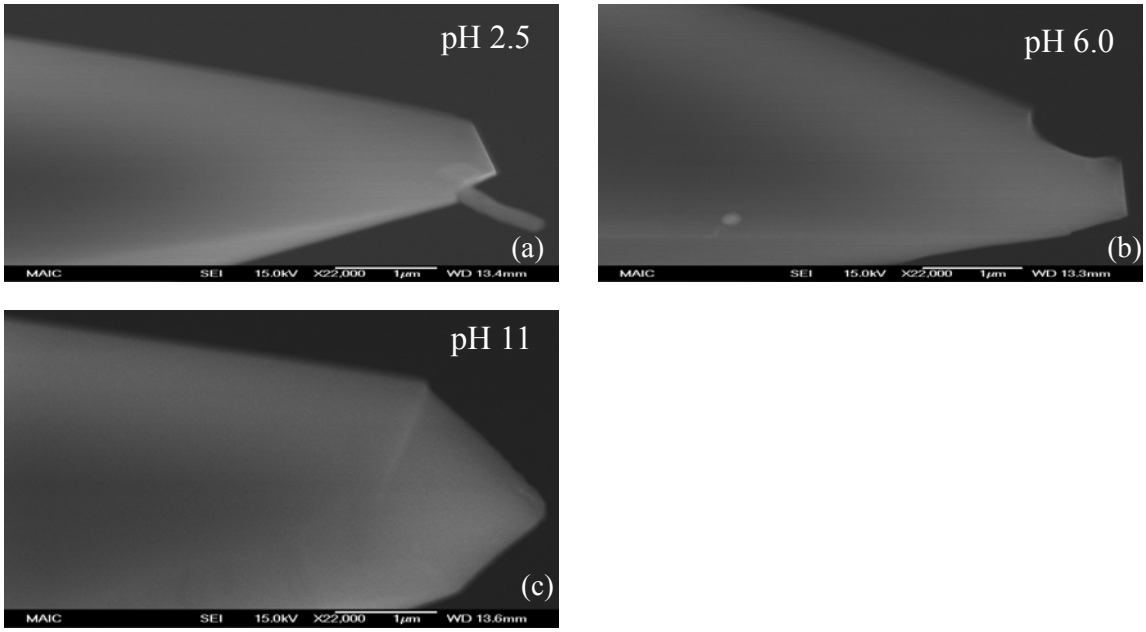

Figure 6-10 Cantilever wear against a silica substrate a) pH 2.5, b) pH 6.0, c) pH 11.

Summary

The proposed ceria-silica chemical reaction was verified using XPS, SEM, and AFM measurements. Force measurements were conducted with a ceria thin film deposited by PLD and a silica particle using an AFM. The most extensive interaction was electrostatic in nature and occurred at pH 4.5. This is in agreement with the measurements of zeta potential and friction force and the semi-quantitative predictions

based on the product of the ceria and silica zeta potentials presented in Chapter 5 of this work.

XPS analysis indicates that the most extensive reaction occurs at pH 6.0, which is the pH that gave the highest silica removal rate. To ensure that the cerium species were not from residual particles, SEM analysis was conducted on the polished samples. Surprisingly, cerium-rich, island-type structures were found scattered on the silica surface. At pH 2.5, a small contribution to the cerium signal was due to the presence of residual cerium particles.

The ceria thin films were also used to compare the wear of silica coated AFM cantilevers at pH 2.5, 4.5, 6.0, and pH 11.0.Thermally oxidized AFM cantilevers were rastered against ceria thin films and silica substrates in various pH environments. SEM image and compositional analysis was conducted after cantilever-film abrasion. For all conditions, the tip assumed a blunted appearance from the original sharp shape. Ce was only detected at pH 6.0. Also, the most extensive tip wear occurred at pH 11.0. In the case of silica-silica, the tip shape indicates a transition from primarily mechanical to chemically-assisted wear at high pH.

CHAPTER 7
SUMMARY, CONCLUSIONS, AND SUGGESTIONS FOR FUTURE WORK

Summary

The continued miniaturization of microelectronic devices requires tighter control of the chemical mechanical polishing (CMP) process. Also, the implementation of CMP in the manufacturing process of other areas like shallow trench isolation (STI), micro electromechanical systems (MEMS), and flat panel displays requires a new set of CMP consumables (pads, polishers, slurries, etc.). To meet the stringent planarity requirements of these novel processes, the fundamental interactions at the pad-slurry-wafer interface must be understood. This is especially critical in STI CMP.

The STI CMP process requires the global planarity of conventional interlevel dielectric (ILD) CMP, with the additional complication of preferential polishing of oxide layers to nitride or polysilicon. The factors that control oxide erosion, nitride overpolishing, particulate residue, and other sources of defectivity (surface scratches from particles or pad) must be known and eliminated. Traditionally, this has been accomplished by altering the chemistry of the polishing slurry. Ceria-based slurries and fixed abrasive pads, which consist of ceria abrasives surrounded by a polymeric material, are two proposed solutions for STI CMP. Therefore, the most critical interactions during STI CMP occur at the ceria-silica interface. A thorough understanding of the mechanisms at the particle-substrate interface will allow tighter control of the STI CMP process. The ceria-silica interactions that determine the output of the CMP process are reported.

Chapter 1 started the dissertation with the motivation for implementation of CMP in integrated circuit (IC) manufacturing. The growth of CMP to other areas like STI, were also discussed. In Chapter 2, the current understanding of the CMP process was summarized. This chapter also included a basic description of the multilevel metallization process that is critically dependent on CMP. Silica CMP may be considered a specialized form of glass polishing. Hence, glass polishing mechanisms were reviewed. For silica-silica CMP, the effect of particle size, concentration, and particle size distribution on the silica removal rate and surface finish was covered. The basics of shallow trench isolation along with three proposed models for ceria-silica CMP were detailed. Chapter 2 ended with a discussion on the ceria surface chemistry. Chapter 3 detailed the materials and methods used in this work.

In Chapter 4 the effect of pressure, pH, and velocity were studied using statistically based experimental methods based on the Box Behnken design. There are more than forty variables, effects, and output parameters involved in CMP process design. It is impossible to investigate the effects of each simultaneously, using conventional experimental techniques. Statistically based experimentation allows prediction of the optimum combination of the respective variables for the desired performance. Furthermore, mutual or joint effects can be examined with statistically based techniques that are not readily apparent in laboratory experiments. The optimum removal rate and surface finished was found to be strongly dependent on the slurry pH and rotational velocity of the polisher. The pressure effect on the removal rate was slight. However, the applied pressure has a pronounced effect on the surface finish.

A major feature in all ceria-silica polishing models is the proposed chemical reaction between the abrasive particles and the silica substrate. The chemical tooth theory is the most widely accepted model to explain the removal of silica by ceria. In this formulation, the polishing performance is controlled by the interactions between surface functional groups on the abrasive and substrate surface. To date, no experimental evidence has been provided in support of this proposed mechanism. There is also a lack of fundamental studies on ceria-silica polishing. In Chapter 5, the effect of pH on the silica removal rate, friction force, and surface morphology was studied. The removal rate, friction force, and surface roughness are dependent on the slurry pH, with the maximum removal rate occurring just below the isoelectric (IEP) point of ceria. A qualitative comparison of the extent of the electrostatic interactions was obtained by analyzing the product of the ceria and silica zeta potentials at various pH values. The maximum in friction force occurred in the pH range wherein the electrostatic attraction was most extensive. Zeta potential and particle size analysis of the post-CMP slurry indicated the ceria abrasives adsorb silicate species during polishing. The effect of pH on the ceria surface chemistry was correlated with the CMP observations.

In Chapter 6, the silica substrates polished with ceria slurries at different pH values were examined by x-ray photoelectron spectroscopy (XPS), field emission scanning electron microscopy (FE-SEM), and atomic force microscopy (AFM). If the ceria particle indeed reacts with the silica substrate during polishing, residual cerium should be present on the silica surfaces after CMP. XPS analysis determined ceria was present on the surface after polishing. To ensure the residual cerium was not because of particulate impurities, FE-SEM analysis was conducted. At both pH 2.5 and pH 6.0, isolated patches

termed cerium-rich ‘islands’ were found on the silica substrates. Elemental analysis by XPS and energy dispersive spectroscopy (EDS) indicated the most cerium, and therefore, the most extensive ceria-silica reaction was at pH 6.0.

To understand the ceria-silica polishing mechanisms, a ceria thin film deposited by pulsed laser deposition and thermally oxidized silicon cantilevers were used for wear measurements as a function of pH. The cantilevers were rastered against the ceria thin film at pH 2.5, 4.5, 6.0, and pH 11.0. These measurements provide further confirmation of the ceria-silica polishing mechanism. From the change in cantilever shape and composition as measured by EDS, the abrasion mode is similar at all pH values. However, at pH 6.0, residual cerium was detected on the cantilever tip. The presence of cerium in the absence of particles confirms the ceria-silica reaction indeed occurs.

Conclusions

Three models have been proposed for ceria-silica polishing: chemical tooth [Coo90, Oss02], surface defects [Kal91, Kal98], and particulate generation [Hos01]. In light of these findings, it seems Cook’s model provides the most accurate description of the ceria-silica polishing mechanism. The existence of a chemical reaction between the ceria particle and the silica surface has been confirmed, which was predicted in all three models. Zeta potential measurements of the post-CMP slurry indicate that a ceria-silicate surface complex indeed forms, which was predicted by the chemical tooth theory. And electron microscopy has confirmed the existence of Ce^{3+} ions at the ceria particle surface [Gill04], which are formed by reduction of the Ce^{4+} ions. The conversion of Ce^{4+} to Ce^{3+} ions is facilitated by the formation of oxygen vacancies [Sko02]. The reduction of ceria may be the driving force for the solid-state ceria-silica reaction. Particle size

measurements indicate that silica is accumulated on the ceria particles as predicted by the particulate generation mechanism.

Several ceria-silica interfacial phenomena are considered to contribute to the ceria-silica CMP mechanism: the extent of chemical reaction between the abrasives and the substrate, the magnitude of electrostatic interactions, the change in particle size with slurry pH, and surface chemical phenomena due to ceria surface properties, which lead to the formation of a ceria-silica complex. The enhanced polishing of silica by ceria may be explained in three ways. Figure 7-1 shows the silica polish rate along with schematic diagrams for the three mechanisms (chemical or dissolution, surface chemical or physicochemical, and/or mechanical) that may control the silica removal rate.

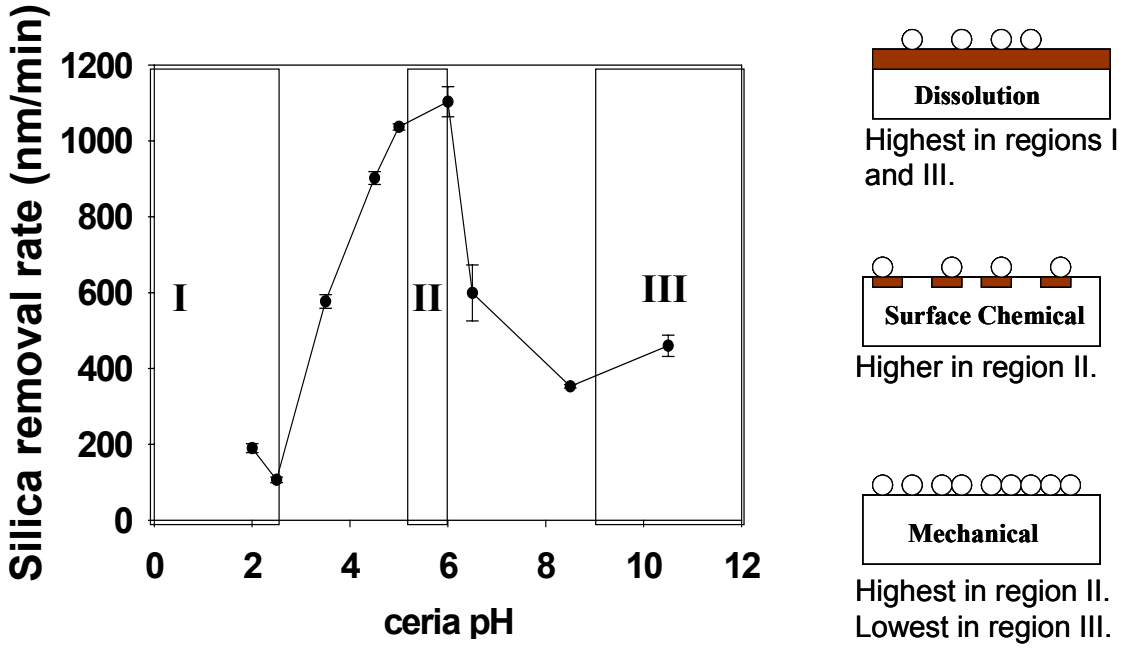

Figure 7-1 Schematic depiction of pH-dependent ceria-silica removal mechanism.

In the chemical mechanism (top schematic in figure 7-1), ceria-silica bonding results in dissolution of the silica substrate similar to the dissolution of silica by water in very acidic media. The AFM wear measurements presented in chapter 6 indicate ceria does not chemically modify silica. Therefore, any dissolution of the substrate may be

attributed to the slurry pH during polishing. Silica dissolution is expected to be highest in very basic or acidic media (regions I and III in figure 7-1). In the surface chemical mechanism, ceria-silica bonding results in increased shear at the abrasive-substrate interface, which leads to higher removal rates. The reactivity of the ceria particles results in an enhancement of the mechanical contribution to polishing. According to the results of this work, the surface chemical mechanism predominates in region II, the area of maximum polishing. Finally, because of particle instability and enhanced abrasive-substrate interaction, a purely mechanical mechanism is possible in which the increased number of abrasives available for polishing are responsible for the enhanced polishing rate. Mechanical contributions are expected to be highest in region II because of slurry instability and lowest in region III because of repulsive electrostatic interactions. Even for reactive abrasive particles like ceria, dielectric CMP is primarily mechanical in nature.

Suggestions for Future Work

STI CMP will continue to be a fertile research area for the foreseeable future. The efforts in this study can be further extended by studying the effect of ceria particle size on the silica removal rate, friction force and surface morphology. The ceria-silicon nitride interactions are also important for STI CMP and should be studied. To enhance selectivity, the nitride removal rate should be low with respect to the oxide. This can be accomplished by inhibiting the abrasive-nitride interaction. Surfactant-based slurries are currently in development for STI CMP. However, the fundamentals of surfactant adsorption are not well understood. By studying surfactant-nitride bonding, mechanisms of surfactant adsorption can be understood. Fourier transform infrared spectroscopy (FTIR) is a surface sensitive technique that identifies chemical bonding. FTIR is a

promising, well understood technique for in-situ characterization of surfactant adsorption on nitride surfaces. The possibility of reduced defectivity is an additional benefit of surfactant-based slurries.

To tailor surfactant adsorption for desired STI CMP performance, an understanding of the silicon nitride surface layer properties is required. The slurry chemistry can then be tailored to inhibit the surface modification process that favors nitride removal over nitride passivation. Recent studies have suggested that conversion of the nitride to an oxide layer is required for chemically assisted removal of the nitrides surface. Along with FTIR, spectroscopic ellipsometry and nano-indentation are ideal techniques for determining surface layer chemical and mechanical properties. This information is valuable for STI CMP with ceria-based slurries and fixed abrasive pads.

Although ceria-based slurries have many promising attributes, STI polishing processes that utilize fixed abrasive pads seem most promising. Further research into the morphology of the abrasive-polymer composite is needed. Also since slurry stability is not a concern with fixed abrasive pads, more extensive investigations into pH and chemical additive effects can be conducted. The proposed studies in the two preceding paragraphs are also directly applicable to STI CMP with fixed abrasive pads.

APPENDIX A
DEFINITION OF COMMON STATISTICAL TERMS [MAS89]

Block – group of homogeneous experimental units.

Confounding – one or more effects that can not be unambiguously attributed to a single factor

Contour plot – series of lines or curvew that identify values of the factorfor which the response is constant

Covariate – an uncontrollable variable that influences the response but is unaffected by any experimental factors

Design – complete specification of experimental test runs, including blocking, randomization, repeat tests, replication, and assignment of factor-level combinations to experimental units

Effect – change in the average response between two factor-level combination or between two experimental conditions.

Factor – a controllable experimental variable that is thought to influence the response

Homogeneous experimental units – are as uniform as possible on all characteristics that could affect the response

Interaction – existence of joint effects in which the effect of each factor depends on the levels of the other factors.

Level – specific value of a factor

Repeat tests – two or more observations that have the same levels for all factors

Replication – repetition of an entire experiment or a portion of an experiment under two or more sets of conditions

Response – outcome or result of an experiment

Response surface – geometric representation obtained when a response variable is plotted as a function of one or more quantitative factors.

Test run – single combination of factor levels that yields an observation on the response

Unit – entity on which a measurement or an observation is made

APPENDIX B
BOX BEHNKEN DESIGN AND RESPONSES

Experimental variables:

A: Pressure (2-10 psi)

B: pH (2-6)

C: Rotational velocity (75-150 RPM)

Responses:

Silica removal rate (RR) nm/min

RMS surface roughness (nm)

$$RR = 436.0 + 141.0 * A + 139.13 * B + 151.13 * C + 47.50 * A^2 - 29.75 * B^2 * - 94.25 * C^2 + 71.25 * A*B + 83.25 * A * C + 213.0 * B* C$$

$$\text{RMS roughness} = 0.31 + 0.21 * A + 0.16 * B – 0.019 * C + 0.25 * A^2 + 0.21 * B^2 + 0.047 * C^2 – 0.16 * A *B + 0.10 * A * C.$$

Table B-1 Box Behnken design for three factor experiment.

Std	Run	Factor A Pressure (psi)	Factor B pH	Factor C Velocity (RPM)	Response RR (nm/min)	Response RMS (nm)
5	1	2	4	75	180	0.5
14	2	6	4	112.5	440	0.3
11	3	6	2	150	90	0.35
12	4	6	6	150	810	0.8
7	5	2	4	150	342	0.2
10	6	6	6	75	108	0.7
15	7	6	4	112.5	438	0.32
2	8	10	2	112.5	405	0.95
9	9	6	2	75	240	0.4
4	10	10	6	112.5	810	0.9
13	11	6	4	112.5	430	0.3
3	12	2	6	112.5	360	0.9
6	13	10	4	75	270	0.8
1	14	2	2	112.5	240	0.3
8	15	10	4	150	765	0.9

LIST OF REFERENCES

Adl01 J. J. Adler, *Interactions of Non-Ideal Surfaces in Particulate Systems*, Ph.D. Dissertation, University of Florida, Gainesville, Fl., (2001).

Bas00 G. B. Basim, et al., *J. of Electrochem. Society,* **147,** (2000), p. 3523.

Bas02a G. B. Basim, *Formulation of Engineered Particulate Systems for Chemical Mechanical Polishing Applications*, Ph.D. Dissertation, University of Florida, Gainesville, Fl., (2002).

Bas02b G. B. Basim and B. M. Moudgil, *J. of Colloid and Interface Science*, **v256**, (1), (2002), p. 137.

Bas03 G. B. Basim, I. Vakarelski, and B. M. Moudgil, *J. of Colloid and Interface Science,* **v263**, (2003), p. 506.

Bas03b G. B. Basim, S. C. Brown, I. U. Vakarleski, and B. M. Moudgil, *J. of Dispersion Science and Technology*, **v24**, (3&4), (2003), p. 499.

Bey00 K. Beyer, *Future Fab Intl.*, **v9**, (2000).

Bie98 M. Bielmann, *Chemical Mechanical Polishing of Tungsten,* Master's Thesis, University of Florida, Gainesville, Fl., (1998).

Bin92 J. B. Bindell, in *Encyclopedia of Materials Characterization*, edited by C. R. Brundle, C. A. Evans Jr., and S. Wilson, Butterworth-Heinemann, Boston, (1992), p. 699.

Biz04 San Jose/Silicon Valley Business Journal, http://sanjose.bizjournals.com/sanjose/stories/2004/08/30/daily2.html Last visited 10/16/04.

Box78 G. Box, W. Hunter, and J. Hunter, *Statistics for Experimenters*, Wiley and Sons, New York, (1978).

Bro81 N. J. Brown, P. C. Baker, and R. T. Maney, *Proc. SPIE,* **v306,** (1981), p. 42.

Bro84 N. Brown and L. Cook, *Tech. Digest,* Topical Meeting on the Science of Polishing, Optical Society of America, (1984), paper TuB-A4.

Bru92 C. R. Brundell, in *Encyclopedia of Materials Characterization*, edited by C. R. Brundle, C. A. Evans Jr., and S. Wilson, Butterworth-Heinemann, Boston, (1992), p. 282.

Bud61 S. M. Budd, *Phys. Chem. Glasses*, **v2**, (1961), p. 111.

Chan04 N. Chandrasekaran, *Mat. Res. Soc. Symp.*, **v816**, (2004), p. K9.2.1.

Che97 Y. L. Cheng et al., *J. of Electrochem. Soc.*, **v144**, (1), (1997), p. 315.

Chen00 Z. Chen, *Silicon Wafer–Contaminant Interactions in Dilute Hydroflouric Acid Solutions and Related Fundamentals in Colloid and Interface Science,* Ph.D. Dissertation, University of Florida, Gainesville, FL, (2001) p. 32.

Chen03 Z. Chen, and R. K. Singh, *J. Electrochem. Soc.*, **v150**, (11), (2003), p. G667.

Cho01 W. Choi, S-M, Lee, and R. K. Singh, *Mater. Res. Soc. Symp. Proc.,* **v671**, (2001), p. M5.

Cho03 W. Choi, *Study of Interfacial Interactions During Chemical Mechanical Polishing (CMP) of Dielectric Silicon Dioxide*, Ph.D. Dissertation, University of Florida, Gainesville, Fl., (2003).

Cho04a W. Choi, et al., *J. of Electrochem. Soc.,* **v151,** (3), (2004), p. G185.

Cho04b W. Choi, et al., *J. of Electrochem. Soc.,* **v151,** (5), (2004), p. G368.

Cho04c W. Choi, et al., *J. of Electrochem. Soc.,* **v151,** (8), (2004), p. G512.

Cho04d W. Choi, et al., *Electrochem. and Solid-State Letters.,* **v7,** (7), (2004), p. G141.

Coo90 L. M. Cook, *J.l of Non-Cryst. Solids,*

Cor63 Cornish, D., and Watt, L., *Br. Sci. Instr. Res. Assoc. Rep.*, (1963), R295.

Dav96 K. M. Davis, et al., *J. of Non-Cryst. Solids,* **v203**, (1996), p. 27.

Der87 B. V. Derjaguin, N. V. Churaev, and V. M. Muller, *Surface Forces,* Consultants Bureau, New York, (1987).

Dov92 P. M. Dove, and S. F. Elston, *Geochim. Cosmochim. Acta*, **v56,** (1992), p. 4147.

Eva02 D. Evans, *MRS Bulletin,* **v27**, (10), (2002), p. 779.

Eva04 D. R. Evans, *MRS Symp. Proc.*, **v816**, edited by, D. Boning, M. Voss, and A. Philloposian, Materials Research Society Proceedings, San Francisco, Ca, (2004) p. K9.1.1.

Ewa99 R. Ewasiuk, S. Hong, and V. Desai, in *Chemical Mechanical Polishing in IC Device Manufacturing III*, edited by Y. A. Arimoto, R. L. Opila, J. R. Simpson, K. B. Sundaram, I. Ali, Y. Homma, Electrochemical Society Proceedings Series, Pennington, NJ, (1999), p. 408.

Fran99 J. Franz, P. Erichson, and J. Kross, *Optik*, **v110**, (9), (1999), p. 426.

Gag02 J. Gagliardi et al., *CMP-MIC*, (2002).

Gar02 R. Garcia and R. Perez, *Surface Science Reports*, **v47**, (2002), p. 197.

Gil04 S. R. Gilliss, J. Bentley, and C. B. Carter, *MRS Symp. Proc.*, **v818**, Materials Research Society Proceedings, San Francisco, (2004), p. M1.8.1.

Gor03 V. R., Gorantla, et al., *J. of the Electrochem.l Soc.,* **v150**, (12), (2003), p. G821.

Gry93 G. W. Grynkewich, and J. N. Helbert, in *Handbook of Multilevel Metallization for Integrated Circuits,"* Noyes Publications, New Jersey, 1993, Ch. 7.

Han90 W-T. Han, and M. Tomozawa, *J. of Non-Cryst. Solids,* **v122**, (1990), p. 90.

Han91 W-T. Han, and M. Tomozawa, *J. of Non-Cryst. Solids,* **v127**, (1991), p. 97.

Hie89 T. Hiemstra, W. H. Van Riemsdijk, and G. H. Bolt, *J. of Colloid and Interface Sci.*, **v133**, (1989), p. 133.

Hir87 K. Hirao and M. Tomozawa, *J. Am. Ceram. Soc.,* **v70,** (7), (1987), p. 497.

Hog73 J. M. Hogan, et al., *J. Cellular Plastics*, September/October (1973), 219.

Hol64 L. Holland, *The Properties of Glass Surfaces*, Chapman & Hall, London, (1964).

Hom03 Y. Homma, et al., *J. of Electrochem. Soc.*, **v150**, (12), (2003), p. G751.

Hos97 S. Hosali, D. Evans, et al., *CMP–MIC Conference*, ISMIC–200P, Feb. (1997), p. 52.

Hos01 T. Hoshino et al., *J. of Non-Cryst. Solids,* **v283**, (2001), p. 129.

Hou92 W. A. House, and D. R. Orr, *J. Chem. Soc. ,* Faraday Trans., **v88**, (1992), p. 233.

Hun01 R. J. Hunter, *Colloids and Surfaces A: Physicochemical and Engineering Aspects*, **v195**, (1-3), (2001), p. 205.

Ile79 R. Iler, *The Chemistry of Silica*, Wiley, New York, (1979).

Ire97 P. J. Ireland, *Thin Solid Films*, **v304,** (1-2), (1997), p. 1.

ITRS03 International Technology Roadmap for Semiconductors (2003).

Izu79 T. Izumitani, in *Treatise on Materials Science and Technology,* eds. M. Tomozawa and R. Doremus, Academic Press, New York, (1979), p. 115.

Izu84 T. Izumitani, *Tech. Digest, Topical Meeting on the Science of Polishing,* Optical Society of America, April 17 (1984), TuB-A1.

Jai94 R. Jairath, et al., *MRS Symp. Proc.,* v337, (1994) p.121.

Kal56a A. Kaller, *Naturwissenschaften*, **v43**, (7), (1956), p. 156.

Kal56b A. Kaller, *Silikattechnik*, **v7**, (10), (1956), p. 380.

Kal91 A. Kaller, *Glastech. Ber.*, **v64**, (9), (1991), p. 241.

Kal98 A. Kaller, *Glastech. Ber. Glass Sci. Tech.*, **v71**, (6), (1998), p. 175.

Kat03 T. Katoh, H-G. Kang, U. Paik, and J-G. Park, *Jpn. J. of Appl. Phys.*, **v42**, (2003), p. 1150.

Kel98 A. Kelsall, *Glass Technology,* **v39**, (1), February (1998), p. 6.

Kim02 S-K. Kim et al, *J. Vac. Sci. Tech. B*, **v20**, (3), (2002), p. 918.

Kim03 S-K. Kim et al, *Jpn. J. of Appl. Phys.*, **v42**, (2003), p. 1227.

Kul04 M. Kulawski, *MRS Symp. Proc.*, **v816**, (2004), p. K7.2.1.

Lee03 S-M. Lee, *Characterization of Chemical Interactions During Chemical Mechanical Polishing of Copper,* Ph.D. Dissertation, University of Florida, Gainesville, Fl., (2002).

Lin99 C. F. Lin et al,*Thin Solid Films*, **v347**, (1999), p. 248.

Mah99a U. Mahajan, M. Bielmann, and R. K. Singh, *Electrochem. and Solid- State Letters*, **2,** (1), (1999), p.46.

Mah99b U. Mahajan, M. Bielmann, and R. K. Singh, *Electrochem. and Solid- State Letters*, **2,** (2), (1999), p.80.

Mah00 U. Mahajan, *Fundamental Studies on Silicon Dioxide Chemical Mechanical Polishing,* Ph.D. Dissertation, University of Florida, Gainesville, Fl., (2000).

Mar03 H. Martin, B. Bournique, B. Blanchi, and C. Lerche-Langrand, *Analytical Biochemistry*, **v319**, (2003), p.56.

Mar03b A. Martin et al, *Mat. Res. Soc. Symp. Proc*, **v767**, (2003), p. F5.10.1.

Mas89 R. L. Mason, R. F. Gunst, and J. L. Hess, *Statistical Design and Analysis of Experiments with Applications to Engineering and Science,* J. Wiley and Sons, New York, (1989).

Mou95 J. F. Moulder et al, *Handbook of X-ray Photoelectron Spectroscopy: A Reference Book of Standard Spectra for Identification and Interpretation of X-ray Photoelectron Spectroscopy Data,* eds. J. Chastain and R. C. King II., Physical Electronics, Eden Prairie, MN (1995).

Mur93 S. P. Murarka, *Metallization Theory and Practice for VLSI and ULSI,* Butterworth-Heinemann, Boston (1993). p. 100.

Mur94 S. P. Murarka, and R. Gutmann, *1994 Annual Report of the New York State SCOE,* Semiconductor Research Corporation, Research Triangle Park, NC (1994).

Nab93 M. Nabavi, O. Spalla, and B. Cabane, *J. Colloid and Interface Sci.*, **v160**, (1993), p. 459.

Ngu01 V. H. Nguyen, et al., *Microelectronic Engineering*, **v55**, (1-4), Mar (2001), p. 305.

Obe98 Y. K. Obeng et al., Electrochemical Society Proceedings Series, **98-7**, 151, (1998).

Ols93 J. Olsen, and F. Moghadam, in *Handbook of Multilevel Metallization for Integrated Circuits,"* Noyes Publications, New Jersey, 1993, Ch. 6.

Oss02 K. Osseo-Asare, *J. of Electrochem. Soc.*, **v149**, (12), (2002), p. G651.

Pai88 P. L. Pai, C. H. Ting, and W. G. Oldham, *5th VMIC IEEE*, Santa Clara, Ca., Cat. No. 88CH2624-5, IEEE, NY (1988), p. 108.

Par04 S. Park, *IEEE Transactions on Semiconductor Manufacturing,* **v17**, (3), (2004), p. 362.

Par04b J.-G. Park, T. Katok, and U. Paik, *J. of Mater. Res.*, **v19**, (6), (2004), p. 1783.

Pour66 M. Pourbaix, *Atlas of Electrochemical Equilibria in Aqueous Solutions*, Pergamon Press Ltd. (1966), p. 194.

Pre27 F. Preston, *J. Soc. Glass Technol.*, **v11**, (1927) p. 247.

Qin04 K. Qin, C. Park, and B. Moudgil, *Thin Solid Films,* **v446,** (2), (2004), p.277.

Ren94 P. Renteln and J. Coniff, *MRS Symp. Proc.*, **v337**, (1994) 104.

Sab00 R. Sabia, and H. Stevens, *Machining Science and Technology*, **v4**, (2), (2000), p. 235.

Sam73 *The Oxide Handbook*, edited by G. V. Samsonov, Translated from Russian by C. N. Turton and T. I. Turton, Plenum, New York, (1973).

Sch95 J. Schlueter, *SemiCon Southwest*, **95,** (1995), p. 1.

Sch99 J. Schlueter, *Semiconductor International,* October (1999).

Sik01 A. K. Sikder, et al*., J. of Electronic Mat.,* **v30,** (12), (2001), p. 1520.

Sim01 A. Simpson, L. Economikos, F-F. Jamin, A. Ticknor, *Mat. Res. Soc. Symp. Proc.*, **v671**, (2001), p. M4.1.1.

Sin98 P. Singer, *Semiconductor International*, June, 1990.

Sin02 R. K. Singh, et. al., *MRS Bulletin*, **v27**, (2002), p. 752.

Sin03 R. K. Singh, *Slurries for Chemical Mechanical Planarization (CMP) Technology*, Short Course - Particle Engineering Research Center, Summer School in Winter, (2003).

Siv92 S. Sivaram, et al., *Proc SRC, Topical Research Conference on Chemical Mechanical Polishing for Planarization,* SRC, Research Triangle Park, NC, (1992), p. 8.

Sko02 N. V. Skorodumova et al, *Physical Review Letters*, **v89**, (16), (2002), p. 166601-1.

Ste92 F. A. Stevie, in *Encyclopedia of Materials Characterization*, edited by C. R. Brundle, C. A. Evans Jr., and S. Wilson, Butterworth-Heinemann, Boston, (1992), p. 699.

Ste97 J. M. Steigerwald, S. P. Murarka, and R. J. Gutmann, *Chemical Mechanical Planarization of Microelectronic Materials*

Sti97 G. Stix, *Scientific American*, **v276**, (1997), p. 45

Stu92 W. Stumm, *Chemistry of the Sold–Water Interface*

Tro94 J. A. Trogolo, K. Rajan, *J. of Materials Science,* **v29**, (1994), p. 4554.

Tse01 W-T, Tseng, et al., *Electrochem. and Solid-State Letters,* **v4**, (5), (2001), p. G42.

Tye04 H. Tye, *Drug Discovery Today*, **v9**, (11), (2004), p. 485.

Ver48 J. W. Verwey and J. T. Overbeek, *Theory of the Stability of Lyophobic Colloids*, Elsevier, Amsterdam, (1948).

Vie01 N. H. Viet, Ph.D. Dissertation, Universiteit Twente, Netherlands, (2001).

Wal96 W. Wallace, W. L. Wu, and R. A. Carpio, *Thin Solid Films,* **v280**, (1996), p. 37.

Wil 93 S. R. Wilson, C. J. Tracy, and J. L. Freeman, *Handbook of Multilevel Metallization for Integrated Circuits,"* Noyes Publications, New Jersey, 1993, Ch. 1.

Zam03 A. A. Zaman, F. Demir, and E. Finch, *Applied Clay Science*, **v22**, (2003), p. 237.

Zeta Colloidal fundamentals, User's Manual Zeta Reader by Brookhaven, p. IV-1.

Zha99 B. Zhao and F. G. Shi, *Electrochem. and Solid-State Letters*, **v2**, (3), (1999), p. 145.

Zha01 E. Zhao, and C. Shan, *Semiconductor International*, June (2001).

BIOGRAPHICAL SKETCH

Jeremiah Terrell Abiade was born Jeremiah Terrell Grey to Candy and Renee Grey, September 22, 1976, in Chicago, Illinois. Jeremiah attended Southern University and A&M College in Baton Rouge, Louisiana where he received a B.S. in physics. There he was a member of the Timbuktu Academy and recipient of the NASA undergraduate student award for research. Jeremiah began his graduate study at the University of Florida in 1999 under the tutelage of Dr. Rajiv K. Singh and obtained his Ph.D. in 2004. Jeremiah's graduate study was supported by fellowships from the National Science Foundation's Alliance for Graduate Education and the Professoriate Program (NSF-AGEP), UF College of Engineering Graduate Minority Fellowship Program, UF Office of Graduate Minority Programs-Supplemental Retention Award, and the NSF Dissertation Fellowship.